2015-05-04

Stability of Interfaces in a SAGD Steam Chamber

Zhu, Da

UNIVERSITY OF CALGARY

Stability of Interfaces in a SAGD Steam Chamber

By

Da Zhu

A THESIS

SUBMITTED TO THE FACULTY OF GRADUATE STUDIES

IN PARTIAL FULFILMENT OF THE REQUIREMENT FOR THE

DEGREE OF MASTER OF SCIENCE

GRADUATE PROGRAM IN CHEMICAL AND PETROLEUM ENGINEERING

CALGARY, ALBERTA

MAY, 2015

Abstract

Oil sands reservoirs in Western Canada are among the largest petroleum accumulations in the world. Given the high viscosity of the oil, typically in the hundreds of thousands to millions of cP, these oils are recovered from the reservoir by using steam which heats the oil to between 180 and 250°C which lowers its viscosity to less than 10 cP. The key issue faced by these recovery processes is their thermal efficiency and consequent greenhouse gas emissions and water use. The larger the amount of steam used, the greater the greenhouse gas emissions and water use and the lower the economic viability of the recovery process itself. Thus, the thermal efficiency of steam-based recovery processes is a critical measure of process viability. Ultimately, the thermal efficiency is controlled by the efficiency of the growth of the steam chamber in the reservoir. In other words, steam conformance in the reservoir is a critical control on the efficiency of the recovery process. The research documented in this thesis examines the stability of the steam-oil interfaces to further understand the dynamics of steam chambers in oil sands reservoirs. The key reason that we are interested in instability in SAGD is that it potentially plays an important role in the growth of the steam chamber with consequent changes of heat transfer and oil rate. The results show that even in a homogeneous reservoir, instabilities can yield non-ideal steam conformance within the reservoir. The instability takes place in the gas phase beyond the edge of the hot steam chamber in the gas zone that is created due to gas exsolution. The nonlinear instability that is exhibited by the fine grid reservoir simulation results can be triggered by the difference in either viscosity (Saffman-Taylor) or density (Rayleigh-Taylor). To observe fingering at the edges of depletion chambers in steam-based recovery processes, fine grid

simulations are required. Given that the fingers are of order of 30 cm in width, this implies grid blocks of this or smaller orders of length scales are needed.

Acknowledgements

I would like to express my deepest appreciation to my supervisor, Dr. Ian Gates. I feel abashed to say that I have studies and worked in four universities in Northern America. Ian is the best supervisor I have ever seen. Ian is humorous and frank and is always optimistic with things, so that it is a very joyful thing to work with him. He respects students, encourages students and grows students from the bottom of his heart. His very impressive sharpness in capturing the essence of the problem greatly deepens my understanding of petroleum engineering. I am very much grateful to my co-supervisor, Dr. Joule Bergerson for her continuous support of my study and research and for her enthusiasm and immense knowledge. I learned quite a lot of statistical analysis and systems analysis from the discussion with her. Without Ian and Joule's help, this thesis would not be possible.

I also would like to sincerely thank my thesis committee: Dr. Brij Maini, Dr. Hossein Hejazi and Dr. Stephen R. Larter, for their insightful comments and hard questions.

Switching from atmospheric physics to reservoir simulation was not an easy decision. I am indebted to Dr. Nakamura, Dr. Frederick of University of Chicago and Dr. Flierl of MIT for their great encouragement. A lot of my friends helped me through this difficult process with their encouragement, they are: Yuanyuan Ou, Renyu Hu, Nanxi Bian, Bo He, Dawei Li, Le Yang and Junjun Zhang. My colleagues at U of C offered me offered me great help in my study and research, they are: Jacky Wang, Xuemin Huang, Yi Su, Yu Bao, Abhishek Batawara, Bahareh Khansari, Bo Yang and Jie Zhan.

I would like to thank my parents for their consistent supports in past few years.

Finally, I am grateful to my wife, Jing Xu, for her support and unconditional love through peaks and troughs in my life. This thesis is dedicated to her.

Table of Contents

List of Figures

List of Tables

Chapter One: **Introduction**

Over the past few years, the demand for crude oil has stabilized at about 92.9 million barrels per day (U.S. Energy Information Administration 2014). A large fraction, about 74%, of this is converted into transportation fuel which leads to greenhouse gas emissions equal to about 6.63 Gt per year (U.S. Energy Information Administration 2014). The world is heavily dependent on fossil fuel energy and there does not appear to be a clear path to shift it to alternative energy sources. Fossil fuel energy is broadly categorized into conventional and unconventional sources. Conventional sources are those that produce high quality petroleum (oil API gravity above 31.1) from reasonably high quality reservoirs (ones where primary production is possible). Unconventional oil sources are those reservoirs that produce an oil product that requires upgrading to chemically convert it to a synthetic conventional crude oil and/or require significant in situ reservoir treatment to enable production of the oil to the surface. For example, steam injection to produce viscous bitumen to the surface or hydraulic fracturing to produce oil from tight, low permeability, rock.

Heavy oil is typically defined as having API gravity between 10 and 20°API and viscosity between 100 and 100,000 cP whereas bitumen (also referred to as extra heavy oil) has API gravity below 10°API and viscosity greater than 100,000 cP (Gates, 2013; some references define heavy oil viscosity up to 10,000 cP and bitumen viscosity greater than 10,000 cP). A comparison of conventional and unconventional oil production globally over the past few years is displayed in Figure 1.1. The data show that the amount of oil from unconventional sources has increased dramatically over the past two decades and that it is becoming an increasingly

more important source of oil. Heavy oil and oil sands are playing more important role in the energy supply in the world as hydrocarbon resources.

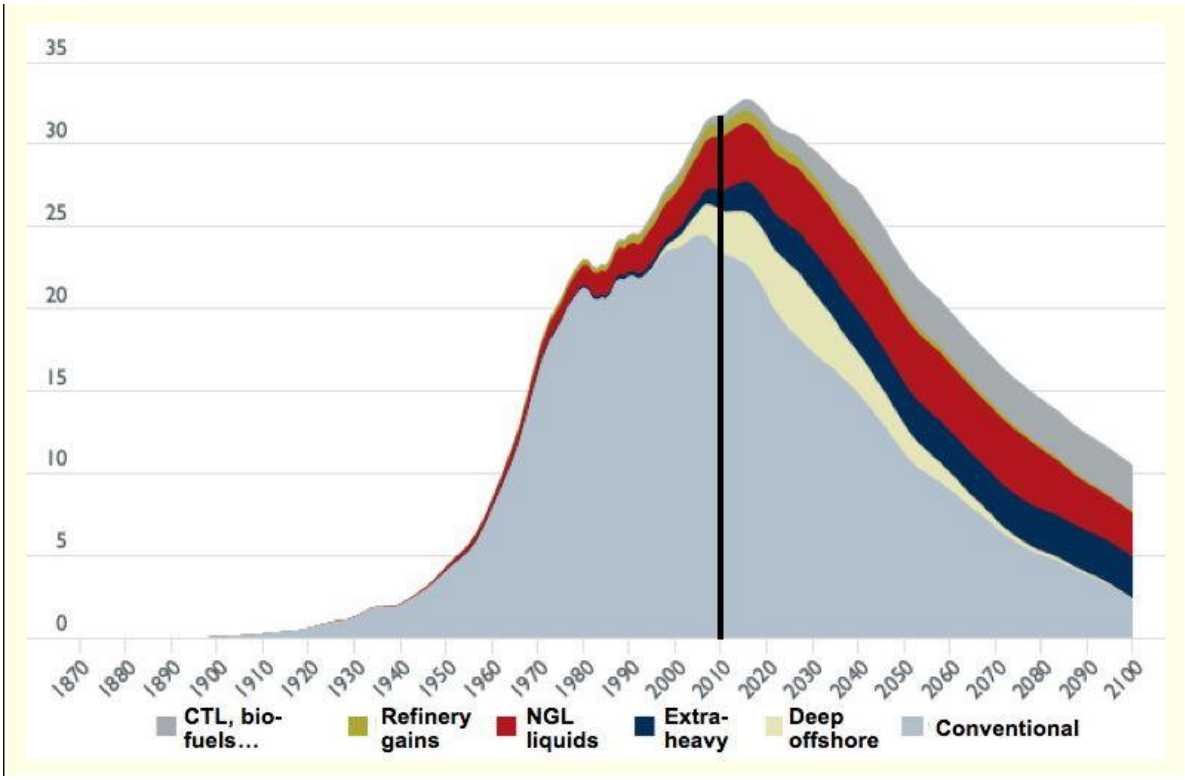

Figure 1-1: Global conventional, heavy oil, and bitumen (extra heavy oil) oil production (Australian Government, Department of Infrastructure 2010).

The research documented in this thesis focuses on production of bitumen from oil sands reservoirs by steam-based recovery processes. Bitumen is the form of petroleum that is found in oil sands reservoirs in Northern Alberta. Given the high viscosity and the resulting very slow movement of the bitumen, conventional recovery methods cannot be used to produce this oil. For bitumen, to enable its movement in the reservoir to the production well, the first technical challenge is to lower its viscosity so that it be produced to the surface. The dependence of

viscosity of heavy oil and temperature is illustrated in Figure 1.2. The viscosity of bitumen can be lowered to 10 cP by increasing its temperature to 250°C. This is the basis for steam-based recovery processes: steam is injected into the reservoir to raise its temperature so that its mobility is high enough so that it can be moved under conventional forces such as gravity. Since steam is required, this implies that fuel is required to generate steam and water will be consumed as part of the recovery process.

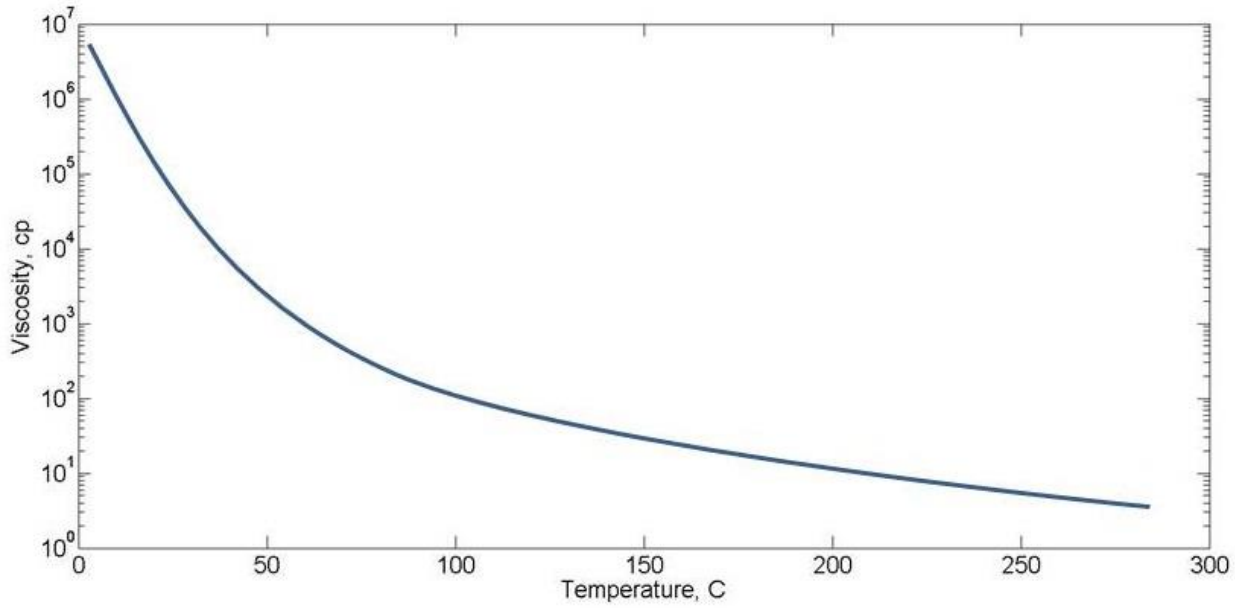

Figure 1-2: Effect of temperature on viscosity of Athabasca crude bitumen (Modified from Mehrotra and Svrcek, 1986).

The two currently commercial steam recovery processes used in Alberta are Cyclic Steam Stimulation (CSS) and Steam-Assisted Gravity Drainage (SAGD). These processes are similar in that steam is injected into the reservoir to heat the bitumen in situ. However, CSS is cyclic and in typical practice applies steam to the reservoir at pressures greater than the fracture

pressure of the reservoir. In SAGD, steam is injected continuously and is typically done at pressures below the fracture pressure.

1.1 Heavy oil and oil sands deposits in World, North America, Canada, Alberta

Globally, the remaining conventional oil resource is equal to about 1.02 trillion barrels whereas the estimated heavy oil resource of the world is approximately 5.6 trillion barrels (Fein 2010). Figure 1.3 displays a map of heavy oil and oil sands resources in the world. In North America, California holds the largest deposits of heavy oil, followed by Texas and Alberta. Alberta hosts most of the bitumen (extra heavy oil) followed by Utah and Alaska (Hein 2006). Heavy oil and oil sands reservoirs in Western Canada contain over 1.7 trillion barrels of heavy oil and bitumen altogether (Alberta Energy Regulator 2013). About 90% of the oil resource in Canada is bitumen (Butler 1997).

The famous pitch drop experiment by Professors Parnell and Mainstone of the University of Queensland, Australia illustrates how slowly viscous bitumen moves at room temperature: in 1930, Professor Parnell cut the seal at the neck of a funnel and let the pitch flow. On April 24, 2014, the 9th droplet of bitumen fell from the funnel. The average period for a droplet to form and fall is equal to about 10 years.

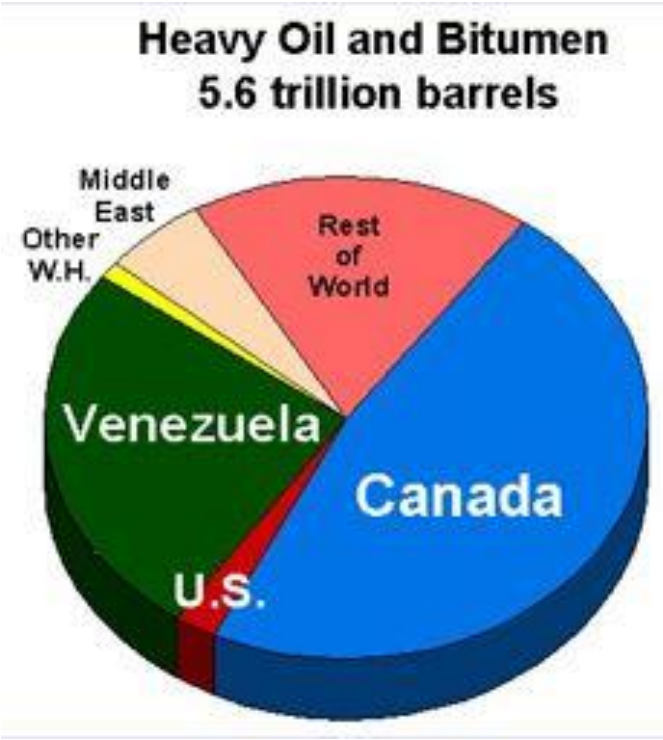

Figure 1-3: Global distribution of heavy oil and bitumen (Elk Hills Petroleum 2013).

Given the resource size of Alberta's bitumen deposits, it is strategically important for Canada to produce these resources for their chemical feedstock and energy values. The key challenge presented with producing these resources is the amount of invested energy and the consequent greenhouse gas (GHG) emissions and water consumption required to produce it. There is an ongoing search for technologies that will reduce the energy, GHG, and water intensities of bitumen recovery processes.

1.2 Basic Geology of Oil Sands Formations

In Alberta, the main productive oil sands formations are the McMurray, Clearwater, and Bluesky Formations. Oil sands deposits in Alberta are usually located at less than depths of 800 m. In these reservoirs, the horizontal permeabilities are relatively high and range from 1 to 10 D. Their porosities are typically high with values between 0.25 and 0.35 and oil saturations from 0.5 to 0.9, and in some cases, even higher. In the McMurray Formation, the oil-bearing rocks are usually poorly cemented quartz which is of high porosity and permeability. A typical high quality oil sands reservoir exhibits a continuous and thick sand column with very few shale barriers. The oil sands deposits are mostly impacted by the underneath Devonian topography. In general, the sands were laid down between 360 and 400 million years ago. The erosion and uplift of the continent to the east led to the eastward exposure f the older Devonian formations, which resulted in an angular unconformity between Devonian and subsequent Cretaceous deposits (Vigrass 1968).

The McMurray formation was laid down in a fluctuating marine environment. The Lower McMurray formation was formed in a fluvial environment and filled the valleys in the underlying Devonian surface with sediments (Hein and Cotterill 2006). Sea level rise resulted in deeper and more sinuous channels, which led to a more tidal environment with larger amounts of sediments being deposited. Multiple, overlying, meandering rivers evolving through time resulted in a stacked channel configuration in the Middle and Upper McMurray Formation. The Upper McMurray was laid down in a more tidal environment (Barson et.al. 2001). The shale caps were formed by the intrusion of the Boreal Sea over the McMurray-Wabiskaw Formation

(Flach 1984). Figure 1.4 illustrates the relative sea change and its corresponding deposition formation.

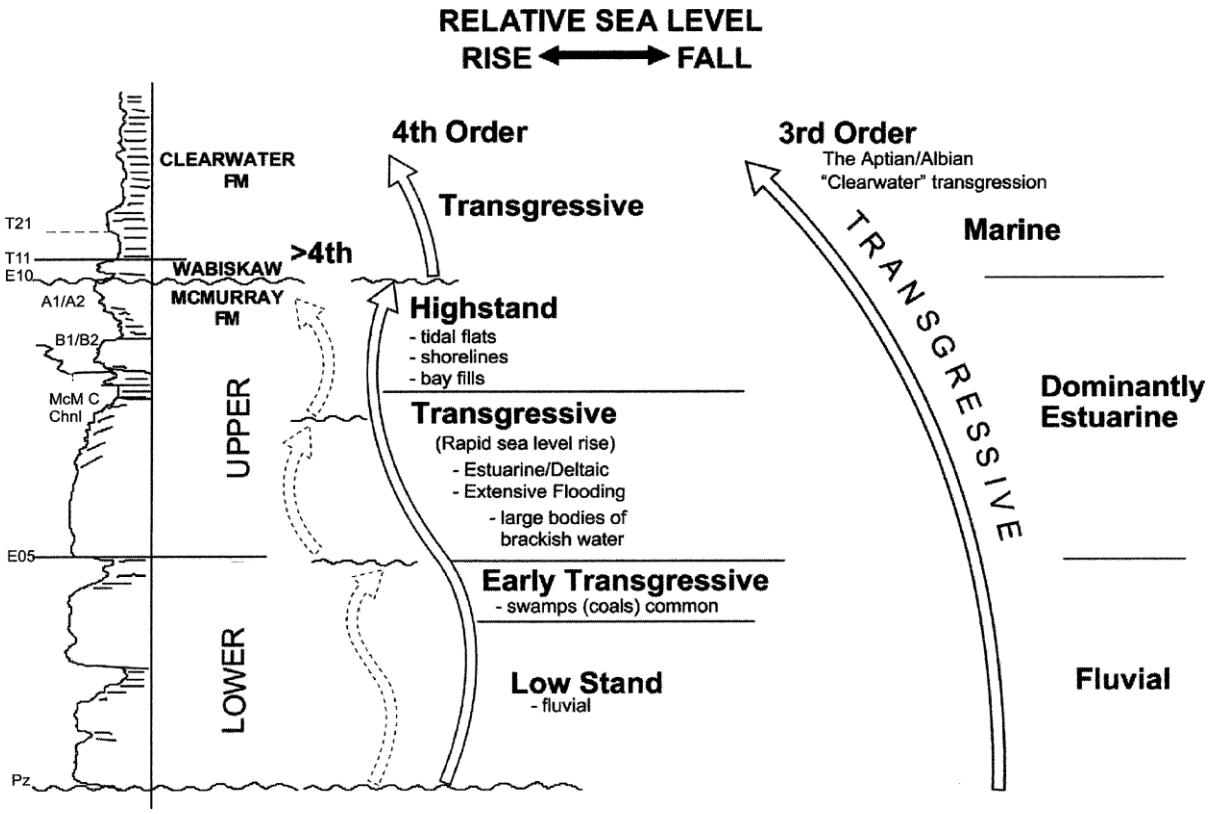

Figure 1-4: Sea level change and McMurray-Wabiskaw-Clearwater formation succession (From Hein and Cotterill 2006)

In the Athabasca deposit, typical oil-bearing sands are contained in the point bars (Hein et al. 2007). Figure 1.5 shows an example of the facies distribution of an oil sands point bar in geological model with mud-filled channel lines.

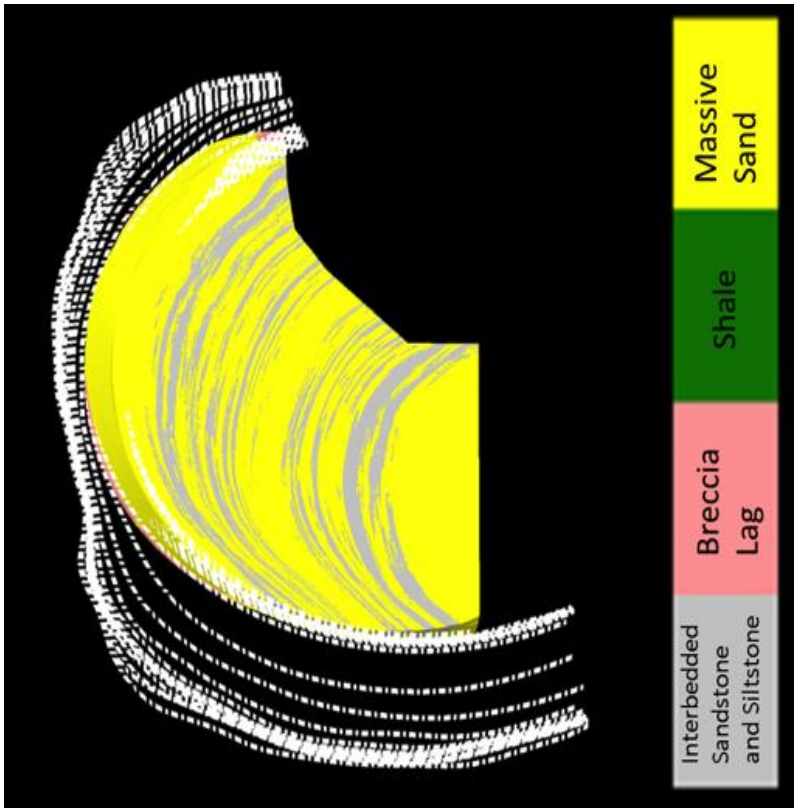

Figure 1-5: Facies distribution of oil sands point bar (Su et al. 2013).

The tidal flat overbank and bay fills led to the formation of low permeability and porosity barriers such as mudstones and clast-brecciated intervals. The length scales of the thicknesses of the barriers vary from centimeters to meters (Hein et al. 2007). Figure 1.6 shows a schematic picture for the cross section in the Athabasca oil sands region.

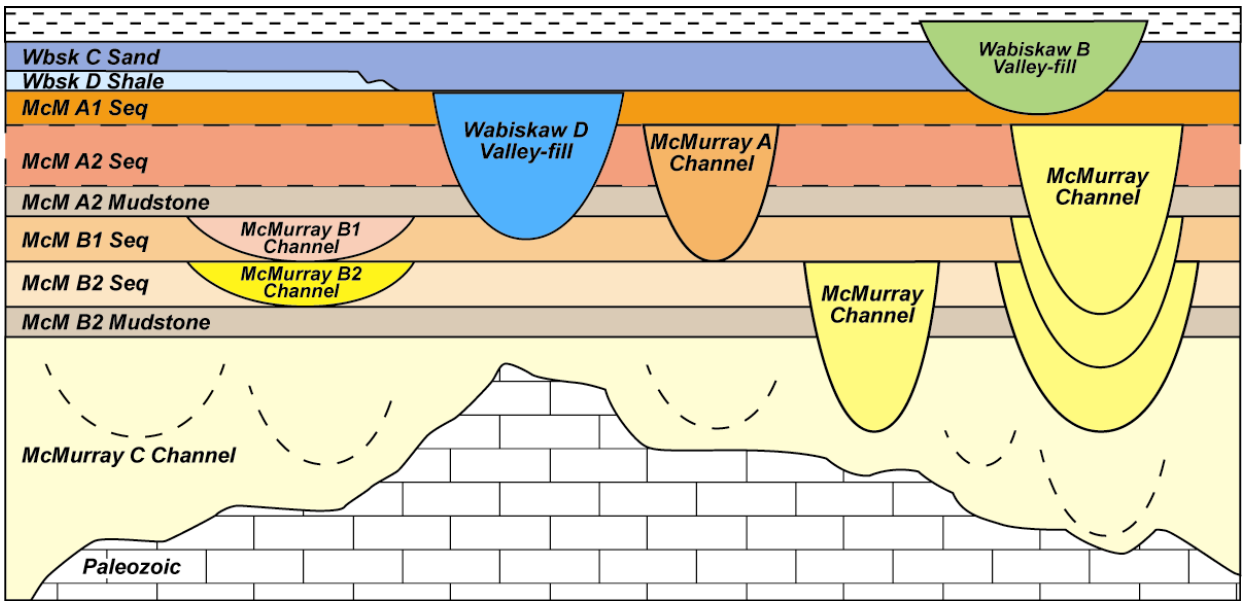

Figure 1-6: Stratigraphic model of McMurray formation in Athabasca region (Alberta Energy and Utilities Board 2003).

1.3 Steam-Assisted Gravity Drainage (SAGD)

SAGD is a steam-based thermal recovery process invented by Roger Butler in 1979. It has now become one of the most widely used methods to recover bitumen from oil sands reservoirs in Northern Alberta. Figure 1.7 displays a typical SAGD well configuration. In this process, two horizontal wells, typically 500 to 1000m long, are placed in the reservoir. The lower well is the production well and it is placed slightly above the bottom of the reservoir whereas the upper well, the injection well, is positioned about 5 to 8 m vertically above the production well. The main idea of SAGD is that steam, of quality of 95% or higher, injected into the upper injection well, flows to the edge of the steam chamber where it releases its latent heat to the oil sands there. As a consequence, bitumen within the oil sands is heated which causes its viscosity to fall. Due to the density difference between the steam (vapour) and mobilized oil, it drains under the

action of gravity to the base of the steam chamber where fluids are removed from the reservoir by the production well. Steam generation is done by combustion of fuel, typically natural gas, which consequently creates large carbon dioxide emissions. Also, as the steam chamber grows in the reservoir, a certain small fraction of water remains in the pore space that results from the removed oil. Thus, the process, providing there is no active water system in the reservoir, will tend to lose water. For many systems, about 5% of the steam injected is lost to the reservoir.

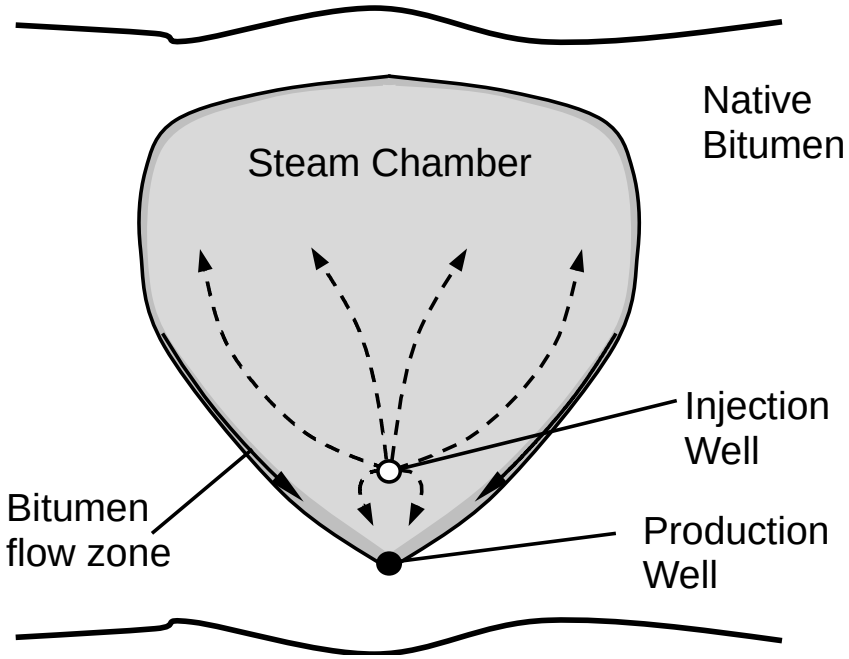

Figure 1-7: Cross-sectional view of the Stream-Assisted Gravity Drainage (SAGD) process The two parallel horizontal wells extend into the page. (Gates 2011)

The SAGD process involves four stages. The first one is called the circulation stage, during which steam is injected through both the injection and production wells so as to establish thermal communication between the wells. In the circulation stage, steam is injected at the reservoir pressure and produced back to surface through each of the injection and production wells. In this

manner, the wells act like line heat sources and conduction is the main heat transfer mechanism. In typical practice, the steam circulation stage takes between 2 and 6 months. After the region surrounding the wells is warm, steam circulation is ceased and SAGD mode starts where steam is injected into the upper well and fluids are produced by the lower well.

During SAGD mode, the second stage of the process is called the rising steam chamber period. In this stage, the steam chamber starts to rise vertically and expands laterally. Since the chamber is fully enclosed within the oil sands reservoir, all heat losses go to the oil sand formation – thus this stage of the process is typically thermally efficient. The measure of the thermal efficiency, the steam-to-oil ratio (SOR, steam expressed as cold water equivalent) At the top of the chamber, cold bitumen sits on the top of hot steam, steam condensate, and mobilized bitumen. Thus, there are opportunities for instability associated with Rayleigh-Taylor type instabilities. These instabilities can explain the fluid dynamics of oil recovery during this stage (to be discussed in more detail in Chapter 4). In this stage, the oil production rate rises as the height of the steam chamber increases and the SOR drops.

After the steam chamber reaches the top of the reservoir, SAGD enters the third stage often referred to as the depletion stage or laterally spreading stage. The oil rate usually peaks just as the steam chamber has reached the top of the oil sands formation. In the third stage, the extent of the steam chamber increases outwards from the injection and production wells with the increase of steam injection. The width of the steam chamber becomes greater than that of the height and convection of steam versus that of steam condensate and draining oil changes the dynamics at the edge of the chamber. In this case, viscous shear type instabilities dominate at the edge of the

chamber. As the chamber spreads, heat losses to the cap rock rise since as the chamber evolves, it contacts greater amounts of cold cap rock. Since a greater fraction of the energy contained in the injected steam is being lost to the cap rock (non-productive rock), the thermal efficiency of the recovery process starts to suffer and the SOR starts to rise.

In the final stage of SAGD, the steam chamber from adjacent well pairs merge. Since there is no cold overburden between the SAGD well pairs, heat losses to the cap rock drop but since the oil now has a long distance to drain to the production wells, the oil rate is relatively low and thus, the thermal efficiency drops significantly and the SOR rises.

The key to a successful SAGD operation is heat transfer – it controls the temperature of the bitumen at the edge of the steam chamber and thus its viscosity. If heat transfer is poor, then ability to heat the oil sand beyond the edge of the steam chamber is impaired and the thermal efficiency is less than ideal. Thus, at its most fundamental level, the success of SAGD (and other steam-based recovery processes) is strictly linked to heat transfer at the edge of the chamber. Thus, means to enhance heat transfer at the edge of the chamber will improve the thermal efficiency of the recovery process. As with all conductive heat transfer, it can be enhanced by increasing the thermal conductivity of the medium or by raising the heat transfer area or by raising the temperature gradient.

1.4 Instability and Its Role in SAGD

The concept of instability in the context of fluid flow is perhaps most clearly explained by the transition from laminar to turbulent flow in pipe flow. At low flow rate, the flow is perfectly parallel and liquid flow in a pipe is dominated by viscous and pressure forces. As the flow rate increases, the speed of the fluid rises and inertial forces start to grow larger as streamlines within the flow stray from parallel flow (the onset of flow features which shift the flow away from parallel flow are referred to as perturbations). At a critical flow rate, the inertial forces dominate and the flow changes state to turbulent flow with multiple scale recirculations. The critical flow rate marks the onset of instability which shifts the flow from one state (laminar flow) to another state (turbulent flow). Below the critical flow rate, any perturbations that decay with time and the base flow state (laminar flow) persists. With the onset of the instability, perturbations grow with time and the change to the new flow state occurs.

From a mathematical point of view, instability can be explained in the context of the momentum and mass continuity equations, referred to as the Navier-Stokes (N.S.) equations, that govern bulk flow. All bulk fluid flows are mathematical solutions of the N.S. equations subject to certain initial and boundary conditions. However, some flow solutions which satisfy N.S. equations are never observed in reality because they are unstable to the small perturbations – in other words, the mathematical flow state does not exist physically since it is unstable. Perturbations, even at the molecular scale, grow and shift the physical flow state to another state. We say a flow profile is unstable if and the perturbation grows when it is perturbed (from whatever source e.g. noise) from its original mean base state. We need to pay great attention to

the adjectives “small” and “mean”. The perturbation has to be “small” compared to the mean base state. The definition of “mean state” is a very complicated problem that it arguably could be either a temporal, special, or ensemble-averaged state. For example, people are talking about climate change, but we first have to understand the mean climate system that the instantaneous system deviates from which is still a great puzzle faced by the climate scientists.

In the linear stability regime, the initial small perturbation grows exponentially with time. Linear stability analysis applies to systems only when the magnitude of perturbation is small compared to the mean state. Once the magnitude of perturbation is comparable to or larger than that of the mean state, nonlinear effects will be important. The flow will be equilibrated by the nonlinearity and enter into another regime of mean state and a new instability cycle could start. Fluid nonlinearity and its consequent turbulence are arguably among the most difficult concepts to understand. Heisenberg is reported to have said “When I meet God, I am going to ask him two questions: Why relativity? And why turbulence? I really believe he will have an answer for the first” (Marshak 2005). Modern turbulence research was pioneered by Kolmogrov’s 1941 theory that energy spectrum in the inertial range of turbulence follows a -5/3 power law with wavenumber. Nowadays, a lot of mathematicians and physicists are still trying to understand turbulence and its physical and mathematical characterizations.

The two main instabilities that will be discussed in later chapters are Rayleigh-Taylor instability and Orr-Sommerfeld instability, both of which are based on linear instability analysis. The mathematical models for both of them are straightforward. Rayleigh-Taylor instability occurs when a heavy fluid is above a light fluid. This happens during the chamber rising period. In this

case, the system is unstable in that the denser phase will descend and the less dense phase will rise. Orr-Sommerfeld instability is a viscous shear instability in parallel flow which describes that when the ratio of inertial force to the viscous force is greater than a given threshold, which occur mainly in the lateral spreading stage. For the case of parallel flow of two phases, the flow will be unstable leading to waviness of the interface between the two phases. Although the mathematical derivation of the shear instability system is relatively simple and numerical solutions are well known, the underlying physics that describes why strong shear will induce instability is still poorly resolved. People have proposed a lot of explanations for the generation of shear instability, for example, the Orr mechanism and the non-normal mechanism, but none of them has gained universal agreement.

The key reason that we are interested in instability in SAGD is that it potentially plays an important role in the growth of the steam chamber with consequent changes of heat transfer and oil rate. Steam chamber growth and heat transfer efficiency are key issues in SAGD operations – they control thermal efficiency which in turn influences process economics and environmental impact. Heat transfer at the edge of the steam chamber is controlled by latent heat release, conduction of heat into the oil sands beyond the edge of the chamber, and potential convection of heat by hot water flow beyond the edge of the chamber. Conduction of heat at the chamber edge is controlled by the thermal conductivity of the oil sand and area of the interface. At the microscopic level, heat transfer occurs by integrated small-scale random movement of molecules across the whole surface area of the interface as shown in Figure 1.8(a). Given the fixed temperature difference between steam and oil layers, the rate of molecular movement is a constant. Therefore, the other way to increase the heat transferred from steam to oil is to enlarge

the area of steam-oil interface. In the presence of flow instability, perturbations of the interface occur. When perturbed, the interface becomes wavier which in turn implies that its area will be enlarged. The idea is illustrated in Figure 1.8. Note that in the case with a wavy interface, as depicted in Figure 1.8(b), heat is still transferred by small-scale molecule movement, but the contact area/interface is larger. This means the effective heat diffusivity is greatly enlarged and the heat transfer rate is enhanced. The concept of effective diffusivity in the presence of external stirring (eddies) has been proposed and explored by Nakamura and Zhu (2010a, 2010b).

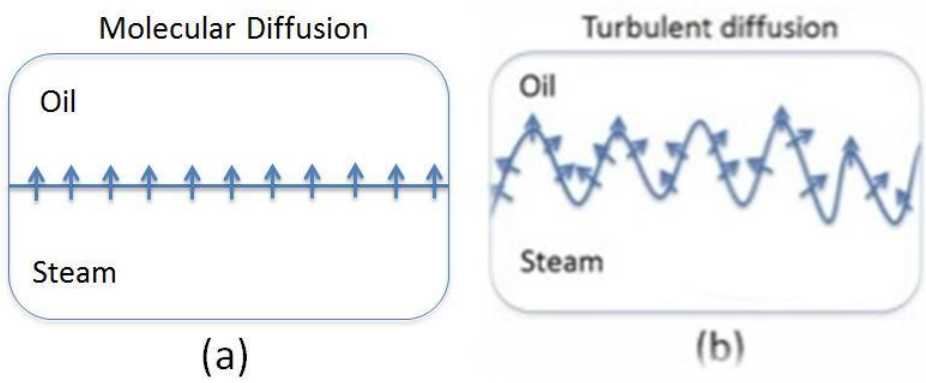

Figure 1-8: Schematic pictures for heat transfer by (a) flat interface and (b) perturbed interface

Steam conformance within oil sands reservoirs along wells is a key control on the thermal efficiency utilization of the wells. If the conformance along the wells is less than ideal, then the steam-to-oil ratio suffers. Most practitioners of steam-based recovery processes such as Cyclic Steam Stimulation and Steam-Assisted Gravity Drainage believe that poor steam conformance arises from the heterogeneity of the reservoir. This is undoubtedly the case as demonstrated by Su et al. (2013) and there is a belief that steam conformance would be ideal in an ideal reservoir – that is one that is perfectly homogeneous with respect to the geology and fluid (oil)

composition in the reservoir. However, if the system is unstable, poor steam conformance could result even in ideal homogeneous reservoirs. As yet, no studies have demonstrated that this is the case. Most reservoir simulations demonstrate ideal steam conformance and chamber shape in homogeneous oil sands reservoirs.

1.5 Research Questions

The research questions addressed by the research documented in this thesis are as follows:

1. Is the edge of the steam chamber stable?
2. What types of instabilities happen at the edge of the steam chamber? Can these instabilities occur in homogeneous reservoirs? If yes, what is the mechanism of the instability?
3. What are the impacts of these instabilities on the steam chamber growth? How can we control them to improve the performance of the recovery process?

1.6 Outline of Thesis

Chapter 2 contains a literature review which is composed of an introduction to oil sands recovery processes, production mechanisms, and previous work on instabilities in SAGD. Chapter 3 introduces the instability analysis of parallel flow model in a heated sub-pore. In Chapter 4, large amplitude instability of SAGD chamber is analyzed. Chapter 5 lists conclusions and recommendations that arise from the research documented in this thesis.

Chapter Two: **Literature Review**

2.1 Introduction to Oil Sands Recovery Processes

The three main oil sands deposits in northern Alberta are the Athabasca-Wabiskaw, Cold Lake, and Peace River deposits as shown in Figure 2.1. In total, they hold about 1.7 trillion barrels of heavy oil and bitumen, of which about 10% is considered recoverable, making Alberta the third largest reserves globally after Saudi Arabia and Venezuela.

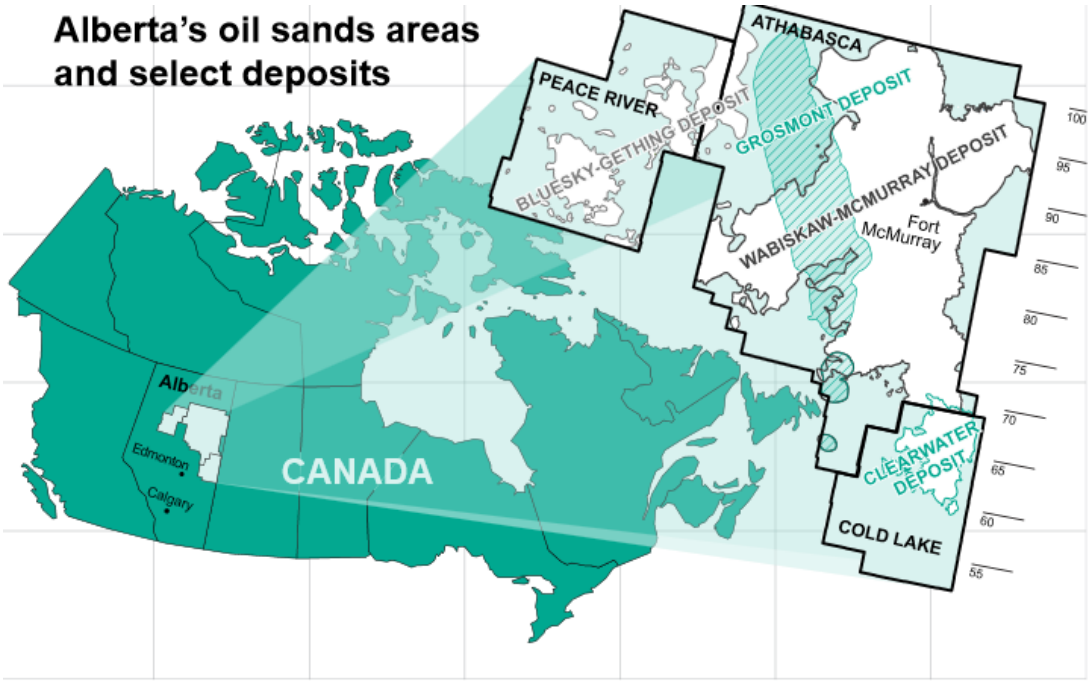

Figure 2-1: Deposits of Alberta' crude bitumen (Alberta Energy Regulator, 2013).

For heavy oil, the major recovery processes are cold production with or without sand production. For cold producible reservoirs, the in-situ viscosity of the dead oil has to be lower than about 35,000 cP and the solution gas-to-oil ratio has to be high enough so that the oil can be recovered under foamy oil flow and solution-gas drive. The recovery factor of cold production, whether with or without sand production, is equal to about 10%. In 2012, around 25% of heavy oil is recovered by cold and non-thermal methods.

For bitumen, the in situ dead oil viscosity is too high and the solution gas content is too low for cold production. In most cases, the viscosity of the dead oil exceeds 100,000 cP and the solution gas content is very low since these reservoirs tend to be relatively shallow. In the McMurray Formation in the Athabasca deposit, the viscosity of bitumen tends to range from 100,000 cP up to 10 million cP with the majority between 1 and 5 million cP. Therefore, despite the high permeabilities of the sand, bitumen is virtually immobile in situ and there is not enough natural drive energy to drive the oil to the surface.

There are two main challenges faced by in situ oil sands recovery processes. The first is that the bitumen must be mobilized so that it can be moved from the reservoir to the production well. The second is that a drive mechanism must be provided to move the mobilized oil from the reservoir to the production well. The key constraint is that this must be done such that the process is economic and generates revenues. Although there are several agents that can be used to mobilize bitumen e.g. heat, solvent dilution, and in situ upgrading (leading to an upgraded lower viscosity oil phase), the most used is steam due to its high latent heat, low viscosity when

in vapour phase, and cost and availability. In Alberta, the two currently commercial thermal processes being used are Cyclic Steam Stimulation (CSS) and Steam-Assisted Gravity Drainage (SAGD). In both of these methods, steam is injected into the oil sands formation to heat the oil and lower its viscosity. After the oil becomes mobile, drive mechanisms move the oil to the production wellbore. In CSS, the major drive mechanisms are thermal expansion, solution-gas and steam flashing drive, formation recompaction, and gravity drainage. In SAGD, the major drive mechanisms are thermal expansion and gravity drainage.

In field operations, CSS uses a single well (vertical, deviated or horizontal). There are three periods in CSS operation: 1. steam injection, 2. soak, and 3. production. During the first cycle, in the injection period, a specified target volume of wet steam is injected into the oil sands reservoir. Since the steam is injected a pressure higher than the reservoir fracture pressure, the formation is fractured and the steam is distributed in the reservoir. After the target volume of steam is injected, the well is shut down and process enters the soak period. In this period, heat from the steam fractured zone warms the reservoir in the neighborhood of the fractured zone. After the soak period is complete, the well is put on production and mobilized bitumen, formation water, steam condensate, and gas are produced. After the oil rate has dropped below the economic limit, the process is repeated and a new CSS cycle begins. The main mechanisms of CSS production are: pressure difference due to production, re-compaction of formation, solution-gas drive, steam flashing, thermal expansion, changes in capillary pressure force and gravity drainage (Gates 2013). In the first few cycles, the re-compaction of formation and solution-gas drive are two major mechanisms. The formation is dilated by the injected steam and the porosity and permeability is increased. After the well is put on production, the overburden

re-compacts the formation and drives the fluids out from the reservoir. Also, when the well is put on production, the pressure will decline. The gas which was originally dissolved in the oil exsolves from the oil (and water). The gas then expands and displaces the oil to the low-pressure production wellbore. A similar mechanism with solution-gas drive is steam-flashing. When pressure declines to the saturation point, the condensate will flash to the vapor phase and the expanded bubbles will push the oil to the production well. In later cycles when the steam chambers are large, gravity drainage becomes important as the mobilized oil moves under gravity to the production well. In numerical simulation of CSS, modeling of the evolution of geomechanics is a big challenge (Cokar et al. 2012). If we want to model the microscopic propagation of fractures in the formation we have to solve the stress tensor at any point throughout time in addition to the mas continuity, multiphase flow, and thermodynamic equilibrium equations, which requires great computing power. Currently, many researchers use the Quad model developed by Beattie et al. (1991) to model the deformation of formation during steam injection (Cokar et al. 2012).

A description of the SAGD process is presented in Chapter 1. The major mechanisms in SAGD are thermal expansion and gravity drainage. There are steam-solvent variants of CSS and SAGD, for example, solvent-aided process (SAP, Gupta and Gittins, 1999), expanding-solvent SAGD (ES-SAGD, Nasr and Isaacs, 2001) and liquid addition to steam for enhanced recovery (LASER, Leaute and Carey, 2005). In these processes, a small fraction of solvent (typically 1 to 5% by volume butane or diluent) is added to the steam. The solvent reduces the viscosity of the oil below that which can be achieved by steam heating alone and thus the oil production rate is enhanced.

In the future, the development of recovery methods for oil sands will probably involve more advanced technology such as smart well technology aided by nanosensor and 4-D seismic imaging to capture the sweet spots and to monitor the conformance of steam chambers and more efficient solvent agent to optimize the oil production and solvent recovery (Gates and Wang, 2011).

2.2 Previous Studies on Instability at the Edge of Steam Chambers

As illustrated in Figure 1.7, the steam chamber releases the latent heat to the oil sands at the edge of the chamber to heat and mobilize the cool bitumen. The mobile oil flows to the production well under the action of gravity and the size of depletion chamber increases within the reservoir. From field data, Ito et al. (2005) observed that the steam chamber grows both upward and laterally at the same time. To prevent live steam production, a liquid pool sits above the production well. The height of the pool has to be maintained such that it does not permit coning of steam into the production well (Gates and Leskiw 2010). The results of Gates and Leskiw (2010) suggest that there is a critical phenomena that describes the onset of steam coning and the loss of steam trap control. Steam trap control can be difficult over the length of the wellbore (Ito and Suzuki 1999, Edmunds 1999).

Chung and Butler (1987) stated the thermal recovered heavy oil is always in the form of water/oil emulsion. They conducted two lab experiments to illustrate the geometrical effect of injected steam on the water/oil emulsion in SAGD. In the first experiment, the steam is injected

slightly above the producer whereas in the second experiment the steam injected is at the top of the formation. They found that much higher water/oil emulsion content exists when the steam is injected at the bottom. The higher emulsion ratio, the higher the viscosity, therefore the lower the heavy oil production. The experiments did not make clear how the interface instability affects production rate. One of the key limits on physical model experiments is that the length scale of the experiments is small (especially in the down well direction) and thus they may constrain the growth of instabilities in the oil sand. Sasaki et al. (2001) observed the water/oil emulsion at the edge of steam chamber in a two-dimensional lab experiment. They observed steam fingering in the vertical direction at the top of the steam chamber. The length scales that were calculated by Gotawala and Gates (2008) were consistent with those observed in Sasaki et al.'s experiments.

Maini and co-workers (2011) have conducted experiments on estimating the molecular diffusion and convective dispersion in porous media. Their results suggest that the diffusion coefficient is greatly enhanced by the interfacial boundary movement. This suggests that interfacial instability could potentially enhance mass transfer between a solvent-carrying vapour and oil phases.

Pritchard (2004) used a linear stability analysis to investigate the stability of viscous steam fingers in the porous media with the injected fluid containing different composition and temperature. He did the analysis for the extent of instability due to specific property of each fluid. His results suggest that the growth rate of interfacial instability will be changed greatly by the coupling effects between compositional and thermal properties.

It has been suggested that when steam is injected into the chamber, the interface between the steam and the oil is advancing in the form of ragged steam fingers and the boundary surface is quite wavy (Butler 1987, 1994; Ito et al. 2005; Gotawala and Gates 2008a-c). Butler (1987, 1994) and Ito et al. (2005) suggested the steam fingers, of the order of meters in length, exist at the edge of steam chamber. Gotawala and Gates (2008a) corrected Butler's theory and found that the extent of the steam fingers is of order of millimeters to tens of centimeters. This changes the vision of the edge of the steam chamber that had at first been reported by Butler and others. Instead of long extended steam fingers penetrating the oil sand, it exists as shallow steam undulations at the edge of the chamber. Gotawala and Gates' (2008a) steam finger analysis is based on a quasi-steady flow and does not describe the stability of the edge of the steam chamber.

Islam and Azaiez (2006) conducted numerical studies on the thermal-viscous fingering in the non-isothermal miscible displacements in the porous media. They found that at large Lewis number (ratio of thermal diffusivity to mass diffusivity), the instability of the thermal-viscous flow is controlled by the viscous contrast between the injected and original fluids. Hejazi and Azaiez (2012) examined the stability of the interface between the solutions of two reactants under gravity. Their results demonstrate that the transverse flow can destabilize an initially stable interface given the initial interface of reactants with same viscosity.

The classical mathematical model for SAGD, pioneered by Butler (1981) did not consider convection as a means for heat transfer, i.e. all heat transfer was obtained by conduction. Farouq-Ali (1997), Edmunds (1999), Ito and Suzuki (1996), Sharma and Gates (2011) and Irani

and Gates (2013a) considered the problem of heat transfer by thermal convection at and beyond the edge of SAGD steam chamber. Their results and analyses are inconsistent with some authors stating that convection beyond the edge of the steam chamber is important whereas others reporting that it is insignificant relative to conduction. Some of the differences in the results are explained by the differences of the reservoir and oil physical properties, steam chamber pressure, and initial reservoir pressure. If the chamber pressure is higher than the initial reservoir pressure, then steam condensate at the edge of the chamber flows into the oil sands enhancing heat transfer there.

Sharma and Gates (2011) examined interfacial instability of thermal-solvent recovery processes (ones where solvent is co-injected with steam into the formation) and showed that the system exhibits capillary instabilities. Their results confirms experimental results of Nasr and Isaacs (2001) that show that heptane appeared to provide the greatest enhancement of oil rate when added to steam.

Gotawala and Gates (2011) examined the stability of a vertical section of the steam chamber edge by using a one-dimensional Boussinesq model which considered perturbations of the oil, steam and water velocities, temperature and steam saturation (fraction of pore space occupied by water vapor). Their results demonstrated that Rayleigh-Taylor type of instability exists at the edge of the steam chamber when the steam quality was greater than a threshold value. They derived an analytical relationship between the scale of most unstable mode and steam quality at the chamber edge and the Darcy-Rayleigh number. Their results demonstrate that Rayleigh-Taylor instability can occur in vertical sections of the steam chamber.

Irani and Gates (2013b), by examining perturbations of the pressure in an analysis of the steam condensate pressure diffusion equation, showed that the instability is controlled by the speed of the translating chamber edge and the water hydraulic diffusivity. The water hydraulic diffusivity controls the diffusion of pressure beyond the edge of the steam chamber.

Although the results of experiments and instability analyses of the edges of the steam chamber are available, all use linear stability analysis which limits the results to the application of infinitesimal perturbations. Despite all of these analytical studies, no study has yet confirmed the onset of instability at the edge of a steam chamber.

2.3 SAGD Reservoir Simulation

Reservoir simulation is used to simultaneously solve sets of partial and algebraic differential equations representing the behavior of petroleum reservoir. The basic equations of reservoir simulation are a) conservation of mass, b) conservation of momentum, c) conservation of energy, d) Darcy's equation, e) equation of state, and f) auxiliary conditions such as the sum of saturations in each phase.

There are several types of reservoir simulators, described briefly as follows:

a) Gas simulator which deals with single phase component with no mobile water.

b) Black-oil simulator in which there exist three phases: water, oil and gas. The gas component can exist in gas phase and dissolved in oil phase and mass exchange can occur between these two phases depending on pressure.

c) Compositional reservoir simulators – there are two basic forms: the first solves the full equation of state for phase transition whereas the second one use K-value tables or correlations to determine phase equilibrium behavior.

The effort to evaluate the reservoir recovery processes by with the aid of computer started in the 1950s pioneered by Bruce et al. (1953). Reservoir simulation has become an indispensable tool and gained great success for reservoir economic evaluation, recovery technology development, and production strategy optimization. That being said, reservoir simulators have drawbacks mainly based in its continuum approach to treating porous media. First of all, petroleum reservoirs consist of multiple rock types with variable micro scale pores or fractures or vugs. The length scale of the reservoir to that of its pores is on the order of 10^{14}. The vast scale difference brings a dilemma between the macroscopic features of the reservoir such as oil rate, steam-to-oil ratio, steam conformance etc. which are actually the manifestation of microscopic physical and chemical mechanisms occurring at pore scales. How to model small scale features in a reservoir simulation? What grid sizes should we use to represent multiple scales of phenomena that interact across those length scales? Are these features physical or just numerical? They seem to be very fair questions faced by every reservoir engineer.

Moreover, every textbook on reservoir simulation talks about using Darcy's law to model flow in the porous media. The use of the Darcy's law is a double-bladed sword. Darcy's law is a

linearized steady-state Navier-Stokes equation with the viscous force replaced by a linear drag force. It captures the feature of the velocity of fluid flow in the porous media and greatly simplifies and enhances the stability of numerical calculations. However, since the nonlinearity in the N.S. equation is removed, reservoir simulators are incapable of providing multiple solutions at the same input parameter set as can be done when solving the full Navier-Stokes equations. Many bulk flows exhibit multiple states, especially ones with interfaces.

In the research documented in this thesis, we consider a fluid dynamical instability problem at the pore scale. Due to the incapability of reservoir simulators to model small scale features at that scale, a new software model for interfacial instability within a pore was constructed.

2.4 SAGD Field Operations

In most field operations, it usually takes between 2 and 5 cubic meters of steam (cold water equivalent, CWE) to produce 1 cubic meter of bitumen (Gates, 2013). The major concerns of SAGD operations are on the cost of steam generation (the cost of fuel), the amount of emitted greenhouse gas (GHG), and post-production water treatment and recycling.

Beyond surface facility concerns, the other major concern faced by SAGD operators is the productivity of the oil. This is measured by the steam-to-oil ratio (SOR). At present, the best SORs being achieved by industry are typically between 1.8 and 2.5 m^3/m^3 whereas the worst are greater than 10 m^3/m^3. From an in situ point of view, the SOR is raised in many operations due

to poor steam conformance along the SAGD well pair. The main reasons that interfere with efficient steam delivery to the oil sands formation are:

1. The heterogeneity of the reservoir inhibits the conformance of steam chamber growth. Complex geology such as the existence of shale barrier sometimes prohibits the vertical propagation of steam, drainage of mobilized oil, and the growth of the steam chamber (Bois et al. 2011, Hubbard et al. 2011, Su et al. 2013, Su et al. 2014).
2. Fluid compositional variations that cause lower viscosity portions of the reservoir to be produced earlier than higher viscosity parts (Larter et al. 2008; Gates et al. 2008).
3. Wellbore hydraulics due to non-horizontal wells. This can lead to loss of steam-trap control at one or more positions along the well pair.
4. The injection of steam is not controlled "smartly" such that the steam is continuously injected to the formation even though the chamber has reached the overburden and the heat is lost to the caprock. Moreover, once SAGD enters the gravity drainage period, a large fraction of the heat carried by the steam is to maintain the temperature of the depleted steam chamber.

In the following, two field operations are briefly described – Cenovus Christina Lake SAGD – an industry leading operation and the Nexen-CNOOC Long Lake SAGD operation.

2.4.1 Cenovus Christina Lake SAGD

A contour map of the net pay for the Christina Lake SAGD operation is displayed in Figure 2.2. The average net pay is equal to about 28 m with average porosity equal to about 34%. The average oil saturation in the project lease is equal to about 79%. The layout of the seven SAGD

pads is superimposed on the net pay map. The image reveals that the pads have been drilled in the parts of the reservoir with the greatest net pay.

The performance of the Christina Lake operation is displayed in Figure 2.3. The results show that the cumulative steam-to-oil ratio (cSOR) is industry leading value of about 2.2 m^3/m^3 with a steady decline indicating that the operation is thermally very efficient and among the best of SAGD practitioners worldwide. The rate profiles show that as the steam injection rate to the field increased as new well pairs were added, the oil rate increases too. The water return is positive with slightly more water being produced than is injected into the reservoir. Also shown is the gas injection rate which reveals that with a significant addition of natural gas to the well pairs, the oil rate increased at nearly constant steam injection rates. The average pressure of the injected steam (and natural gas) is less than 2,500 kPa. The data reveals that the cSOR is declining.

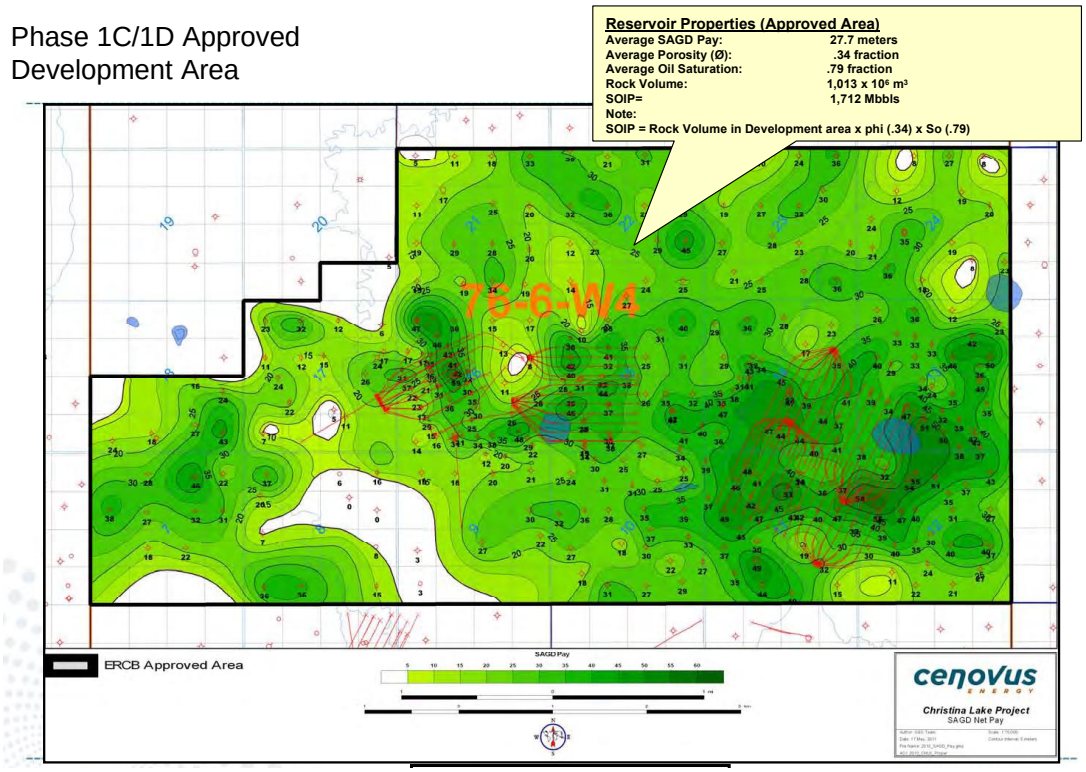

Figure 2-2: Contour map of the net pay for the Christina Lake SAGD operation with SAGD pads indicated (courtesy Cenovus).

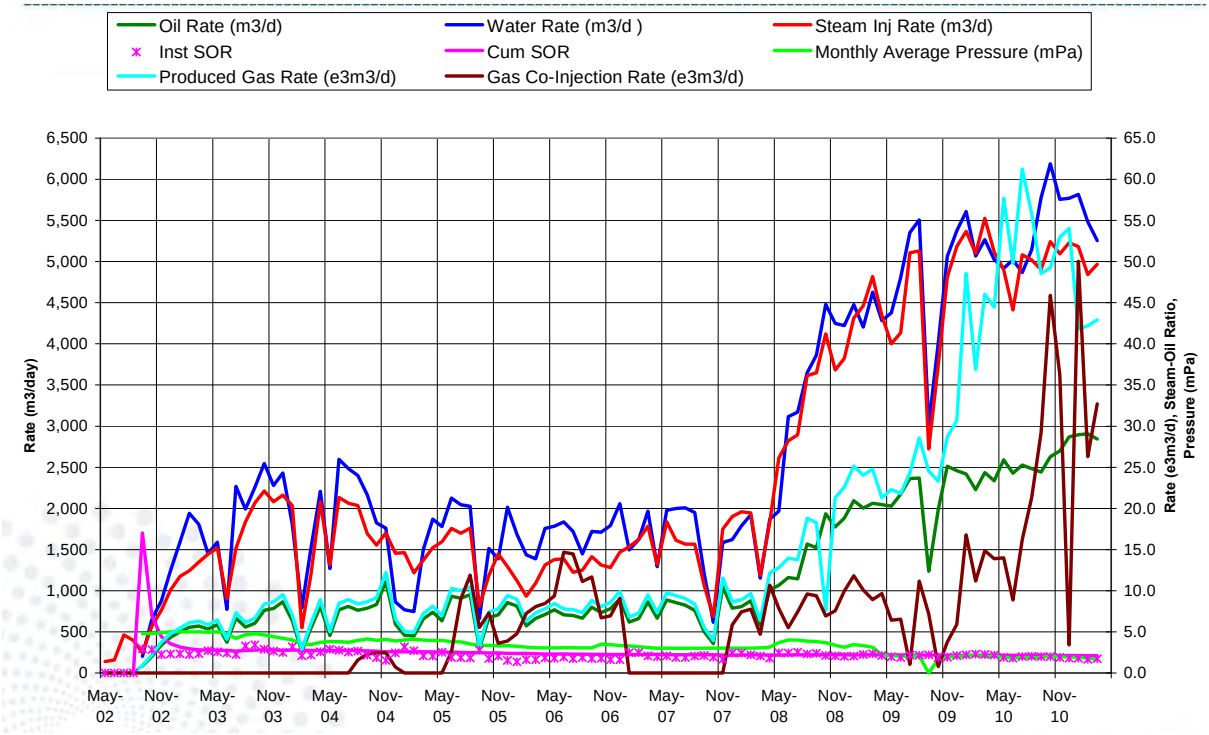

Figure 2-3: Christina Lake SAGD operation performance (courtesy Cenovus).

Figure 2.4 displays 4D seismic images of the Christina Lake SAGD operations. The results show that the steam chambers are not uniform. This could be attributed to either heterogeneities of the reservoir and/or instabilities occurring at the edge of steam chambers. As discussed above, the greater the growth rate of instability at the edge of steam chamber, the meandering and larger the contact surface between the steam/condensate and oil zones will be, and the more efficient the heat transfer. Therefore, when there are differences in geological properties and fluid properties at the edge of steam chamber, the growth rates and the subsequent heat transfer efficiencies at the vicinities will be different, which leads to the non-uniform growth of steam chamber.

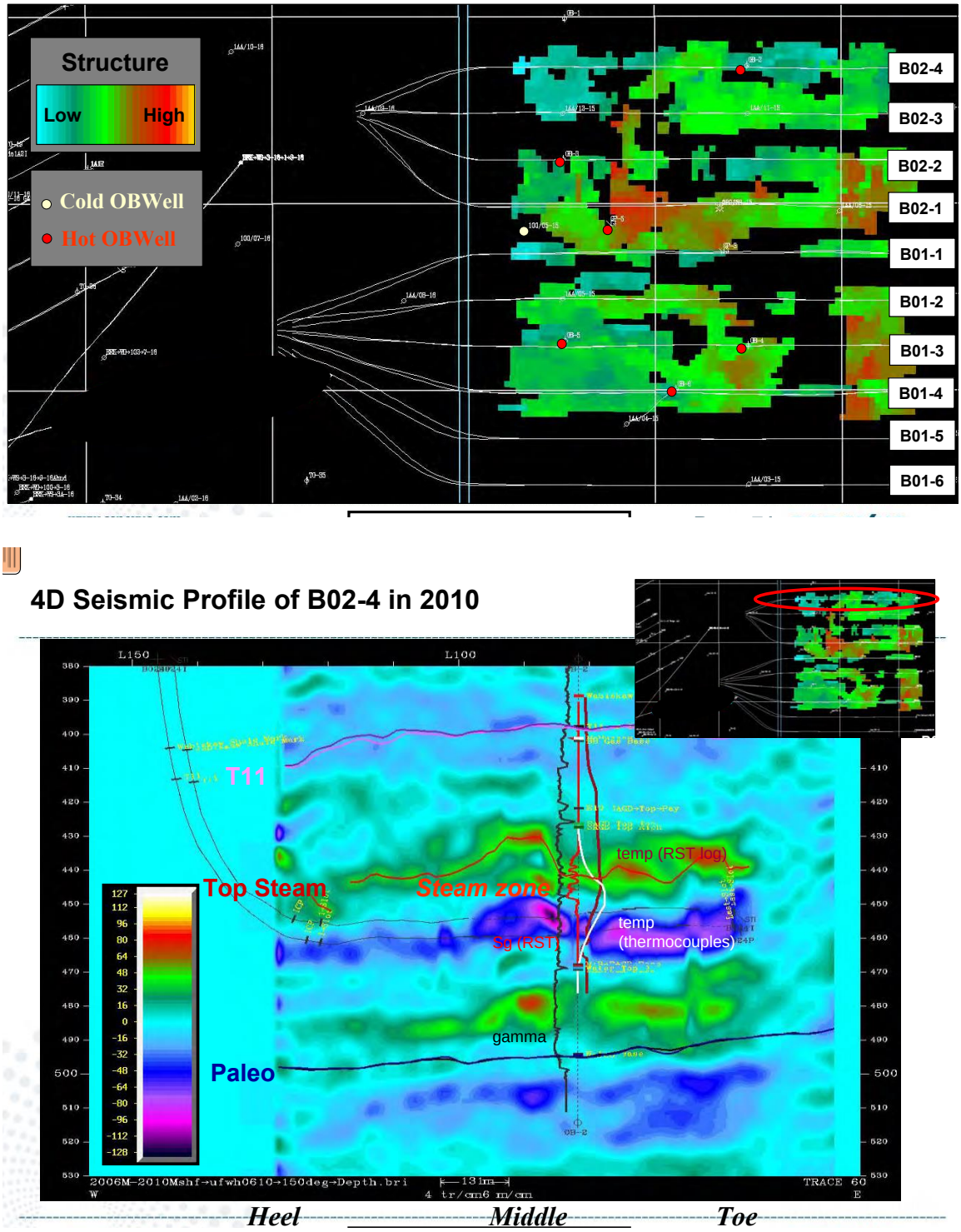

Figure 2-4: 4D Seismic interpretation for Christina Lake SAGD steam chamber conformance for the B Pad in 2010 (courtesy Cenovus).

2.4.2 Nexen-CNOOC Long Lake SAGD Operation

The layout of SAGD well pairs in the Long Lake SAGD operation and the net pay is shown in Figure 2.5. The wells have been drilled in the thickest parts of the reservoir. The performance of the Long Lake SAGD operation is shown in Figure 2.6. The results show that although oil rate increases in recent years, SOR is still really high (~4.5 m^3/m^3), which means the performance of the Long Lake project is not ideal.

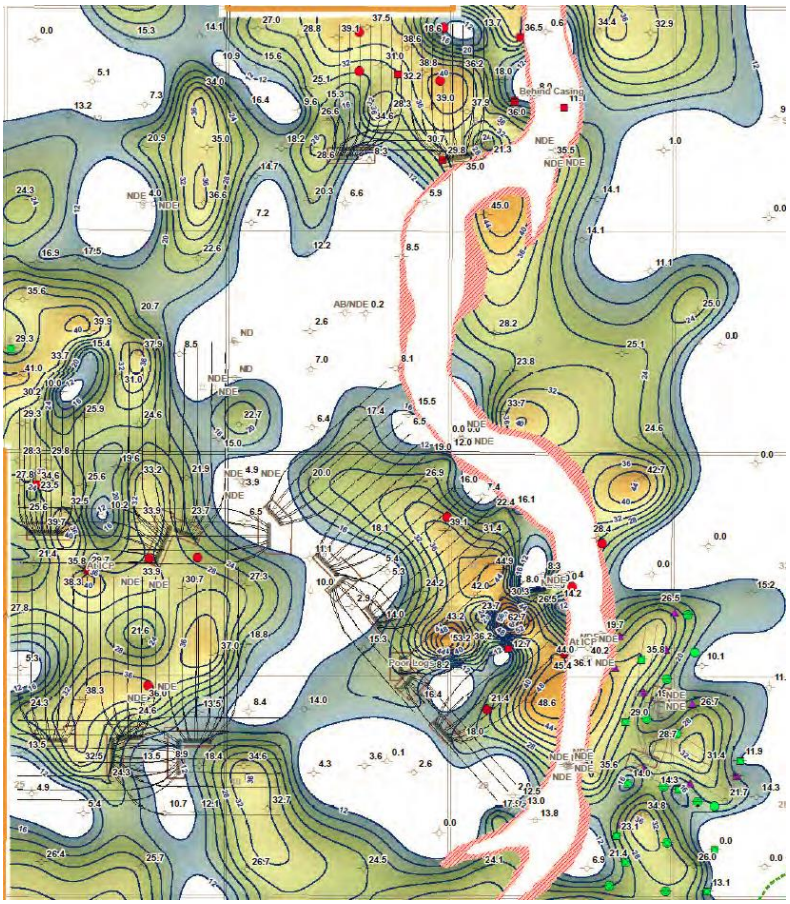

Figure 2-5: Contour map of the net pay for the Long Lake SAGD operation with SAGD pads indicated (courtesy Nexen-CNOOC).

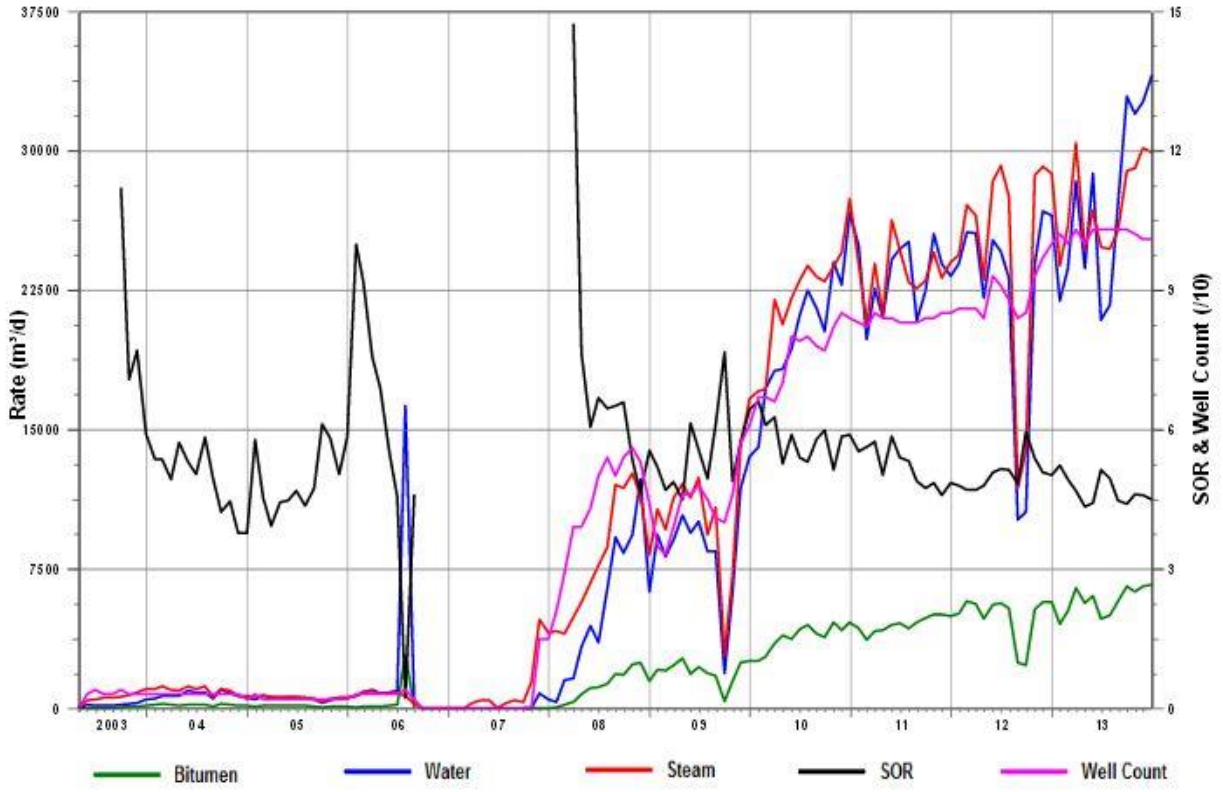

Figure 2-6: Long Lake SAGD operation performance (courtesy Nexen-CNOOC).

2.5 What is missing in the Literature?

From the literature review, we find that

1. the fluid shear instability happening at the interface between the fluid components at pore scale and its impacts on heat transfer is yet to be explored, and

2. thermal reservoir simulation has not yet demonstrated instability in an homogeneous reservoir.

As yet, it has not been established how steam conformance can be affected by the onset of fluid mechanical instabilities that occur in oil sands systems and that even in homogeneous reservoirs, poor steam conformance can result.

Chapter Three: **Parallel Flow in a Heated Pore – Stability Analysis**

3.1 Introduction

Figure 1.7 displays a typical steam chamber configuration that occurs in the SAGD recovery process. As described earlier, steam injected into the upper horizontal well, flows to the edge of the steam chamber where it releases its latent heat to the oil sands there. Bitumen within the oil sands is heated and as a consequence, its viscosity falls and due to the density difference between the steam and oil, it drains under the action of gravity to the base of the steam chamber. The production well removes the mobilized oil and steam condensate from the reservoir to the surface. In this manner, the steam chamber continuously expands as more and more bitumen is mobilized and drained from the reservoir.

SAGD is considered both energy and carbon intensive for the production of oil compared to conventional oil production processes (Gates and Larter 2013). The steam is generated by combustion of fuel, typically natural gas, which creates large CO2 emissions. Providing combustion is ideal, for each mole of methane consumed, a mole of carbon dioxide is emitted to the environment. This means that between 250 and 2,000 kg of carbon dioxide is emitted per tonne of bitumen produced depending on the steam-to-oil ratio (Gates and Larter 2013). There is motivation from all stakeholders including industry, regulators, and environmentalists to lower the amount of steam injected per unit volume oil recovered. The lower the steam-to-oil ratio (SOR), the smaller the greenhouse gas emissions per unit volume of produced oil, the smaller the water consumption and the lower the operation costs (of the fuel consumed for steam generation

and post-processing of water). Thus, there exists strong motivation to improve the heat efficiency at the edge of the steam chamber to ensure that steam is being used as effectively as possible.

Heat transfer at the edge of the steam chamber is controlled by latent heat release, conduction of heat into the oil sands beyond the edge of the chamber, and potential convection of heat by steam and/or hot water flow beyond the edge of the chamber. Conduction of heat at the chamber edge is controlled by the thermal conductivity of the oil sand and area of the steam-oil interface. Notice that when the steam-oil interface is wavy, the heat is still transferred by conduction but in this case, the heat transfer area is larger. This means the heat transfer rate is enhanced.

There have been many efforts to model the dynamics and instabilities that occur in the SAGD process (Farouq-Ali 1997, Edmunds 1999, Ito and Suzuki 1996, Gotawala and Gates 2011, Sharma and Gates 2011, and Irani and Gates 2013a and 2013b). But as mentioned in Chapter 2, all previous stability analyses were based on the assumption that the porous media can be represented by using a continuum approach. However, heating of oil sand at the edge of the steam chamber starts with pore scale phenomena. Furthermore, the onset of wavy interfaces could potentially lead to greater opportunities for formation of oil droplets within the pores which in turn may lead to emulsion formation at pore scale in the sand. There has not been a published study on the instability of steam-oil interfaces at the pore scale – this is the focus of the research documented here.

3.2 Model for Thermal Stability Analysis

Here, the stability of the draining mobilized oil-hot water interface at pore scale is analyzed by following Orr-Sommerfeld's (1907,1908) approach. The physical situation being analyzed is displayed in Figure 3.1. The system consists of a single planar pore which is inclined with an angle, θ, with respect to the vertical axis. Packed sand grains in the McMurray Formation are largely angular grains with patches of planar gaps between them – as a first approximation, we examine the case where the sand grain surfaces are perfectly parallel. As shown in the Figure, mobilized oil drains under gravity. To simplify the system, the steam condensate is neglected. The parallel pore has dimensionless width from y = -1 to y = +1 with no slip at the pore walls. The interface between the steam and draining liquid is located at y = 0.

On the oil-side of the interface, the capillary (ratio of viscous force to capillary force) and Bond numbers (ratio of gravity force to capillary) for a typical bitumen-steam condensate system are equal to $Ca = \mu_o U_{oil}/IFT = O(10^{-6})$ to $O(10^{-11})$ and $B_o = \rho g L^2/IFT = O(10^8)$ and $O(10^9)$, respectively (typical oil phase viscosity, μ_o, ranges from 10 to 1 million cP for steam and cold conditions, oil density varies from 950 to 1,000 kg/m^3 for steam and cold conditions, the speed of the draining oil, U_{oil}, is taken to be 5.0 and 10^{-8} cm/day for steam and cold conditions, IFT, is equal to 5 and 35 mN/m for steam and cold conditions, and length scale of the oil zone is of order of the thickness of the reservoir, L, is of order of 20 m). The ranges of the capillary and Bond numbers suggest that capillary forces can be important relative to viscous forces but both capillary and viscous forces are smaller than that of gravity forces.

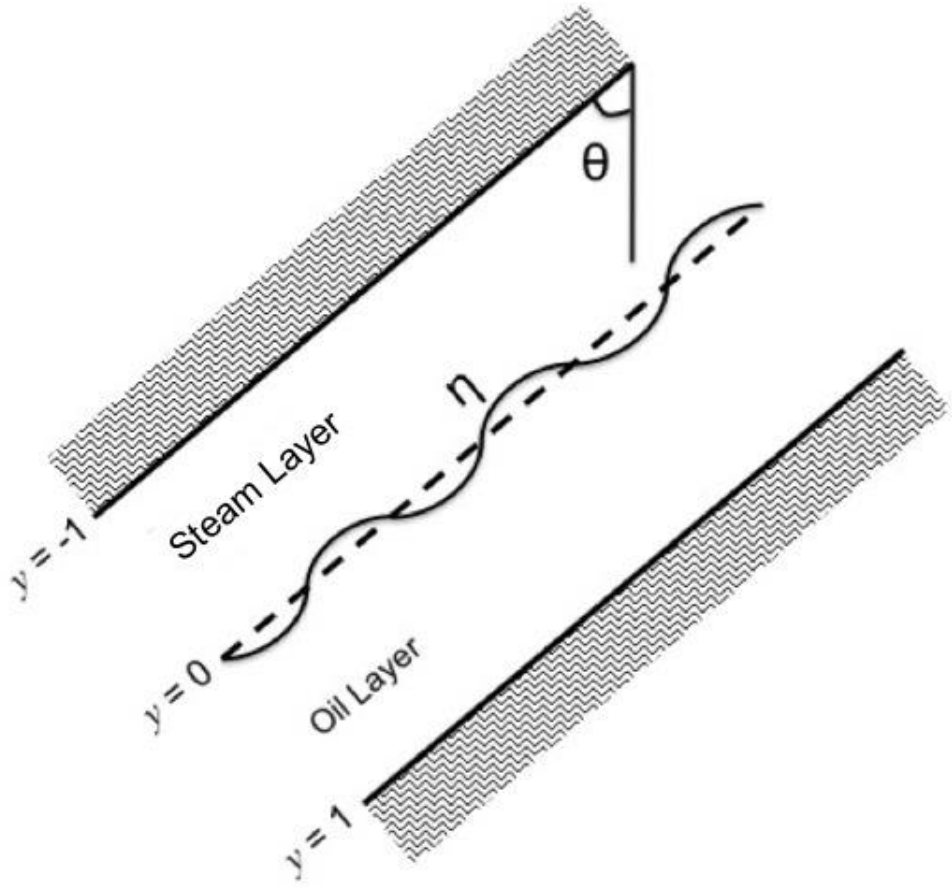

Figure 3-1: Interface between steam and oil within idealized planar pore at the edge of the steam chamber.

3.3 Theory

3.3.1 Orr-Sommerfeld Theory

In the cross-pore direction, y, the steady-state base flow is parallel and is denoted by U(y). The velocities u and v are perturbed values of the oil velocities in the streamwise and normal directions to the pore boundaries. In the steady base case, the flow is parallel and thus the flow

component in the normal direction to the pore walls is equal to zero. The Navier-Stokes equations, governing both oil and water flow in the plane of the pore, are given by:

$$\frac{\partial u_t}{\partial t} + u_t \frac{\partial u_t}{\partial x} + v_t \frac{\partial u_t}{\partial y} = -\frac{\partial p_t}{\partial x} + \frac{1}{Re} \nabla^2 u + \frac{\cos\theta}{F^2} \tag{3-1}$$

$$\frac{\partial v_t}{\partial t} + u_t \frac{\partial v_t}{\partial x} + v_t \frac{\partial v_t}{\partial y} = -\frac{\partial p_t}{\partial y} + \frac{1}{Re} \nabla^2 v + \frac{\sin\theta}{F^2} \tag{3-2}$$

$$\frac{\partial u_t}{\partial x} + \frac{\partial v_t}{\partial y} = 0 \tag{3-3}$$

Here, $u_t = U + u, v_t = v$ are the total velocities in the x and y directions and u and v are the x and y components of the perturbed velocities, respectively, and $p_t = P(x, y) + p'$ is the total pressure where P is the pressure of steady state base state and p is the perturbation pressure. $Re = \rho UL/\mu$ is the Reynolds number (measures the ratio of the inertial to viscous forces) and $F = \frac{U}{\sqrt{gL}}$ is the Froude number (measures the ratio of the inertial to gravity forces) where g is the acceleration due to gravity and L and U are the characteristic scales of length and velocity and ρ is the density of fluids and μ is the dynamic viscosity.

Since both U and P satisfy the base flow, the x and y components of the linearized momentum equations for the flow fluids are given by:

$$\frac{\partial u}{\partial t} + U\frac{\partial u}{\partial x} + U'v = -\frac{\partial p'}{\partial x} + \frac{1}{Re}\nabla^2 u \tag{3-4}$$

$$\frac{\partial v}{\partial t} + U\frac{\partial v}{\partial x} = -\frac{\partial p'}{\partial y} + \frac{1}{Re}\nabla^2 v \tag{3-5}$$

$$\frac{\partial u}{\partial x} + \frac{\partial v}{\partial y} = 0 \tag{3-6}$$

The vorticity in the direction normal to the x-y plane is defined as:

$$\zeta = \frac{\partial v}{\partial x} - \frac{\partial u}{\partial y} \tag{3-7}$$

The operation $\left[\frac{\partial}{\partial x}\left(\text{Equation 3-5}\right) - \frac{\partial}{\partial y}(\text{Equation 3-4})\right]$ leads to

$$\frac{\partial}{\partial t}\zeta + U\frac{\partial}{\partial x}\zeta - U''v = \frac{1}{Re}\nabla^2\zeta \tag{3-8}$$

The velocities u and v are related to the streamfunction $\tilde{\phi}(x, y, t) = \phi(y)e^{i\alpha(x-ct)}$ by:

$$u = -\frac{\partial \tilde{\phi}}{\partial y} = -\phi'(y)e^{i\alpha(x-ct)} \tag{3-9}$$

and

$$v = \frac{\partial \tilde{\phi}}{\partial x} = i\alpha\phi(y)e^{i\alpha(x-ct)} \tag{3-10}$$

where α is the wave number. After substituting Equations (3-9) and (3-10) into Equation (3-7), the result is:

$$\zeta = (-\alpha^2\phi + \phi'')\, e^{i\alpha(x-ct)} \tag{3-11}$$

In this travelling wave form, the growth rate of disturbance is $-i\alpha(ic_i) = \alpha c_i$, where c_i is the imaginary part of the phase speed, c. After substituting Equation (3-11) into Equation (3-8), the result is the Orr-Sommerfeld equation in streamfunction form:

$$[i\alpha(U-c)(\phi''-\alpha^2\phi) - U''(i\alpha)\phi] = \frac{1}{Re}(\phi'''' - 2\alpha^2\phi'' + \alpha^4\phi) \quad (3\text{-}12)$$

For a two-layer flow system, if ϕ and ψ are the streamfunctions of the top layer 1 and bottom layer 2, respectively, then their corresponding Orr-Sommerfeld equations are:

$$(\phi'''' - 2\alpha^2\phi'' + \alpha^4\phi) = i\alpha Re_1[(U_1-c)(\phi''-\alpha^2\phi) - U''\phi] \quad (3\text{-}13)$$

and

$$(\psi'''' - 2\alpha^2\psi'' + \alpha^4\psi) = i\alpha Re_1 \frac{\gamma}{m}[(U_2-c)(\phi''-\alpha^2\phi) - U''\phi] \quad (3\text{-}14)$$

where $\gamma = \frac{\rho_2}{\rho_1}$ and $m = \frac{\mu_2}{\mu_1}$. We assume at the interface between the two layers, the base velocities of layers 1 and 2, U_1 and U_2 respectively, satisfy velocity and shear stress continuity:

$$U_1 = U_2$$

and

$$\mu_1 \frac{\partial U_1}{\partial y} = \mu_2 \frac{\partial U_2}{\partial y}$$

3.3.2 Boundary Conditions

At the pore walls, due to the no-slip conditions at the pore walls, the velocity is equal to zero which yields:

$$\phi = \phi' = 0 \tag{3-15}$$

and

$$\psi = \psi' = 0 \tag{3-16}$$

at y = -1 and y = +1, respectively.

At the interface, $y = 0$, there are four boundary conditions:

1) The continuity of normal velocity $v_{t1=}v_{t2}$. From Equation (3-10), this implies

$$\phi = \psi \tag{3-17}$$

2) The continuity of horizontal velocity $u_{t1=}u_{t2}$. The kinematic condition at the steam-oil interface is expressed by $v_t = \frac{d\tilde{\eta}}{dt} = \frac{\partial\tilde{\eta}}{\partial t} + u_t\frac{\partial\tilde{\eta}}{\partial x}$, where η is the displacement of the interface from $y = 0$. In linearized form, it can be written as:

$$v = \frac{\partial\tilde{\eta}}{\partial t} + U\frac{\partial\tilde{\eta}}{\partial x} \tag{3-18}$$

If the perturbation at the interface is given by $\tilde{\eta} = \eta e^{i\alpha(x-ct)}$ and making use of Equation (3-10), we have $i\alpha\phi = -i\alpha c\eta + U_0 i\alpha\eta$ which yields:

$$\eta = \frac{\phi}{-c+U_0} \tag{3-19}$$

The horizontal velocity is continuous, the linearized approximation of velocity leads to:

$$U_0 + U_1' \frac{\partial \eta}{\partial y} + u_1 = U_0 + U_2' \frac{\partial \eta}{\partial y} + u_2$$

where $U_0 = U_1(0) = U_2(0)$. Making use of Equation (3-9), the result is:

$$\phi' - \psi' = (U_2' - U_1') \frac{\phi}{c-U_0} \tag{3-20}$$

3) Tangential stress continuity such that at $y = 0$, we have

$$\mu_1 \left(\frac{\partial v_1}{\partial x} + \frac{\partial u_1}{\partial y} \right) = \mu_2 \left(\frac{\partial v_2}{\partial x} + \frac{\partial u_2}{\partial y} \right)$$

Making use of Equations (3-9) and (3-10), we have

$$-(\alpha^2\phi + \phi'') + DU_1 + D^2U_1\eta = m\{-(\alpha^2\psi + \psi'') + DU_2 + D^2U_2\eta\}$$

Since $DU_1 = mDU_2$, we obtain:

$$\alpha^2\phi + \phi'' = m(\alpha^2\psi + \psi'') \tag{3-21}$$

4) Normal stress continuity at the interface. The normal stress of two layers satisfy:

$$\gamma\left(-p_{2t} + \frac{2}{Re_2}\frac{\partial v_2}{\partial y}\right) - \left(-p_{1t} + \frac{2}{Re_1}\frac{\partial v_1}{\partial y}\right) - S\frac{\partial^2\eta}{\partial x^2} = 0 \tag{3-22}$$

Here $S = \frac{1}{We}$, where $We = \frac{\rho U^2 L}{\sigma}$ is the Weber number which measures the ratio of inertial to interfacial forces.

Let the perturbation pressure be equal to $p' = pe^{i\alpha(x-ct)}$. Substituting it into Equation (3-4), we get:

$$(-i\alpha c)(-\phi') + U(i\alpha)(-\phi') + U'(i\alpha)\phi = -(i\alpha)p + \frac{1}{Re_1}(\alpha^2\phi' - \phi''')$$

which implies that

$$p = \frac{1}{i\alpha Re_1}(\alpha^2\phi' - \phi''') - c\phi' + U\phi' - U'\phi \tag{3-23}$$

After linearizing Equation (3-22), we get

$$\gamma\left(-p_2 - P_0 - \frac{\partial P_2}{\partial y}\eta + \frac{2}{Re_2}\frac{\partial v_2}{\partial y}\right) - \left(-p_1 - P_0 - \frac{\partial P_1}{\partial y}\eta + \frac{2}{Re_1}\frac{\partial v_1}{\partial y}\right) - S\frac{\partial^2\tilde{\eta}}{\partial x^2} = 0$$

or, after rearrangement:

$$(p_1 - \gamma p_2) + \left(\frac{2\gamma}{Re_2}\frac{\partial v_2}{\partial y} - \frac{2}{Re_1}\frac{\partial v_1}{\partial y}\right) + \left(-\gamma\frac{\partial P_2}{\partial y}\tilde{\eta} + \frac{\partial P_1}{\partial y}\tilde{\eta} - S\frac{\partial^2\tilde{\eta}}{\partial x^2}\right) = 0$$

Substituting the travelling wave form of Equation (3-23) yields

$$\frac{1}{i\alpha Re_1}(\alpha^2\phi' - \phi''') - c\phi' + U\phi' - U'\phi - \frac{\gamma}{i\alpha Re_2}(\alpha^2\psi' - \psi''') + \gamma(c\psi' - U\psi' + U'\psi)$$
$$+ \frac{2\gamma}{Re_2}(i\alpha\psi') - \frac{2}{Re_1}(i\alpha\phi') + \left(-\gamma\frac{\sin\theta}{F^2} + \frac{\sin\theta}{F^2} + S\alpha^2\right)\eta = 0$$

Since $\eta = \frac{\phi}{-c+U_0}$, we have:

$$(\alpha^2\phi' - \phi''') + [(U-c)\phi' - U'\phi](i\alpha)Re_1 - m(\alpha^2\psi' - \psi''') + \gamma[(c-U)\psi' + U'\psi](i\alpha)Re_1$$
$$+ i\alpha Re_1\left[(1-\gamma)\frac{\sin\theta}{F^2} + S\alpha^2\right]\frac{\phi}{-c+U_0} - 2\alpha^2 m\psi' + 2\alpha^2\phi' = 0$$

After rearranging the terms, we get:

$$-i\alpha Re_1[(c-U)\phi' + U'\phi] - \phi''' + 3\alpha^2\phi' + i\alpha Re_1\gamma[(c-U)\psi' + U'\psi] + m(\psi''' - 3\alpha^2\psi')$$
$$= i\alpha Re_1\left[(1-\gamma)\frac{\sin\theta}{F^2} + S\alpha^2\right]\frac{\phi}{c-U_0} \qquad (3\text{-}24)$$

3.3.3 Heat Transfer Equation

Since the steam is at saturation conditions, the perturbations of temperature in the steam layer are taken to be equal to zero. Heat transfer occurs from the hot steam-oil interface to the oil side in the oil layer from $y = 0$ to $y = 1$. If the temperature of the oil layer, T_t, is decomposed into the steady mean part $T(y)$ and a perturbation $T'(x, y, t)$, such that $T_t = T(y) + T'(x, y, t)$, the linearized non-dimensional convection-conduction equation becomes:

$$\frac{\partial T'}{\partial t} + U_2\frac{\partial T'}{\partial x} + v\,\overline{T}' = \frac{1}{Pe}\nabla^2 T' \qquad (3\text{-}25)$$

subject to the boundary conditions $T'(y = 0) = T'(y = 1) = 0$ (the perturbations of the temperature are taken to be equal to zero at the interface and pore wall). Here, the Peclet number is defined by $Pe = LU/\alpha_{TH}$, where α_{TH} is the thermal diffusivity which provides a measure of the relative roles of convective to conductive heat transfer modes and $\overline{T}'$ represents $\frac{dT}{dy}$. By assuming $T' = \widetilde{T}(y)e^{i\alpha(x-ct)}$, such that the temperature perturbation amplitude $\widetilde{T}(y) \in \mathbb{C}$, the result is:

$$-i\alpha c\widetilde{T} + U_2(i\alpha)\widetilde{T} + v_2\overline{T}' = \frac{1}{Pe}\left(-\alpha^2 + \frac{\partial^2}{\partial y^2}\right)\widetilde{T} \qquad (3\text{-}26)$$

which can be simplified to:

$$i\alpha\psi\overline{T}' + \left[i\alpha U_2 - \frac{1}{Pe}\left(-\alpha^2 + \frac{\partial^2}{\partial y^2}\right)\right]\widetilde{T} = i\alpha c\widetilde{T} \tag{3-27}$$

3.3.4 Coordinate Transformation

Equations (3-13) and (3-14) subject to boundary conditions (3-17), (3-20), (3-22), and (3-24) and Equation (3-27) subject to zero perturbations of the temperature represent two fourth order eigenvalue and a single first order eigenvalue problems all in the complex plane. The Orr-Sommerfeld equations are actually fourth order ordinary differential equations in the complex domain. To solve the coupled set of eigenvalue problems, we use a Galerkin approach where the unknown perturbation amplitudes are represented by a set of basis function. Here, a spectral Chebyshev collocation approach is used (Dongarra et al. 1996).

To solve the problem with the Chebyshev collocation spectral method, first, the Orr-Sommerfeld equations are transformed from $[-1,0]$ and $[0,1]$ to $[-1,1]$ by the following linear transformation

$$\begin{cases} z = -2y - 1, & \text{for } -1 \le y \le 0 \\ z = 2y - 1, & \text{for } 0 \le y \le 1 \end{cases}$$

We will implement the D^2 Chebyshev tau method introduced by Dongarra et al. (1996). First, we define the differential operators L_1 and L_2 and two dummy variables, ξ and ω:

$$L_1\phi \equiv \left(4\frac{d^2}{dz_1^2} - \alpha^2\right)\phi$$

$$L_1\phi = \xi$$

$$L_2\psi \equiv \left(4\frac{d^2}{dz_2^2} - \alpha^2\right)\psi$$

$$L_2\psi = \omega$$

where z_1 and z_2 are coordinates in layers 1 and 2, respectively. Therefore, the two-layer Orr-Sommerfeld system can be written as:

$$L_1\phi - \xi = 0$$

$$L_1\xi - i\alpha Re U_1\xi + i\alpha U_1''\phi = -ci\alpha Re_1\xi$$

$$L_2\psi - \omega = 0$$

$$L_2\omega - i\alpha Re\frac{\gamma}{m}U_2\omega + i\alpha Re\frac{\gamma}{m}U_2''\psi = -ci\alpha Re\frac{\gamma}{m}\omega$$

The rigid boundary conditions at $y = +1$ become (Boundary Conditions 1 to 4):

$$\phi(1) = \frac{d}{dz_1}\phi(1) = 0$$

$$\psi(1) = \frac{d}{dz_2}\psi(1) = 0$$

The interface is now at $y = -1$ and the interface conditions yield:

$$\phi - \psi = 0$$

$$\xi + 2\alpha^2\phi - m\omega - 2\alpha^2 m\psi = 0$$

$$\frac{d\xi}{dz_1} - 2\alpha^2\frac{d}{dz_1}\phi + m\frac{d\omega}{dz_2} - 2m\alpha^2\frac{d}{dz_2}\psi = 0$$

$$U\left(\frac{d}{dz_1}\phi + \gamma\frac{d}{dz_2}\psi\right) + \frac{1}{2}\left(U_1'(0) - \gamma U_2'(0)\right)\phi$$

$$-\frac{1}{U_2'(0) - U_1'(0)}\left((1-\gamma)\frac{\sin\theta}{F^2} + \alpha^2 S\right)\left(\frac{d}{dz_1}\phi + \frac{d}{dz_2}\psi\right) = c\left(\frac{d}{dz_1}\phi + \gamma\frac{d}{dz_2}\psi\right)$$

After transforming the heat transfer equation into the new coordinate $z = [-1,1]$, Equation (3-27) yields:

$$-iPe\ \alpha\bar{T}'\psi - (-\alpha^2 + 4D^2)\tilde{T} + iPe\ \alpha U_2\tilde{T} = iPe\ \alpha c\tilde{T}$$

subject to boundary conditions $\tilde{T}(y = 0) = \tilde{T}(y = 1) = 0$.

3.4 Numerical Method

The magnitudes of streamfunctions, ϕ and ψ and that of temperature $\tilde{T}$ as well as two dummy variables ξ and ω are approximated by the truncated series of the Chebyshev polynomials $T_n(z)$ of the first kind, such that:

$$\phi(z) = \sum_{n=0}^{N+2} \phi_n T_n(z), \xi = \sum_{n=0}^{N+2} \xi_n T_n(z)$$

$$\psi(z) = \sum_{n=0}^{N+2} \psi_n T_n(z), \quad \omega = \sum_{n=0}^{N+2} \omega_n T_n(z)$$

$$\tilde{T}(z) = \sum_{n=0}^{N+2} \tilde{T}_n T_n(z)$$

where the series are truncated at N+2. We need $5(N+3)$ equations to determine the eigenfunctions, i.e. the coefficients, $\phi_n, \xi_n, \psi_n, \omega_n$ and $\tilde{T}_n$ $(n = 0 \ldots N+2)$ and the eigenvalue, c. We collocate the truncation at the Chebyshev nodes in the interval $z = [-1,1]$:

$$x_k = \cos\left(\frac{j\pi}{M}\right), j = 1 \ldots . M-1,$$

which are the roots of $T_k(z)$. Here we follow Dongarra et al. (1996) and Wang (2011) to construct the Chebyshev tau matrices. The system of equations constitutes a generalized eigenvalue problem which can be represented by:

$$(A_R + iA_I)x = c(B_R + iB_I)x \tag{3.28}$$

where $x = \left(\phi_0, \phi_1, \ldots \phi_{N+2}, \xi_1, \xi_2, \ldots \xi_{N+2}, \psi_0, \psi_1, \ldots \phi_{N+2}, \omega_0, \omega_1, \ldots \omega_{N+2}, \tilde{T}_0, \tilde{T}_1 \ldots \tilde{T}_N\right)^T$. Here, the right side real and imaginary component matrices, in block form, are given respectively by:

$$A_R = \begin{pmatrix} 4D^2 - \alpha^2 I & -I & 0 & 0 & 0 \\ 0 & 4D^2 - \alpha^2 I & 0 & 0 & 0 \\ 0 & 0 & 4D^2 - \alpha^2 I & 0 & 0 \\ 0 & 0 & 0 & 4D^2 - \alpha^2 I & 0 \\ 0 & 0 & 0 & 0 & -(4D^2 - \alpha^2) \\ & & \text{Boundary Conditions} & & \end{pmatrix}$$

and

$$A_I = \begin{pmatrix} 0 & 0 & 0 & 0 & 0 \\ \alpha U_1'' & -\alpha Re U_1 & 0 & 0 & 0 \\ 0 & 0 & 0 & 0 & 0 \\ 0 & 0 & \alpha Re \frac{\gamma}{m} U_2'' & -\alpha Re \frac{\gamma}{m} U_2 & 0 \\ 0 & 0 & -\alpha Pe \widetilde{T}' & 0 & \alpha Pe U_2 \\ & & \text{Boundary Conditions} & & \end{pmatrix}$$

The left side real and imaginary components of the generalized matrix eigenvalue problem, in block form, are respectively given by:

$$B_R = \begin{pmatrix} 0 & 0 & 0 & 0 & 0 \\ 0 & 0 & 0 & 0 & 0 \\ 0 & 0 & 0 & 0 & 0 \\ 0 & 0 & 0 & 0 & 0 \\ 0 & 0 & 0 & 0 & 0 \\ & & \text{Boundary Conditions} & & \end{pmatrix}$$

and

$$B_I = \begin{pmatrix} 0 & 0 & 0 & 0 & 0 \\ 0 & -\alpha ReI & 0 & 0 & 0 \\ 0 & 0 & 0 & 0 & 0 \\ 0 & 0 & 0 & -\frac{\alpha Re}{m} I & 0 \\ 0 & 0 & 0 & 0 & \alpha PeI \\ 0 & 0 & 0 & 0 & 0 \end{pmatrix}$$

Note that each block in the four coefficient matrices $A_R, A_I, B_R \text{and } B_I$ have dimensions $(N + 1) \times (N + 3)$, which are evaluated at the inner Chebyshev collocation points. Therefore, before implementing the boundary conditions, the coefficient matrices are $5(N + 1) \times 5(N + 3)$. By adding the ten boundary conditions (four for each of the Orr-Sommerfeld equations and two for the heat transfer equation) to them, we actually add 10 more rows to the original matrix, which yields square matrices. Note that there are zero rows in the B matrices are equal to zero – this implies that the system is a singular generalized eigenvalue problem.

Here, we will implement the MATLAB™ differential matrices suite developed by Weideman and Reddy (2001) for Chebyshev tau matrix methods and the QZ-algorithm proposed by Dongarra et al. (1996) to solve the complex generalized eigenvalue problem described by Equation (3.28). The listing of the MATLAB™ code generated is listed in Appendix A.

3.4.1 Model Validation

The two-layer case has been studied by Dongarra et al. (1996) in the absence of heat transfer. The base flow profile is given by:

$$u_1(y) = A_1 y^2 + a_1 y + 1, \quad 0 < y < n$$

$$u_2(y) = A_2 y^2 + a_2 y + 1, \quad -1 < y < 0$$

where

$$A_2 = \frac{-(m+n) + m u_n}{n(n+1)}$$

$$A_1 = \frac{A_2}{m}$$

$$a_2 = \frac{n^2 - m + m u_n}{n(n+1)}$$

$$a_1 = \frac{a_2}{m}$$

and

$$m = \mu_1/\mu_2$$

$$n = d_2/d_1$$

where u_n is the velocity of the wall at position n and d_* is the thickness of layer * (this follows Dongarra et al.'s somewhat confusing symbol convention). A comparison of the real and imaginary parts of the growth rates obtained by Dongarra et al. and the new MATLAB™ code generated in this study is presented in Figure 3.2. The results reveal that the new stability code generates the same results as that of the previous work especially for the most dangerous modes (the largest real parts).

(a) Re = 125, α = 1, m = 2, n = 10, $u_n = 3$

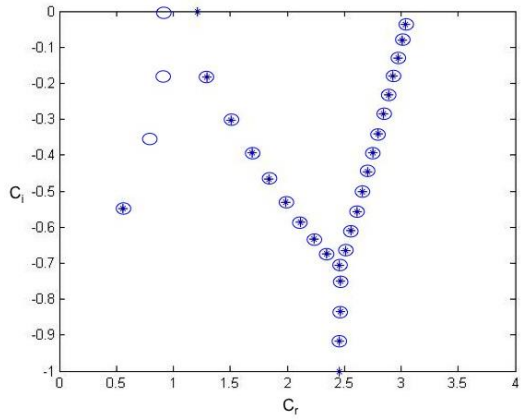

(b) Re = 200, α = 2, m = 2, n = 10, $u_n = 0$

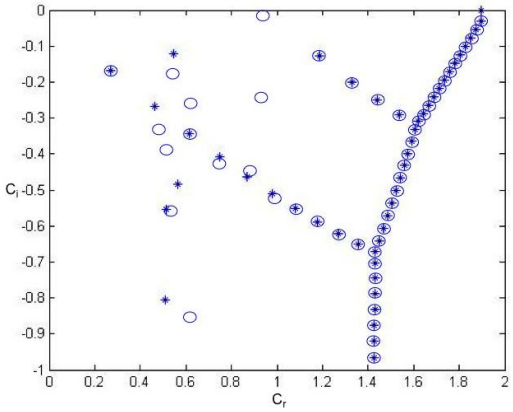

(c) Re = 10000, α = 1, m = 2, n = 2, $u_n = 0$

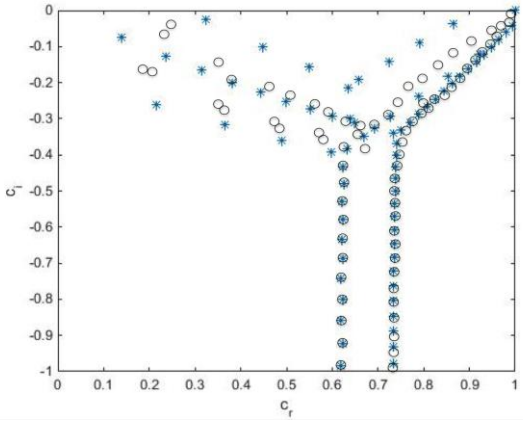

Figure 3-2: Comparison of results of new code versus that of Dongarra et al (1996) Asterisks represent the results from the new code whereas the circles represent Dongarra et al.'s data.

Figure 3.3 displays a test of the new stability code with Pe = 0 (the case where thermal diffusion dominates and the temperature perturbations vanish to zero) versus Dongarra's results by using a viscosity ratio equal to 440, Reynolds' number equal to 1, inclination equal to 90° (vertical), S = 1, and F = 0.1. The comparison shows that the results are the same.

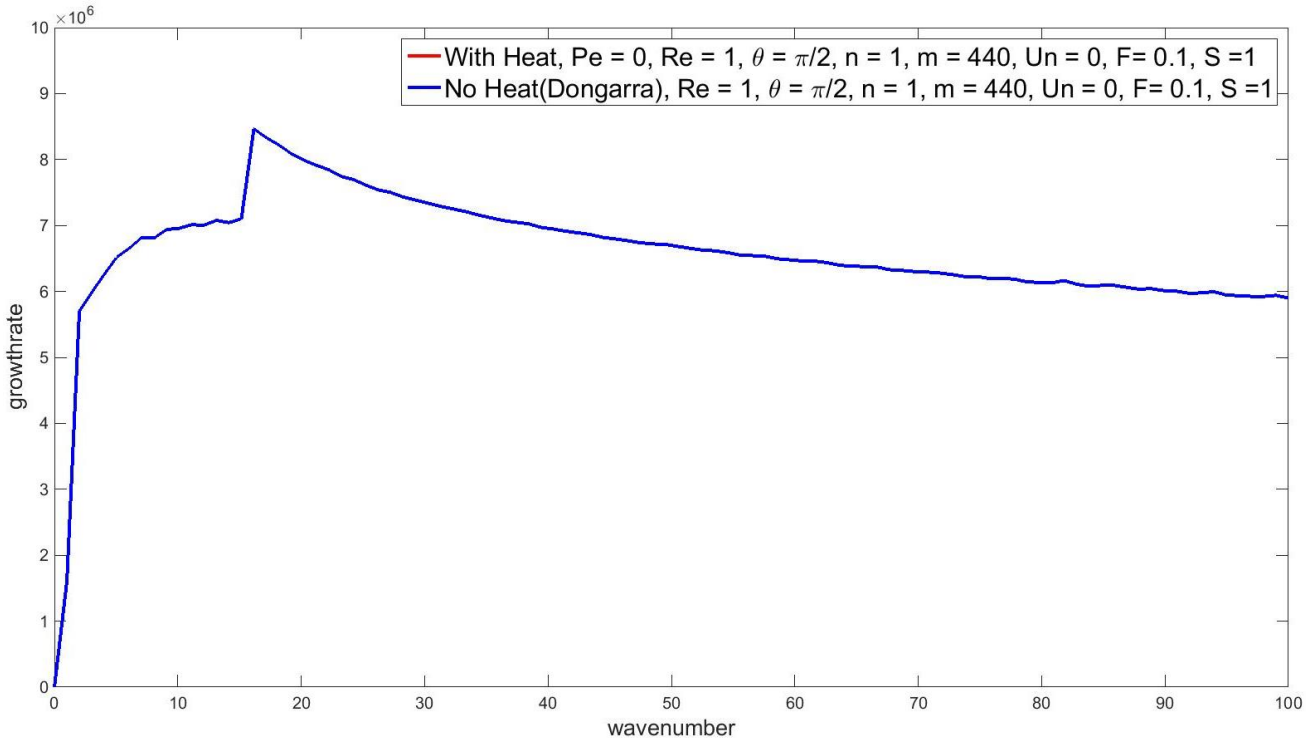

Figure 3-3: Comparison of results of new code with Pe=0 versus that of Dongarra et al (1996).

3.4.2 Base Flow and Temperature Profiles

Now, the code is used to analyze the stability of the interface in the case where heat transfer occurs at pore scale. Firstly, we will construct the base flow profiles U_1 (steam layer) and U_2 (oil layer) in the sub-pores at the edge of steam chamber. Let

$$U_1(y) = a_1 y^2 + a_2 y + a_3$$

and

$$U_2(y) = b_1 y^2 + b_2 y + b_3.$$

Since at $y = -1$, $U_1 = 0$, we know that

$$a_1 + a_2 + a_3 = 0$$

Since at $y = 1$, $U_2 = 0$, we know that

$$b_1 + b_2 + b_3 = 0.$$

At the interface $y = 0$, $U_1 = U_2$, we have

$$a_3 = b_3$$

Also, the shear stress at $y = 0$ should equal to each other, which implies

$$-\mu_1 \frac{\partial U_1}{\partial y} = -\mu_2 \frac{\partial U_2}{\partial y}$$

and since

$$\frac{\partial U_1}{\partial y} = 2a_1 y + a_2, \qquad \frac{\partial U_2}{\partial y} = 2b_1 y + b_2$$

we get

$$-\mu_1 a_2 = -\mu_2 b_2$$

and

$$a_2 = m\, b_2,$$

$$where\ m = \frac{\mu_2}{\mu_1}$$

Let us further assume the steam and oil rate in the pore Q_s and Q_o is defined as

$$Q_s = \int_{y=-1}^{y=0} (a_1 y^2 + a_2 y + a_3) dy$$

$$Q_o = \int_{y=0}^{y=1} (b_1 y^2 + b_2 y + b_3) dy$$

$$6Q_s = 2a_1 - 3a_2 + 6a_3$$

$$6Q_o = 2b_1 + 3b_2 + 6b_3$$

We have now

$$a_1 - mb_2 + b_3 = 0$$

$$b_1 + b_2 + b_3 = 0$$

$$2a_1 - 3mb_2 + 6b_3 = 6Q_s$$

$$2b_1 + 3b_2 + 6b_3 = 6Q_o$$

Therefore,

$$2a_1 - 2b_1 - 2(m+1)b_2 = 0$$

and

$$2a_1 - 2b_1 - 3(m+1)b_2 = 6(Q_s - Q_o)$$

$$(m+1)b_2 = 6(Q_o - Q_s)$$

Therefore,

$$b_2 = \frac{6(Q_o - Q_s)}{m+1}$$

and

$$a_2 = \frac{6m(Q_o - Q_s)}{m+1}$$

Since $b_2 + 4b_3 = 6Q_o$, and $a_3 = b_3$we get

$$a_3 = b_3 = \frac{6Q_o - b_2}{4} = \frac{3(mQ_o + Q_s)}{2}$$

Also,

$$a_1 = -a_2 - a_3 = -\frac{6m(Q_o - Q_s)}{m+1} - \frac{3(mQ_o + Q_s)}{2}$$

and

$$b_1 = -b_2 - b_3 = \frac{6(Q_o - Q_s)}{m+1} - \frac{3(mQ_o + Q_s)}{2}$$

Here the external parameters are $Q_s \; and \; Q_o$ and they are related by

$$Q_s = Q_o \, SOR$$

If we specify $SOR \equiv 3.5$ m^3/m^3, Q_o, which is the dimensionless oil rate will be the only parameter we should consider. Let $Q_{oM} = \frac{\rho_o g \, \delta^3 cos\theta}{3\mu_o}$ be the maximum oil rate (determined for a layer of oil flowing under gravity down an inclined plate), Q_o is defined as:

$$Q_o = \frac{physical \; rate}{Q_{oM}}$$

Secondly, we construct the base temperature profile $\bar{T}(y)$. Based on a temperature gradient ahead of a moving steam chamber under conduction, the dimensional temperature distribution is approximately given by $\bar{T}(y) = T_{stm} - 0.5y$ for a pore of dimensions equal to about 30 microns.

3.5 Results and Discussion

Figure 3.4 displays the results for an inclined pore at 45°, n = 1 (thickness of oil and steam layers are equal), viscosity ratio between oil and steam equal to 440, SOR = 3.5 m^3/m^3, and oil rate at 90% of the maximum oil drainage rate possible. The results show that when the ratio of interfacial forces relative to inertial forces, S, is small, then the flow exhibits a peak growth rate at a very small wavenumber. At large S, the peak is smaller but the wavenumber of the most dangerous mode is also small. At values of S expected at the edge of a SAGD steam chamber, S = 1,000,000, the growth rates are larger and the growth rate curve exhibits multiple modes – one with a peak equal to about wavenumber 5 and other at wavenumber 18. The results of the analysis reveal that at all values, the flow is unstable (has a positive growth rate).

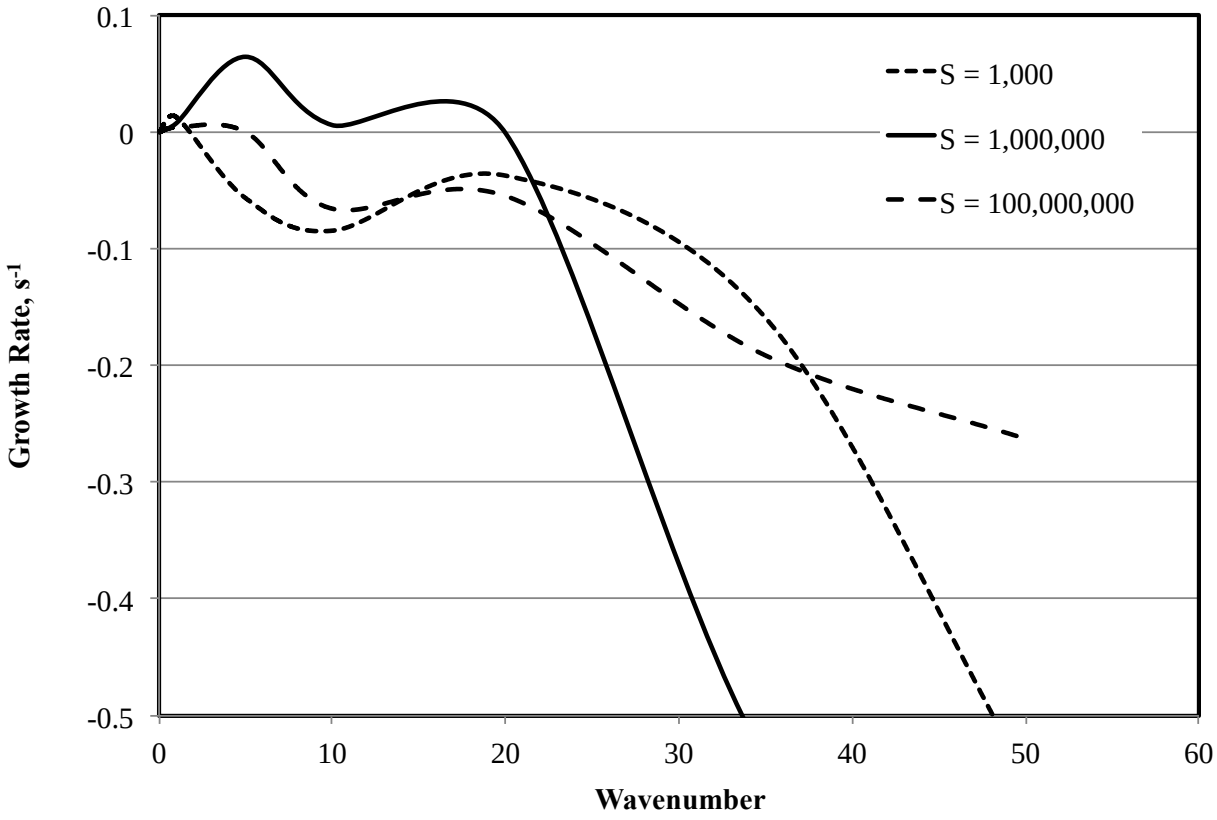

Figure 3-4: Impact of ratio of interfacial forces relative to inertial forces on growth rates (inclination = 45°, Re = 1, Pe = 10, thickness of oil and steam layers equal, viscosity ratio between oil and steam equal to 440, SOR = 3.5, and oil rate 90% of maximum value).

Figure 3.5 displays the impact of the Reynolds' number (ratio of inertial to viscous forces) on the growth rates for the case with for an inclined pore at 45°, n = 1 (thickness of oil and steam layers are equal), viscosity ratio between oil and steam equal to 440, SOR = 3.5 m^3/m^3, and oil rate at 90% of the maximum oil drainage rate possible. The results show that the greater the inertial forces, the higher is the peak growth rate. At the Reynolds' number expected at the edge of the chamber (Re = 1), the flow exhibits two dominant modes of instability with two peaks. As the Reynolds' number rises to 5, the peaks coalesce into a single dominant mode.

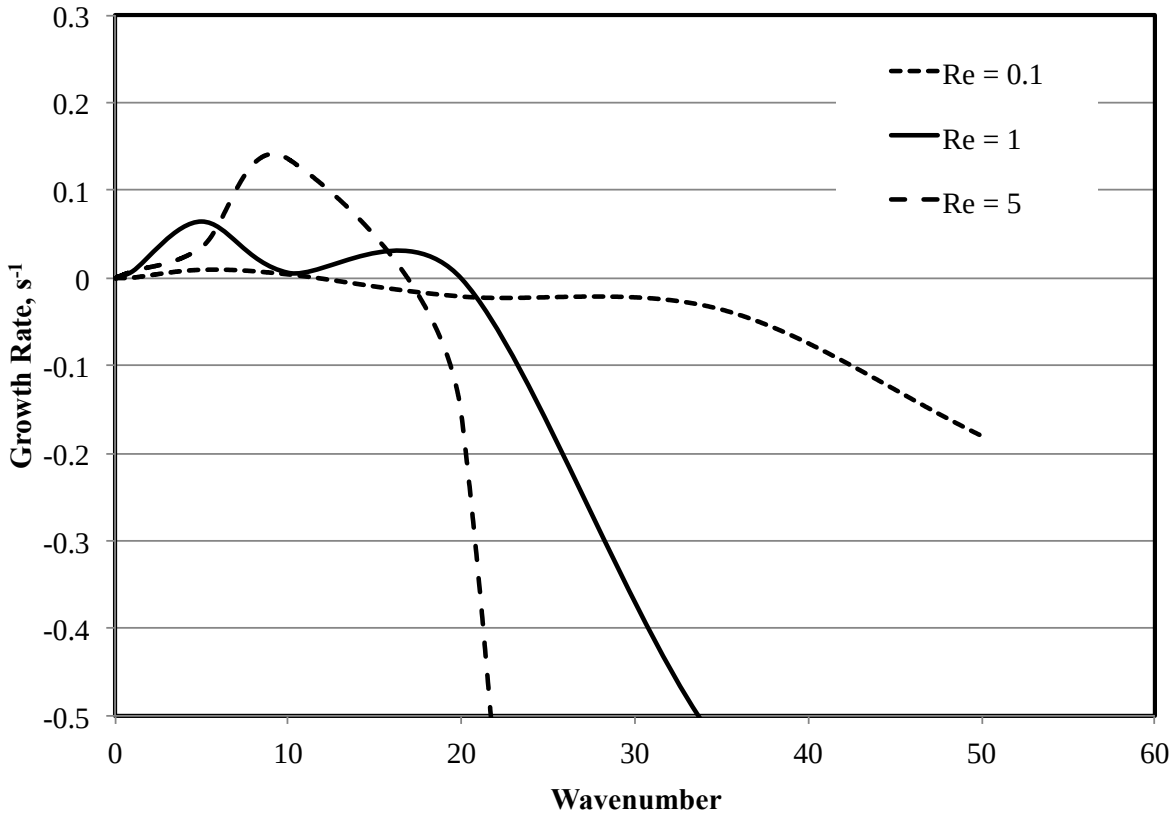

Figure 3-5: Impact of Reynolds' number on growth rates (inclination = 45°, S = 1,000,000, Pe = 10, thickness of oil and steam layers equal, viscosity ratio between oil and steam equal to 440, SOR = 3.5, and oil rate 90% of maximum value).

Figure 3.6 displays the effect of Peclet number on the growth rates. As the Peclet number increases, the growth rate of the most dangerous mode is larger. This implies that as convection becomes more dominant relative to conduction, the system becomes less stable.

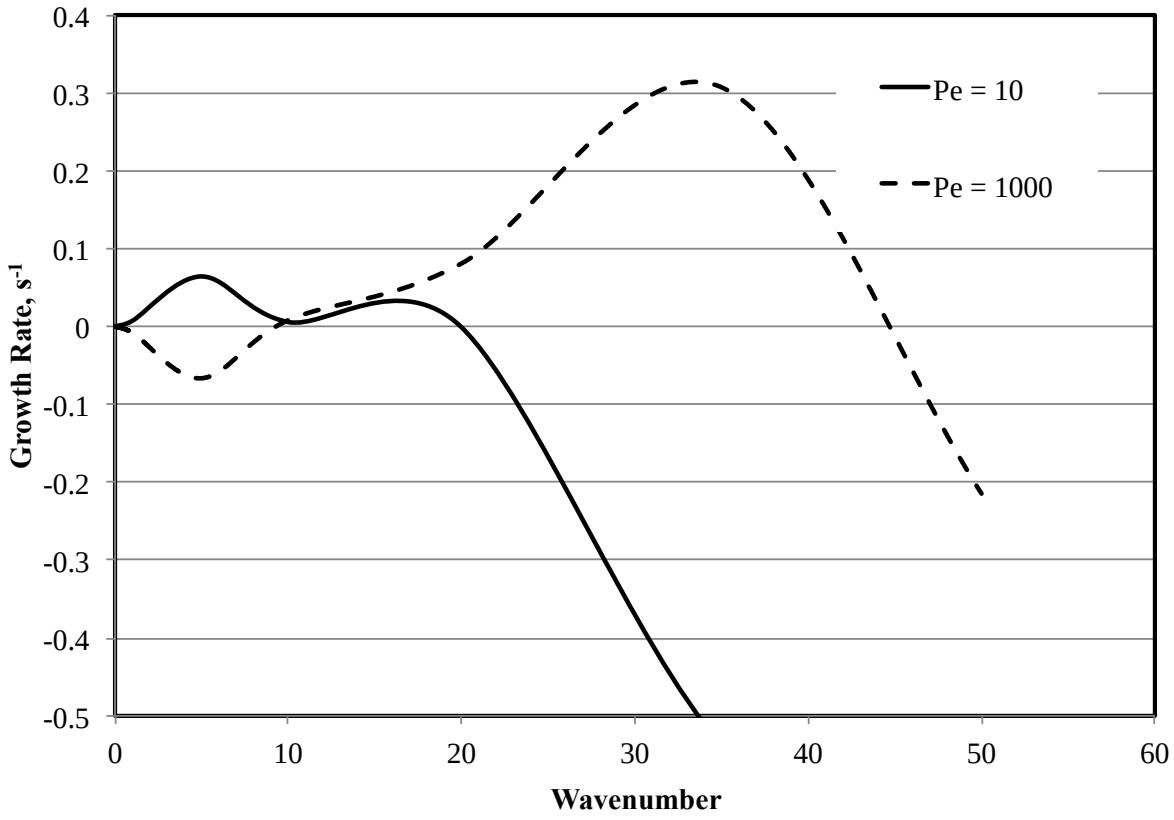

Figure 3-6: Impact of Peclet number on growth rates (inclination = 45°, Re = 1, S = 1,000,000, thickness of oil and steam layers equal, viscosity ratio between oil and steam equal to 440, SOR = 3.5, and oil rate 90% of maximum value).

Figure 3.7 displays the impact of inclination of the pore on the growth rates of the instability. The results show that the greater the inclination, the less stable is the system. This result is intuitive since the greater the inclination, the larger the impact of gravity leading to gravity drainage.

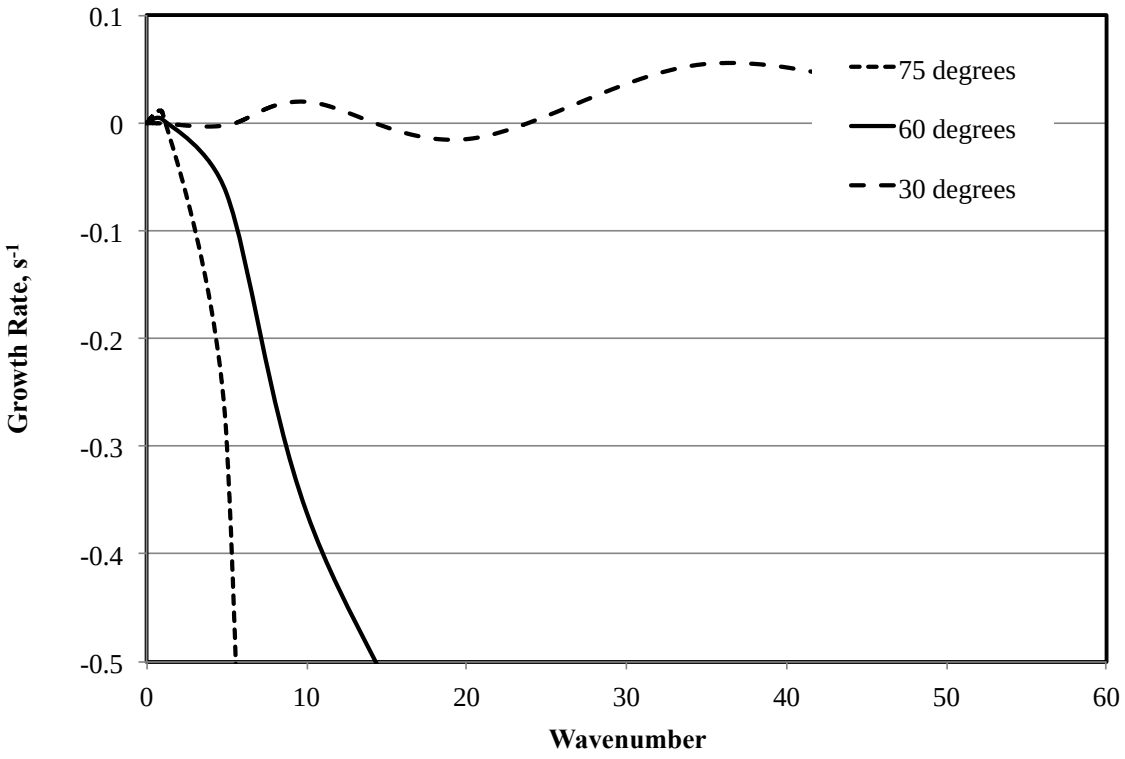

Figure 3-7: Impact of inclination on growth rates (Re = 1, S = 1,000,000, Pe = 10, thickness of oil and steam layers equal, viscosity ratio between oil and steam equal to 440, SOR = 3.5, and oil rate 90% of maximum value).

Figure 3.8 displays the eigenvectors of the most unstable mode for inclination = 45°, Re = 1, S = 1,000,000, Pe = 10, SOR = 3.5, and viscosity ratio = 440. The results show that most of the action of the real part of the eigenvectors is at the interface (y = 0). Thus, this suggests that the onset of the instability will yield perturbations at the interface. Given the analysis is limited to linear stability analysis and infinitesimal perturbations, the eigenvector simply indicates the early time response of the instability. The other realtively large part of the real part of the eigenvector is seen at the wall of the oil layer – this implies that there is a viscous contribution to the instability. In other words, the instability is dominated by shear (viscous) and interfacial modes.

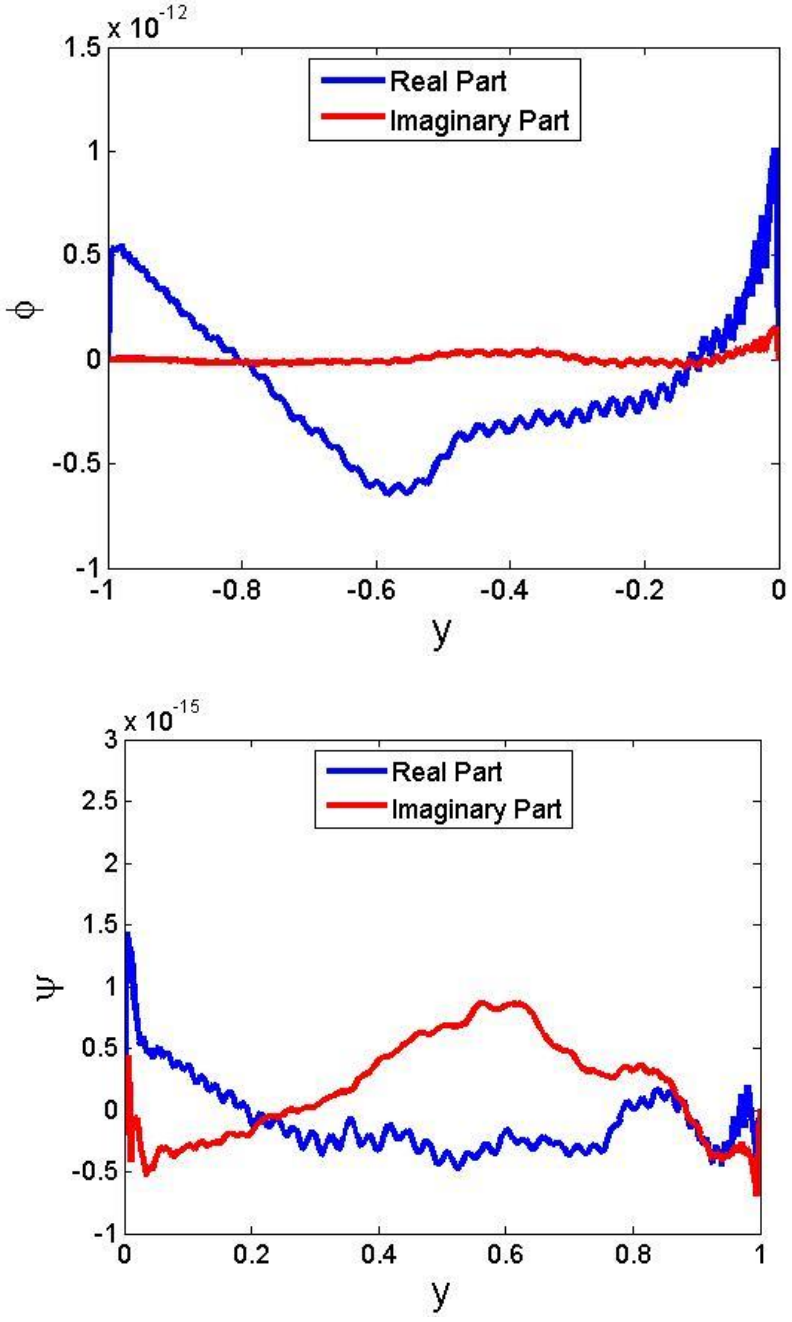

Figure 3-8: Eigenvectors (Φ, Ψ) of the most unstable mode for (inclination = 45°, Re = 1, S = 1,000,000, Pe = 10, thickness of oil and steam layers equal, viscosity ratio between oil and steam equal to 440, SOR = 3.5, and oil rate 90% of maximum value). The interface is at y = 0.

3.6 Implications for SAGD Operations

With respect to implications for the oil sands recovery process, with greater the instability, the more wavy is the interface and thus the heat transfer area is enhanced which in turn implies a greater volume of mobilized oil and thus the recovery process is more productive. This also implies that the more unstable the system, the greater is the energy efficiency of the process, or in other words, the lower is the steam-to-oil ratio.

The results show that the growth rate is positive for all the wavenumbers for all parameters studies which implies that the steam oil interface is unstable for all length scales. The larger the inertial forces, the greater is the growth rates which suggests that inertia is destabilizing the system and interfacial forces are destabilizing the system. Several of growth rate profiles have two or more dangerous modes versus wavenumber which suggest that the mode of instability is changing versus wavenumber. Although, according to linear stability analysis, the peak mode will dominate the instability, that there are other modes can be important with respect to interactions of the instability modes. For the Orr-Sommerfeld system, the two modes of instability are most frequently linked to a shear (viscous) mode and an interfacial based mode – these two modes are reflected in the eigenvectors of the system for the most dangerous mode. This is consistent to the results of Hooper (1989) who showed that the leading two growth rates were associated with interfacial and shear modes.

From the point of view of enhancing drainage rate, the results suggest that if instability occurs, and this leads to greater mixing of the phases at pore scale, this can be achieved by either

decreasing S or by increasing the angle to the vertical θ. Reduction of interfacial tension can be done further beyond that which results from steam heating. For example, the addition of surfactants or thin film spreading agents can lead to lower values of S and thus greater instability which implies greater mixing. Another is the addition of solvent if it lowers the interfacial tension between oil and other phases. Trials of using steam additives to SAGD field operations that lead to reduction of interfacial tension have shown an uplift of oil rate and a reduction of the steam-to-oil ratio (Suncor, 2014). This could be due to not only enhanced relative permeability but also due to enhanced instability and mixing at the edge of the chamber.

Since the analysis used here is that of linear stability which is constrained to infinitesimal perturbations, the interactions of the perturbations are not represented. Thus, the analysis demonstrates that the flow is unstable and that this is the case at pore scales but it does not deal with the propagation of the instability.

3.7 Conclusions

The conclusions from the research documented in this chapter are as follows:

1. Even at low Reynolds' number (equal to about 1 as expected in a pore containing steam and mobilized bitumen), the flow is unstable.
2. The larger is the convective heat transfer relative to conductive heat transfer, the less stable is the system.

3. The smaller is the ratio of interfacial forces relative to inertial forces, the greater is the growth rate of the instability.
4. The larger is the inclination, the greater is the growth rate of the instability.

Chapter Four: **Large Amplitude Instability of SAGD Chambers**

4.1 Introduction

There are two requirements for heavy oil and bitumen in underground reservoirs to be recovered to the surface: first, the oil has to be mobile and second, the mobilized oil has to be moved to the production wells under one or more drive mechanisms. The main control on the efficiency and economics of Steam-Assisted Gravity Drainage (SAGD) operations is in its capability to mobilize the bitumen within the reservoir which suffers from two key challenges. The first one is the conformance of the steam chamber along the SAGD well pair. The second is the efficiency of the steam chamber itself to transfer heat to the cool oil sands formation. The better the steam conformance, the larger the volume of oil produced per unit volume (CWE) of injected steam, the more efficient the SAGD process. As viewed by interpretations of seismic data, steam conformance along SAGD well pairs is not ideal in most cases (see for example, ConocoPhillips 2013, Cenovus 2013, Devon Canada 2013, Imperial Oil 2013).

There are three main factors that can impact SAGD steam conformance. The first of which is the heterogeneity of the geology and geochemistry of the reservoir rock and fluids which contribute to variability of the porosity and oil saturation (oil storage and oil phase relative permeability), permeability (fluid conductivity within the formation rock), and fluid composition (oil phase viscosity). The second factor is wellbore hydraulics, i.e. non-uniform steam pressure along the well pair caused by wellbore flow regime dynamics, multiple steam injection points, non-horizontal well trajectory, and formation damage all of which lead to non-uniform steam

conformance. The last factor are undulations of the steam chamber associated with instabilities of the steam-oil interface – these can potentially occur even in the most uniform oil sand due to small scale perturbations at pore or multi-pore scale that amplify to large scale perturbations of the chamber at reservoir scales. The last factor can cause poor steam conformance even in what are considered excellent quality relatively homogeneous oil sands reservoirs – this is an important concern especially if heterogeneity of the oil sand formation make worse non-uniformities of the steam chamber arising from instabilities. In most cases, analysis of steam conformance issues is centered on geological and fluid compositional variations and issues arising from wellbore hydraulics.

There are a lot of articles on the instability analysis of the fluids in porous media. Hill (1952) and Saffman and Taylor (1958) found that when a fluid phase of low viscosity displaces a fluid phase of higher viscosity, the interface between the phases is unstable and exhibits fingers that grow. This leads to fingering of the invading low viscosity fluid phase (the injectant) into the high viscosity phase. In the context of oil recovery, this can yield adverse effects on the recovery process since the injectant will tend to bypass oil rich zones after the fingers have provided a connected path between the injection well and the production well.

For steam-based recovery processes such as SAGD, the viscosity of the (vapour) steam is of order of micropoise – at about 2,100 kPa saturated steam (corresponding saturation temperature is equal to about 215°C), its viscosity is equal to about 16 μP. For McMurray Formation oil sands reservoirs, the viscosity of the bitumen is of order of 1 million cP at original conditions and at 215°C, it is equal to about 7 cP (Mehrotra and Svcek 1986). Even at steam temperature,

the viscosity of the mobilized oil is several hundred times that of the steam. Thus, even in uniform oil sands reservoirs, the steam-oil interface is unstable and at the edge of the steam chamber, given the results of analytical models, it is proposed that steam advances into the oil formation in the form of viscous fingers (Butler 1987, 1994; Ito et al. 2005; Gotawala and Gates 2008). However, there has not been strong evidence of steam fingering from thermal reservoir simulation or experiments or from field operations. Butler (1987, 1994) suggested that the length scale of the steam fingers would be of order of meters to tens of meters. Gotawala and Gates (2008) corrected Butler's result and found length of steam fingers is on the order of millimeters to tens of centimeters. However, the general approach taken by Buter and Gotawala and Gates is a pseudo-steady approach which pre-supposes fingers at the edge of the chamber and solves for the length scale of them given heat transfer, steam rise, and oil drainage. Thus, dynamics are not represented by the approach.

Prichard (2004) found that for a fluid of different composition and temperature, the interfacial instability is greatly impacted by the coupling between the thermal and compositional effects. In his analysis, he used linear stability analysis based on eigenfunction expansions to determine how the properties of each fluid contribute towards instability. The results showed that the growth rate of the interfacial instability may be altered significantly by the coupling between thermal and compositional effects.

Islam and Azaiez (2006) studied viscous fingering in a non-isothermal miscible displacement by using a Hartley transform-based pseudo-spectral numerical method. In their numerical model, the viscosity of the liquid varied with both temperature and composition as follows:

$$\mu(C,\theta) = e^{\beta_C(1-C)+\beta_T(1-\theta)} \tag{4.1}$$

where C and θ are the dimensionless concentration of the injected fluid and temperature, respectively, and β_C and β_T are parameters that represent dependency of viscosity on concentration and temperature, respectively. The results of their analysis suggested that at large Lewis number, Le = α/D (ratio of thermal diffusivity to mass diffusivity), the instability of the thermal-viscous flow is controlled by the viscous variation between the displacing and displaced fluids and that the effects of viscosity contrast between the invading and original fluids due to thermal and concentration effects are additive. At high Lewis number, due to the high thermal diffusivity, the instability is dominated by the viscosity variations arising from compositional variations.

Here, the stability of the SAGD steam chamber is analyzed by using an analytical and numerical approach to verify that steam chamber conformance can by non-ideal due to instabilities of the steam-oil interface. The analytical theory is adapted from Gotawala and Gates (2011) which is strictly applicable to infinitesimal perturbations. The numerical approach makes use of transient analysis which enables a view of finite scale perturbations of the steam-oil interface.

4.2 Analytical Model – Rayleigh-Taylor Instability Analysis

In this section, the interfacial instability model proposed by Gotawala and Gates (2011) is presented for analysis of SAGD steam chamber dynamics. The schematic diagram of the model is illustrated in Figure 4.1. The approach taken by Gotawala and Gates is an idealization and really only applies to the case where the base case steam-oil interface within the porous medium is perfectly horizontal and perturbations of the interface are infinitesimal. In other words, the perturbations of the interface are very small and the thus the system can be linearized and then analyzed by using Fourier normal modes. Strictly, even though this is sufficient to determine whether the system is stable or unstable subject to small amplitude perturbation, it does not provide meaningful insights as to final form of the flow system that arises if the flow is unstable. For this, non-linear stability analysis is required – this can be done by using transient analysis. One traditional means to measure the length scale of the impacted zone by instability is to calculate the length scale of the most unstable Fourier normal mode. For example, the distance between the troughs and peaks between the westly jet in the atmosphere is around 4000 km, which is actually the length scale of the most unstable mode of the instability (called baroclinic instability). But as we have discussed in the previous chapter, the problem with this means is whether the most unstable mode of the linear instability can go that far, i.e. whether the mean state will change over time such that the original estimate will not valid anymore. Nonlinear stability analysis is one of the most important topics in climate sciences because it tells us where does our climate system origin from, what is maintaining it against external forces (mainly surface friction) and where will it go if we perturb it (for example by emitting CO_2 and water vapor).

For the edge of the oil sands chamber, there are three phases in this model: the oil phase above the interface, the steam phase and the liquid condensate phase underneath of the interface. The steam zone temperature is at its saturated steam chamber temperature, T_c, which corresponds to its injection pressure. The steam quality adjacent to the interface is equal to η_s. Heat is transferred from steam zone to the oil zone is by conduction. The temperature of oil sands sufficiently far away from the interface is assumed to be at the original reservoir temperature, T_R. The fluids in this model are immiscible and Newtonian such that the two fluids do not exchange mass.

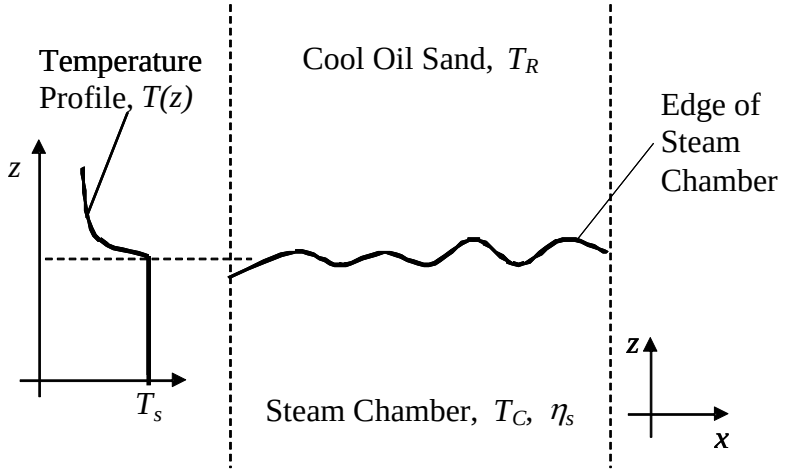

Figure 4-1: Interface between steam chamber and cool oil sands reservoir. Interface between steam chamber and cool oil sands reservoir. The steam chamber is at saturation temperature T_s. The quality of steam at the edge of the chamber is η_s. (Gotawala and Gates 2011)

In the analytical model, the porous medium is assumed to be homogeneous, the top part is saturated with bitumen and the bottom part is saturated with steam. Thermal dispersion is isotropic. Gotawala and Gates imposed the Boussinesq approximation, i.e., the change of density is neglected except when the density term is multiplied by gravity term in the vertical direction. In their analysis, they also neglected capillary forces. The density and viscosity of the oil, steam and condensate depend on temperature.

Gotawala and Gates' used linear stability analysis and expanded the perturbations in terms of Fourier normal modes. The result was an eigenvalue system given by:

$$\begin{pmatrix} l^2 & 0 & 0 & Ra_o l^2 & 0 \\ \gamma_0 l & 0 & 0 & \sigma + l^2 & \sigma(\gamma_w - \gamma_v) \\ 0 & l^2 & 0 & Ra_v l^2 & 0 \\ 0 & 0 & l^2 & Ra_w l^2 & 0 \\ 0 & -\rho_{vs} l & -\rho_{ws} l & 0 & \epsilon\sigma(\rho_{vs} - \rho_{ws}) \end{pmatrix} \begin{pmatrix} \Psi_o \\ \Psi_v \\ \Psi_w \\ \Theta \\ \Phi \end{pmatrix} = \begin{pmatrix} 0 \\ 0 \\ 0 \\ 0 \\ 0 \end{pmatrix} \tag{4.2}$$

where Ψ_o, Ψ_v, Ψ_w are the magnitudes of the perturbation streamfunctions of oil, steam and water phases while Θ and Φ are magnitude of perturbation temperature and steam saturation, respectively, and

$$Ra_v = \frac{k k_{rv} g \rho_{vs} \beta_v d(T_C - T_R)}{\epsilon \alpha_U \mu_{vs}} + m_v(\bar{\theta})^{-(m_v+1)} \tag{4.3}$$

$$Ra_w = \frac{k k_{rw} g \rho_{ws} \beta_w d(T_C - T_R)}{\epsilon \alpha_U \mu_{ws}} + m_w(\bar{\theta})^{-(m_w+1)} \tag{4.4}$$

and

$$\mathrm{Ra_o} = \frac{\mathrm{kk_{ro} g \rho_{oR} \beta_o d(T_C - T_R)}}{\epsilon \alpha_U \mu_{os}} + \mathrm{m_o}(\bar{\theta})^{-(\mathrm{m_o}+1)} \tag{4.5}$$

are respectively the vapour (steam), water (steam condensate), and oil phase Darcy-Rayleigh numbers. The remaining symbols are defined in Table 4.1. When the determinant of the matrix in Equation 4.2 equals zero, the system has non-trivial solutions, which leads to the condition:

$$\sigma + l^2 + l\Delta\mathrm{Ra} = 0 \tag{4.6}$$

where

$$\Delta\mathrm{Ra} = \left[\frac{\gamma_v - \gamma_w}{\epsilon(\rho_{vs} - \rho_{ws})}(\rho_{vs}\mathrm{Ra_v} + \rho_{ws}\mathrm{Ra_w}) - \gamma_o \mathrm{Ra_o}\right] \tag{4.7}$$

and

$$\gamma_v = \frac{\eta_s \rho_{vs} L_v}{(T_C - T_R)(\rho C_p)_U} \tag{4.8}$$

$$\gamma_w = \frac{(1-\eta_s)\rho_{ws} C_{pw}}{(\rho C_p)_U} \tag{4.9}$$

and

$$\gamma_o = \frac{\epsilon \rho_{oR} C_{po}}{(\rho C_p)_U} \tag{4.10}$$

are the thermal lag coefficients of the vapour (steam), water (steam condensate), and oil phases, respectively. Here, $\Delta\mathrm{Ra}$ is the difference between the energy-weighted wet stream ratio of

buoyancy to viscous forces and the energy-weighted oil phase ratio of buoyancy to viscous forces. When ΔRa transitions from positive to negative, the growth rate of linear instability transitions from being stable for all wavenumbers to being unstable over an interval of wavenumbers.

The viscosity of the fluid phases is expressed by:

$$\mu_i = \mu_{is}\left(\frac{T-T_R}{T_C-T_R}\right)^{-m_i} \tag{4.11}$$

where i = o (for oil), s (for steam vapour), and w (for water).

An example calculation, for parameters listed in Table 1, is shown in Figure 4.2. Figure 5 shows growth rate, σ, versus wave number, l, versus ΔRa.

Table 4-1: Definition of symbols

a,b	Steam-water relative permeability curve Corey coefficients	dimensionless
C_p	Specific heat capacity	kJ/kg °C
d	Characteristic length	m
g	Gravitational acceleration	m/s^2
k	Absolute permeability	D
k_r	Relative permeability	dimensionless
l	Horizontal wave number	1/m
L_v	Latent heat of condensation	J/kg
m	Power law coefficient for viscosity-temperature correlations	dimensionless
Ra	Darcy-Rayleigh number	dimensionless
t	Time	s
T	Temperature	°C
Greek		
α	Thermal diffusivity of reservoir	m^2/s
γ_i	Thermal lag coefficient of i^{th} phase	dimensionless
ε	Porosity of porous media	dimensionless
η_s	Steam quality	dimensionless
θ	Dimensionless temperature	dimensionless
μ	Viscosity	kg/m s
ρ	Density	kg/m^3
σ	Growth rate	1/s
$\chi(x,z,t)$	Small disturbance in temperature	dimensionless
$\psi(x,z,t)$	Small disturbance in velocity	dimensionless
$\Psi(z,t)$	Dimensionless velocity perturbation function	dimensionless
$\Theta(z,t)$	Dimensionless temperature perturbation function	dimensionless
$\Phi(z,t)$	Dimensionless saturation perturbation function	dimensionless
ΔRa	Difference between displacing and displaced fluids Darcy-Rayleigh number	dimensionless

The results reveal that as ΔRa changes from positive to negative, the growth rate shifts from being completely negative, that is stable, to being unstable over an interval of wavelength. The neutral stability state occurs at $\Delta Ra = 0$. Negative values of ΔRa indicate that the energy content-weighted Darcy-Rayleigh number for the oil phase is greater than that of the steam+water phases – physically, this is the situation where the energy-weighted buoyancy to viscous forces of the steam+water phases is smaller than that of the oil phase. The physical outcome is that the oil phase drains and the steam+water phases rise. The peak positive values of the growth curves in Figure 4.2 indicate the most dangerous mode of the instability. For oil

sands reservoirs, at typical reservoir conditions and steam injection temperatures, the expected range of ΔRa is between 0 and -50 which suggests that the wavenumber of the most dangerous mode ranges up to 28 m^{-1} which in turn implies that the horizontal wave length of the disturbance ranges down to tens of centimeters. This length scale is consistent with the fingering theory of Gotawala and Gates (2008).

Table 4-2: Reservoir and fluid properties

Item	Value
Reservoir Temperature T_R, ˚C	10
Steam Temperature T_c, ˚C	250
Steam Pressure, kPa	4,000
Characteristic dimension of the steam chamber, m	5
Viscosity correlation of water	μ_{ws} = 0.00106 cP at 250˚C m_w = 0.7692
Viscosity correlation of steam (vapour)	$\mu_{vs} = 1.749(10)^{-5}$ cP at 250˚C m_v = 0.21
Viscosity correlation of bitumen	μ_{os} = 0.003423 cP at 250˚C m_o = 4.0948
Density of water at T_R,, kg/m^3	1,000
Density of steam (vapour) at T_R, kg/m^3	0.017314
Density of oil at T_R, ρ_o kg/m^3	1,003
Coefficient of thermal expansion for water, $\beta_{\rho w}$ ˚C^{-1}	$6.34(10)^{-4}$
Coefficient of thermal expansion for oil, $\beta_{\rho o}$ ˚C^{-1}	$6.90(10)^{-6}$
Coefficient of thermal expansion for vapour, $\beta_{\rho v}$ ˚C^{-1}	$-4.00(10)^{-4}$
Absolute permeability k, mD	5,000
Porosity, ε	0.39
Solid thermal diffusivity, α_U, m^2/s	$7.08(10)^{-6}$
Volumetric heat capacity of upper region, $(\rho C_p)_U$, J/m^3 ˚C	$2.443(10)^6$
Relative permeability of oil, k_{ro}	1
Water-steam relative permeability data (O´Connor, 2001)	S_{wc} = 0.4, S_{gc} = 0.07, k_{rwrg} = 0.55, k_{rgwc} = 0.68, a = 3, b = 2.7

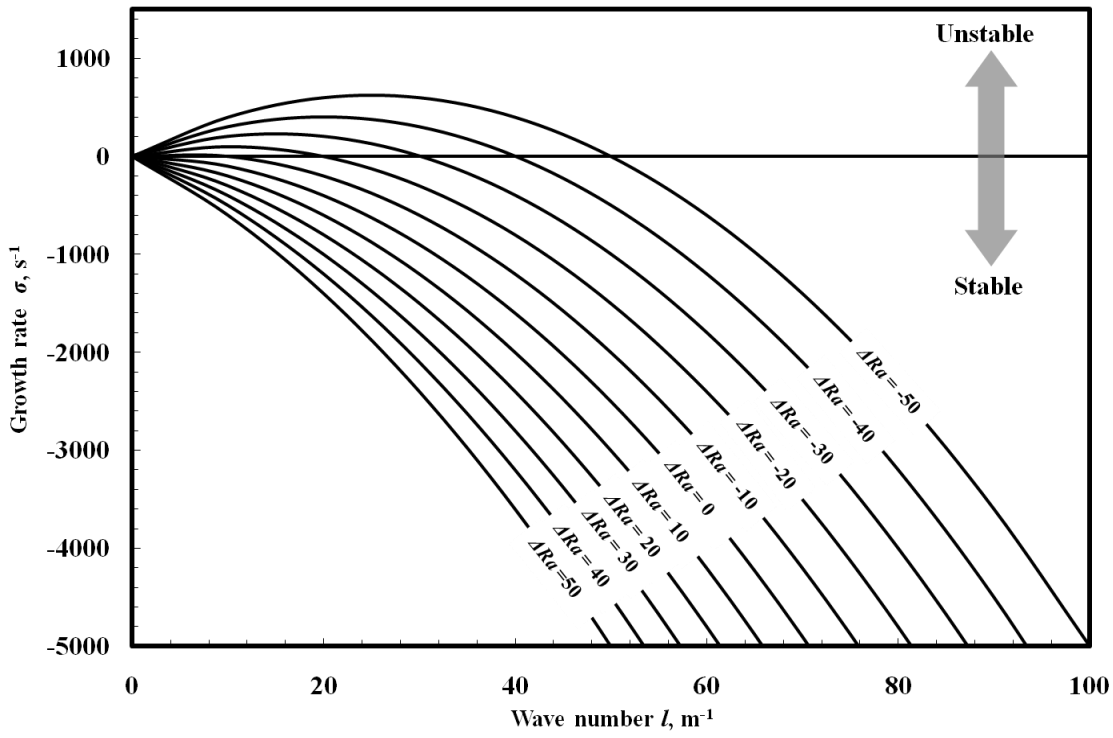

Figure 4-2: Growth rate versus wave number versus Δ*Ra*. The parameters used are listed in Table 4.2 (Gotawala and Gates 2011)

Figure 4.3 shows the impact of temperature and steam quality ΔRa. The results show that above a certain steam quality, above about 50%, the system is unstable for the temperature range over which SAGD is operated (between about 180 and 250°C). Even though steam is injected at about 95% quality (or higher) into the reservoir, after it reaches the edge of the chamber, it has dropped to about 50% (Gates et al. 2007). Thus, this suggests that the steam-oil interface is always unstable over the typical range of SAGD team injection temperatures. The results also suggest that the instability can be increased if the steam quality is higher at the edge of the chamber.

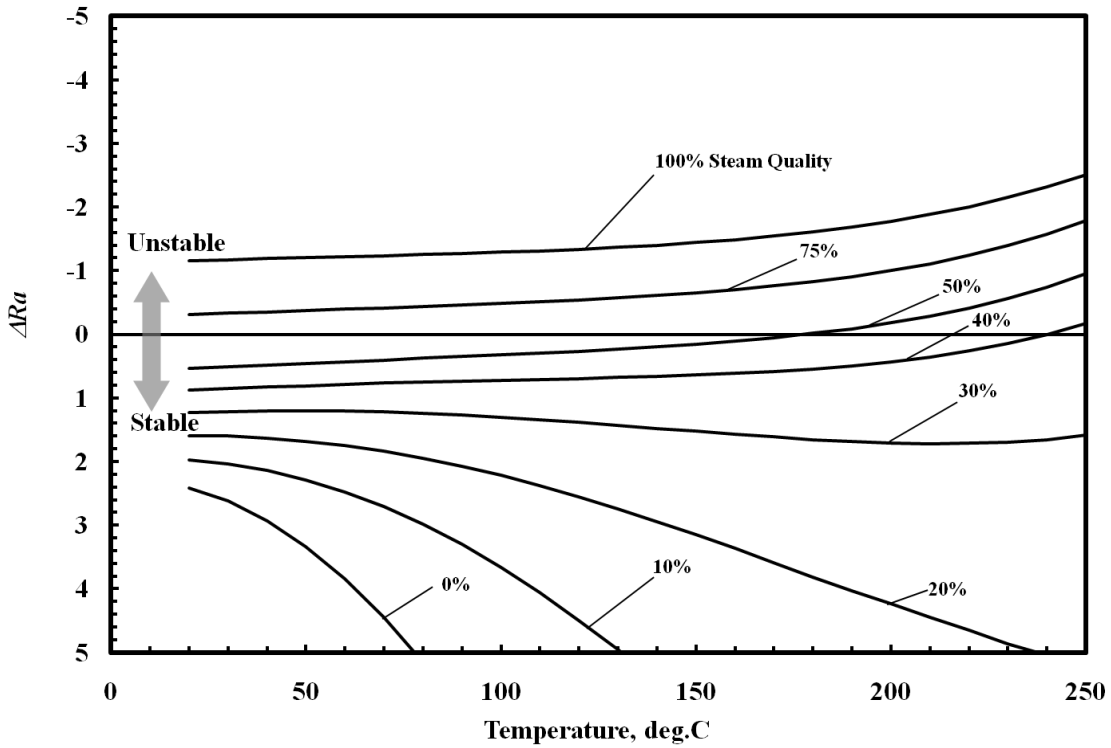

Figure 4-3: ΔRa versus temperature versus steam quality (η_s). The parameters used are listed in Table 4.2 (Gotawala and Gates 2011)

4.3 Reservoir Simulation Model

The reservoir model used here has properties typical of that of a McMurray Formation oil sands reservoir. The model was constructed and run by using CMG STARS™ (CMG, 2013). STARS™ is a commercial thermal reservoir simulator that is commonly used in the oil sands industry to model SAGD; it uses a finite volume approach that solves the mass continuity, multiphase Darcy flow and component mass transport with thermodynamic equilibrium between the vapour, aqueous, and oil phases (in the model used here, water can transition between the aqueous and vapour phases and solution gas can move between the oil and vapour phases).

Since we want to understand instability of the steam-oil interface, the model is a vertical section model that contains a SAGD injection and production well pair. The width of the model is equal to 10 m and its height is equal to 21 m. To make the analysis more straightforward, a two-dimensional model has been used. The average porosity of the model is equal to 0.3. The horizontal permeability is given by:

$$\ln k_H = 7.7319\,\phi - 0.4477$$

which has been taken from the average porosity-permeability transform for the ConocoPhillips Surmont SAGD project (Accumap, 2013); at porosity equal to 0.3, the horizontal permeability is equal to 6.5 D. The vertical permeability is equal to one-quarter of the horizontal permeability. Initially, the water and oil saturations are equal to 0.2 and 0.8, respectively. The separation between the injector and producer is equal to 5 m.

Two cases were run, listed in Table 4.3. The first case, denoted by Case 1, considered uniform fluid composition whereas the second case, denoted by Case 2, used a variable fluid compositional model typical of that of a McMurray oil sands formation.

Table 4-3: List of cases. In all cases, the initial water and oil saturations are equal to 0.2 and 0.8, respectively.

Case Name	Description
Case 1	Homogeneous fluid composition (initial live oil viscosity = 560,000 cP) Homogenous porosity and permeability (porosity = 0.3, horizontal permeability = 6.5D)
Case 2	Heterogeneous fluid composition (oil live viscosity varies from 447,400 cP at reservoir top to 981,600 cP at reservoir bottom) Homogenous porosity and permeability (porosity = 0.3, horizontal permeability = 6.5D)

The solubility of the solution gas is expressed by K-value relationship:

$$\text{K-value} = \frac{k_{v1}}{P} e^{\frac{k_{v4}}{T+k_{v5}}}$$

where k_{v1}= 5.45x10^5 kPa, k_{v4} = -879.84°C, and k_{v5} = -265.99°C (CMG, 2013). Additional properties required for the thermal reservoir simulation model are listed in Table 4.4.

The oil component viscosities are listed in Table 4.5. The oil phase viscosity, at a given temperature, is given by:

$$\ln \mu_{oil} = x_{TOIL} \ln \mu_{TOIL} + x_{BOIL} ln\, \mu_{BOIL} + x_{sg} \ln \mu_{sg}$$

where x_* is the mole fraction of the component and *TOIL*, *BOIL*, and *sg* denote the top oil, bottom oil, and solution gas, respectively.

Table 4-4: Properties used in thermal reservoir simulation model

Parameter	Value		
Dimensions of grid blocks, m	0.05 (horizontal) x 0.05 (vertical) x 1 (downwell direction)		
Depth (at top of model), m	300		
Initial reservoir temperature, °C	15		
Initial reservoir pressure, kPa	2,670 at top of model		
Three phase relative permeability model	Stone's Model II		
Rock (sand, overburden, and understrata) heat capacity, J/m^3 °C	$2.35x10^6$		
Rock (sand, overburden, and understrata) thermal conductivity, J/m day °C	$6.600x10^5$		
Water phase thermal conductivity, J/m day °C	$5.350x10^4$		
Oil phase thermal conductivity, J/m day °C	$1.25x10^4$		
Gas phase thermal conductivity, J/m day °C	$3.200x10^3$		
Thermal conductivity mixing rule and temperature dependence	Anand et al. (1973), Somerton et al. (1974)		
Solution gas to oil ratio, m^3/m^3	3		
Water-oil relative permeability curve (Good et al., 1997)	S_W	k_{rw}	k_{row}
	0.15	0	0.992
	0.2	0	0.979
	0.25	0.0004	0.95
	0.3	0.0012	0.72
	0.35	0.0029	0.6
	0.4	0.0057	0.47
	0.45	0.0098	0.35
	0.5	0.0156	0.24
	0.55	0.0233	0.165
	0.6	0.0331	0.11
	0.65	0.0456	0.07
	0.7	0.0606	0.04
	0.75	0.0787	0.015
	0.8	0.1	0
	0.9	0.1537	0
	0.95	0.1866	0
	1	0.2237	0
Gas-liquid relative permeability curve (Good et al., 1997)	S_L	k_{rg}	k_{rog}
	0.155	1	0
	0.2075	0.95	0.0002
	0.26	0.84	0.0016
	0.3125	0.72	0.0055
	0.365	0.6	0.013
	0.4175	0.47	0.0254
	0.47	0.35	0.044
	0.5225	0.24	0.0698
	0.575	0.165	0.104
	0.6275	0.093	0.148
	0.68	0.075	0.204
	0.7325	0.045	0.271
	0.785	0.027	0.352
	0.8375	0.02	0.447
	0.89	0.01	0.559
	0.9425	0.005	0.687
	0.995	0	0.834
	1.0	0	0.992

Table 4-5: Oil component viscosities. Note that the solution gas viscosities are liquid equivalent values (Gates et al. 2008).

Temperature, °C	Top oil viscosity, cP	Bottom oil viscosity, cP	Liquid equivalent solution gas viscosity, cP
5	4523613.536	14627862.150	115
12	1246217.106	4420687.1044	98.1
20	336922.854	1291721.5943	68.4
30	81167.3762	331656.0328	54.1
40	23833.2916	100864.5923	43.4
50	8256.5612	35419.2117	35.2
60	3286.7421	14062.1725	28.9
70	1471.4227	6203.0386	24.0
80	727.8683	2996.2711	20.1
90	392.1015	1565.6454	17.0
100	227.2724	875.9733	14.6
110	140.3285	520.2501	12.6
120	91.5278	325.5854	10.9
130	62.6183	213.3676	9.56
140	44.6674	145.6378	8.43
150	33.0524	103.0622	7.49
160	25.2599	75.3141	6.70
170	19.8623	56.6370	6.03
180	16.0164	43.6994	5.46
190	13.2065	34.5021	4.97
200	11.1070	27.8104	4.55
210	9.5067	22.8386	4.18
220	8.2649	19.0741	3.86
230	7.2855	16.1745	3.58
240	6.5019	13.9058	3.34
250	5.8666	12.1056	3.12
260	5.3454	10.6583	2.93
270	4.9132	9.4811	2.76
280	4.5512	8.5129	2.61
300	3.9846	7.0349	2.36

Figure 4.4 displays the initial oil viscosity distribution for the heterogeneous fluid composition case. The lower oil viscosity is found at the top of the model whereas the higher viscosity oil is found at the bottom of the oil column.

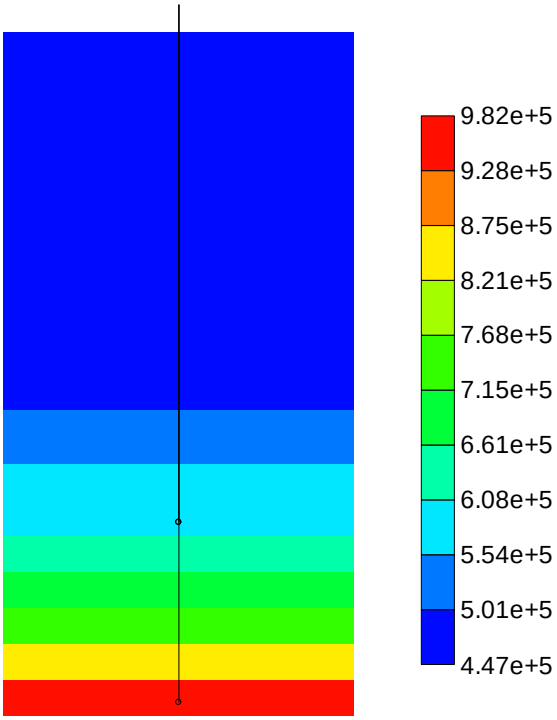

Figure 4-4: Spatial distribution of the initial live oil phase viscosity in cP used in Case 2.

The positions of the injection and production wells are also displayed in Figure 4.4; the top well is the injection well and the lower well is the production well. Prior to SAGD mode, steam circulation is modeled by using line heaters, operated at 200°C, in the locations of the injection and production wells – the circulation period is operated for a total of three months. During the steam circulation period, to relieve the pressure created by thermal expansion of the reservoir fluids in the region near the well pair, temporary production well in the location of the injection well and the lower production wells are opened with bottom hole pressures equal to the initial reservoir pressures at their depths. After the circulation period is complete, the line heaters are switched off, and the temporary production well in the location of the injection well is removed. Thereafter, steam is injected into the top well at injection pressure equal to 4,000 kPa (steam

quality equal to 0.95) and fluids are produced from the production well under a maximum steam production rate constraint equal to 1 m^3(CWE)/day (this mimics steam trap control).

To ensure the results were independent of grid size, the dimensions of the grid blocks were reduced to 1 cm in both directions and the model was re-run for the homogeneous case, Case 1. The fluid rates differed by less than 0.1% and the length scales of the perturbations observed in the simulations changed by less than 5% and thus the results were considered sufficiently accurate at the original grid size. The model, with 5 cm grid blocks, took about 10 hours to run on a quad core personal workstation (3.4 GHz processor).

4.4 Results

The initial temperature of the reservoir is 15°C. Figure 4.4 displays the temperature profile after the steam circulation period is complete for Case 1. The temperature between the wells has been raised to about 70°C which is sufficient for the bitumen between the wells to have mobility so that when steam is injected into the formation, it is displaced from the region between the wells. Note that Figure 4.4 displays a close up view of the reservoir with the length scale indicated by the distance between the injection and production wells (equal to 5 m).

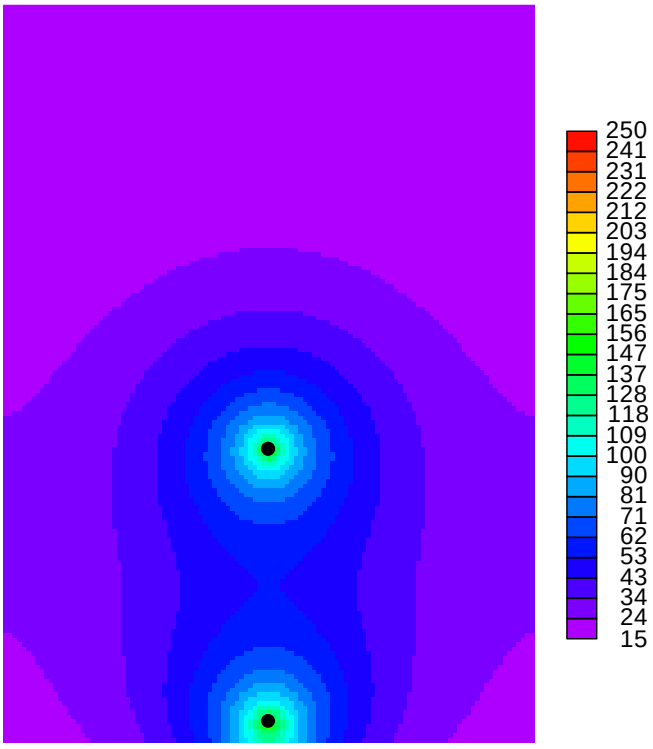

Figure 4-5: Spatial temperature distribution after steam circulation period is complete (Day 96) for Case 1.

Figures 4.5 to 4.10 displays the onset of the creation of the steam chamber after the steam circulation period as well as the formation of fingers at the top of the steam chamber. At Day 97, steam injection into the top well and fluid production from the bottom well cause pressurization of the zone surrounding the injection well to rise to 4,000 kPa and the temperature to rise to the corresponding saturation temperature (about 250°C). The viscosity of the oil phase drops to about 6 cP as a result. The mole fraction of solution gas (methane) in the gas phase distribution indicates that symmetry has been broken even at this stage of the process with the onset of non-infinitesimal perturbations arising surrounding the injection and production wells. The gas saturation is small and at this stage of the process has arisen due to the rise of temperature surrounding the two wells.

Figure 4.6 displays the pressure, mole fraction of solution gas, temperature, and oil phase viscosity after Day 100 for Case 1. The pressure has climbed surround the top well and the pressure wave is traveling towards the lower production well. The mole fraction of solution gas displays that the gas phase has fingered its way from the injection well to the production well through the mobilized bitumen. The finger is not symmetric around the mid plane and exhibits the onset of a pressure-driven viscous fingering instability that connects the two wells after steam injection starts. This is the first time this phenomena has been seen in thermal reservoir simulation. The temperature distribution looks perfectly symmetric around the mid plane of the wells but is misleading given the dynamic that is exhibited by the distribution of the gas phase mole fraction of solution gas. Given that the viscosity is largely responding to the temperature distribution, the oil viscosity distribution appears to be symmetric around the mid place as well.

Figure 4.7 displays the pressure, gas phase mole fraction of solution gas, temperature, and oil viscosity distributions after Day 103. The pressure and temperature distributions are symmetric around the mid plane. The pressure distribution illustrates that the pressure wave has now connected the two wells and the temperature distribution shows that the hot steam chamber now connects the two wells. The fully connected steam depletion chamber between the two wells has now overcome the instability exhibited earlier by gas phase fingering through the mobilized bitumen zone. However, at the top of the steam chamber, the spatial distribution of the solution gas mole fraction in the gas phase displays the onset of finite amplitude chamber fingers at the top of the depletion chamber. If one was to view the pressure and temperature distributions, the onset of the instability would not have been observed. The fingers at the top of the depletion

chamber are coincident with the region above the wells where the pressure gradient is highest and is above the 250°C steam chamber. The temperature has risen sufficiently and the pressure is small enough to cause the onset of solution gas exsolution. The majority of the gas phase at the top of the chamber is solution gas (not steam) and thus the results are showing the creation of a depleted space above the hot steam chamber that is gas filled which suffers from instability. This then creates a pathway for the steam to enter as the steam chamber ascends within the reservoir.

Figure 4.8 displays the results at Day 107. The pressure distribution is uniform and established throughout the domain but the depletion chamber fingering first seen at Day 103 has now grown into mature fingers at the top of the steam chamber. A comparison of the distributions of the solution gas content in the gas phase and the temperature reveal that the fingers exist above the hot steam chamber – this gas zone is largely filled with solution gas. The gas saturation (not shown) shows that the gas saturation is between 0.05 and 0.1 in this zone and thus it is 'seeding' the reservoir above the steam chamber for the steam chamber to grow. The pressure and temperature distributions on their own do not indicate the onset of the instability at all and thus are misleading as to displaying the full dynamics of the steam chamber and its evolution into the reservoir. The gas fingers in the zone above the hot steam chamber have an impact on the oil phase viscosity – the fingers are clearly observed in the oil viscosity distribution. The evolution of the fingers demonstrates that they have grown several meters into the reservoir above the hot steam chamber. This reveals the presence of two depletions chambers within the process – the first is the well established hot steam chamber where the temperature has been raised to the injected steam temperature and the other is a lower temperature depletion chamber above the hot

steam chamber filled with solution gas. The results are consistent with Edmunds (2006) field observations of what he referred to as gas blunting where there appeared to be a blunting of the temperature distribution from observation wells at the top of the steam chamber. He accounted for the blunting by the presence of solution gas at the top of the steam chamber. However, the results here show a different dynamic where there is not only solution gas at the top of the steam chamber but also gas phase fingering above the hot zone. The results also show that the gas fingers above the hot chamber are not symmetric and have widths over order of 5 to 20 cm in width.

Figure 4.9 displays the results at Day 110. The pressure distribution and temperature distributions show the fully established steam chamber between two wells. The distributions of the mole fraction of solution gas in the gas phase and the oil viscosity illustrate the growth of the fingers beyond the edge of the hot chamber into the reservoir. The fingers have grown illustrating that the system is unstable. The fingers have evolved in the vertical direction which reveals that the instability is reinforced in the vertical direction where the contrast between gravity, pressure, and viscous forces are largest. The sides of the chamber, with flow down the inclined edge of the chamber and relatively small pressure differences in the cross-well direction yield no fingering in that direction. Thus, with respect to steam conformance, in the mode of instability viewed here, it affects the vertical growth of the steam chamber within the reservoir. Given an underlying heterogeneity of the oil sands reservoir both vertically and areally as would be the case in a point bar deposit (Su et al. 2013, 2014), vertical fingering coupled with shale/sand sequences in the reservoir would yield non-uniform lateral growth of the chamber as well. This will be examined in future work. Additionally, if the pressure gradient was slightly

greater in the lateral direction (equal to that in the vertical direction at the top of the chamber), there is potential that fingering would occur in the lateral direction as well (to be explored in future work).

Figure 4.10 displays the results for Day 120. The results show that the hot chamber has ascended further into the reservoir and that the fingers have extended further into the reservoir with length scale nearly that of the interwell spacing. The pressure and temperature distributions do not display this dynamic. The fingers that dominated earlier in the process have continued to grow and largely evolved into a single large finger with multiple tips above which is similar to the observations of Saffman and Taylor for their viscous fingering experiments in Hele-Shaw cells. The distribution of the mole fraction of solution gas in the gas phase shows that it is not symmetric around the mid plane and that there are waves on the top surface of the depletion zone above the hot chamber. The oil viscosity distribution displays that lower viscosity oil fingers exist within the viscous oil above the steam chamber.

The results for Case 1 demonstrate that fingering occurs in a completely homogeneous reservoir leading to heterogeneities of the oil phase viscosity in the reservoir. This result, not seen before in previous thermal reservoir simulation studies, reveals that heterogeneity can result from homogeneity due to fluid mechanical instabilities associated with the reservoir process. This implies that even ideal oil sands reservoirs will suffer from steam conformance issues.

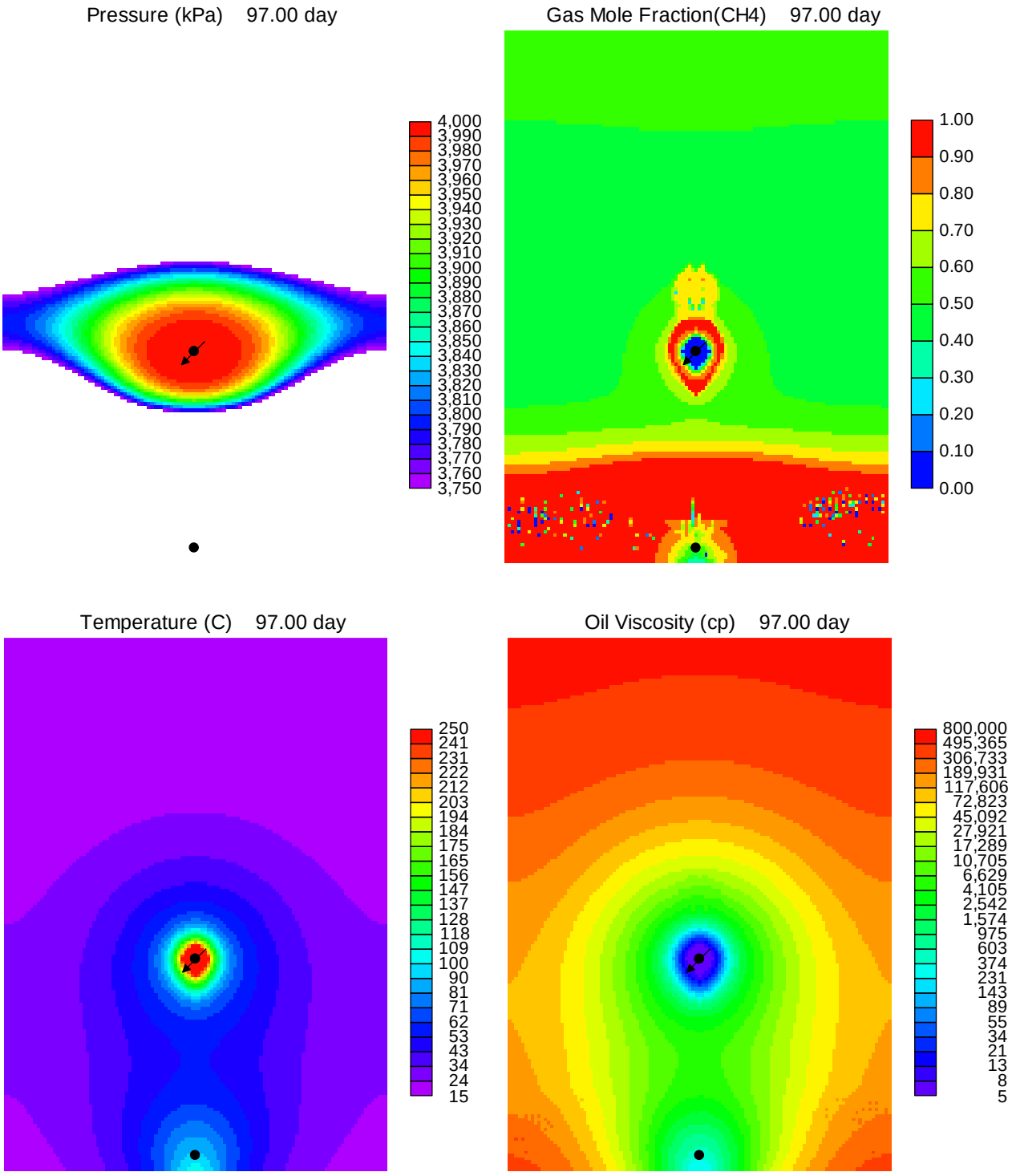

Figure 4-6 Case 1: Pressure, gas mole fraction solution gas, temperature, and oil visscosity distribution at Day 97.

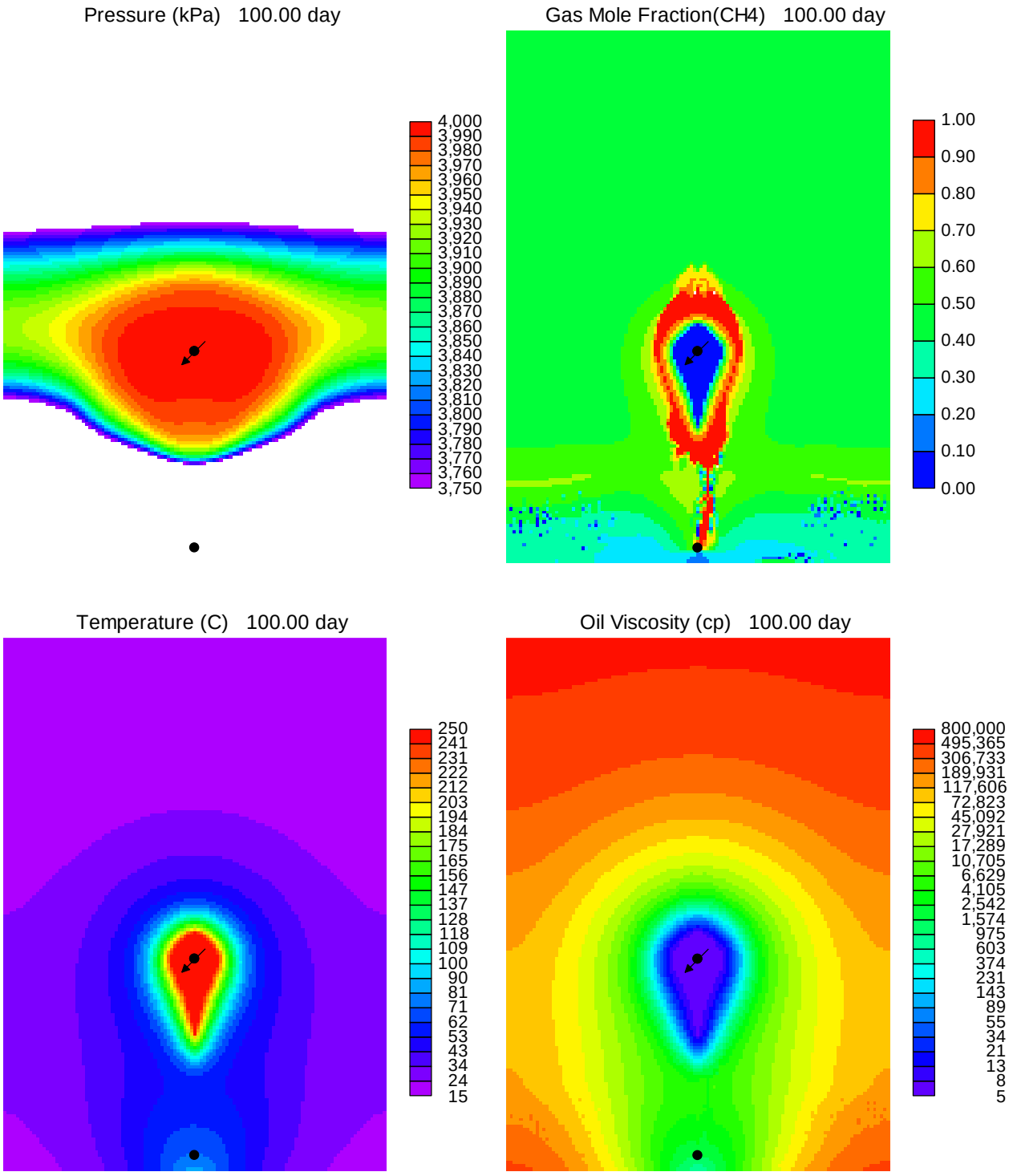

Figure 4-7 Case 1: Pressure, gas mole fraction solution gas, temperature, and oil viscosity distributions at Day 100.

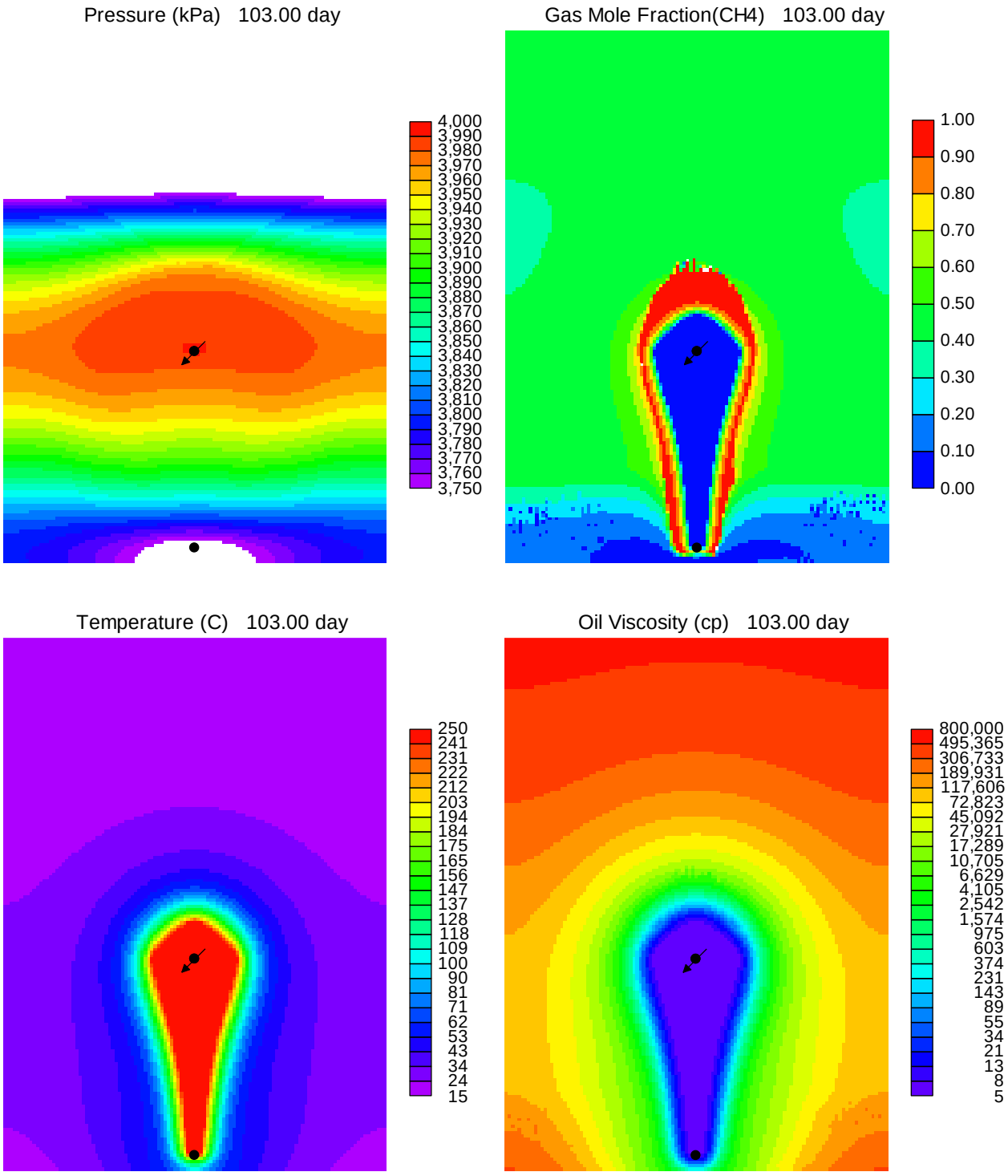

Figure 4-8 Case 1: Pressure, gas mole fraction solution gas, temperature, and oil viscosity distributions at Day 103.

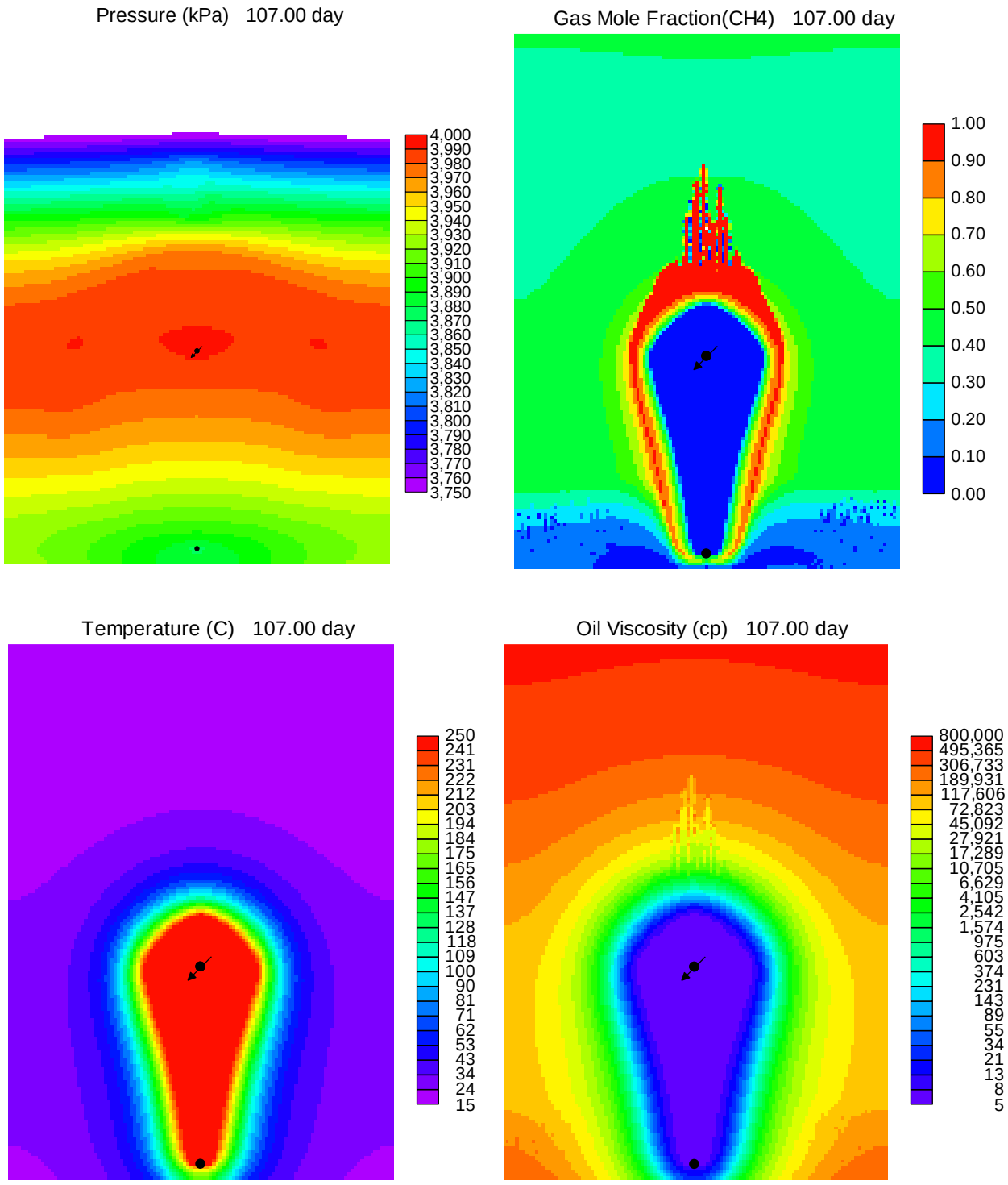

Figure 4-9 Case 1: Pressure, gas mole fraction solution gas, temperature, and oil viscosity distributions at Day 107.

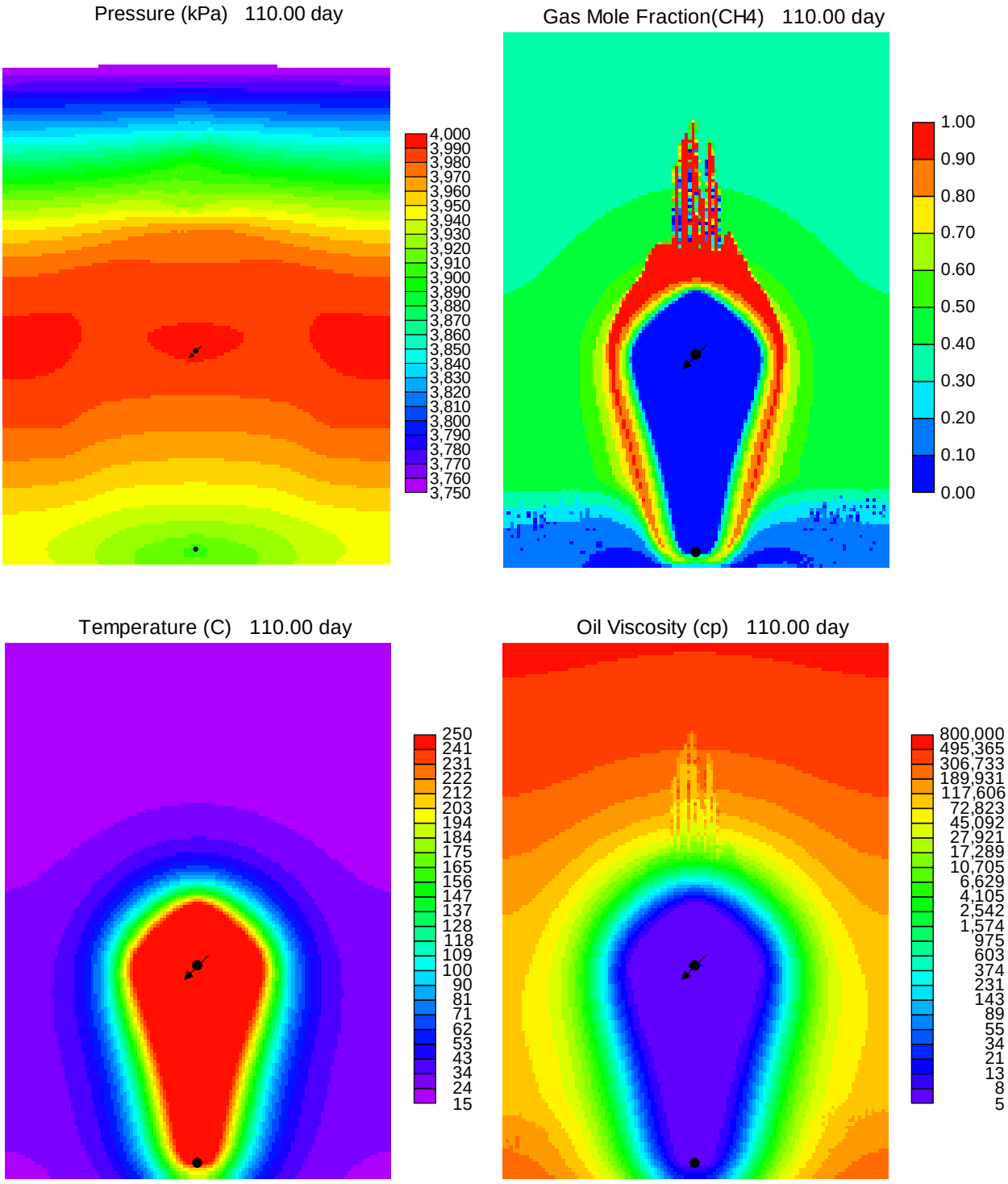

Figure 4-10 Case 1: Pressure, gas mole fraction solution gas, temperature, and oil viscosity distributions at Day 110.

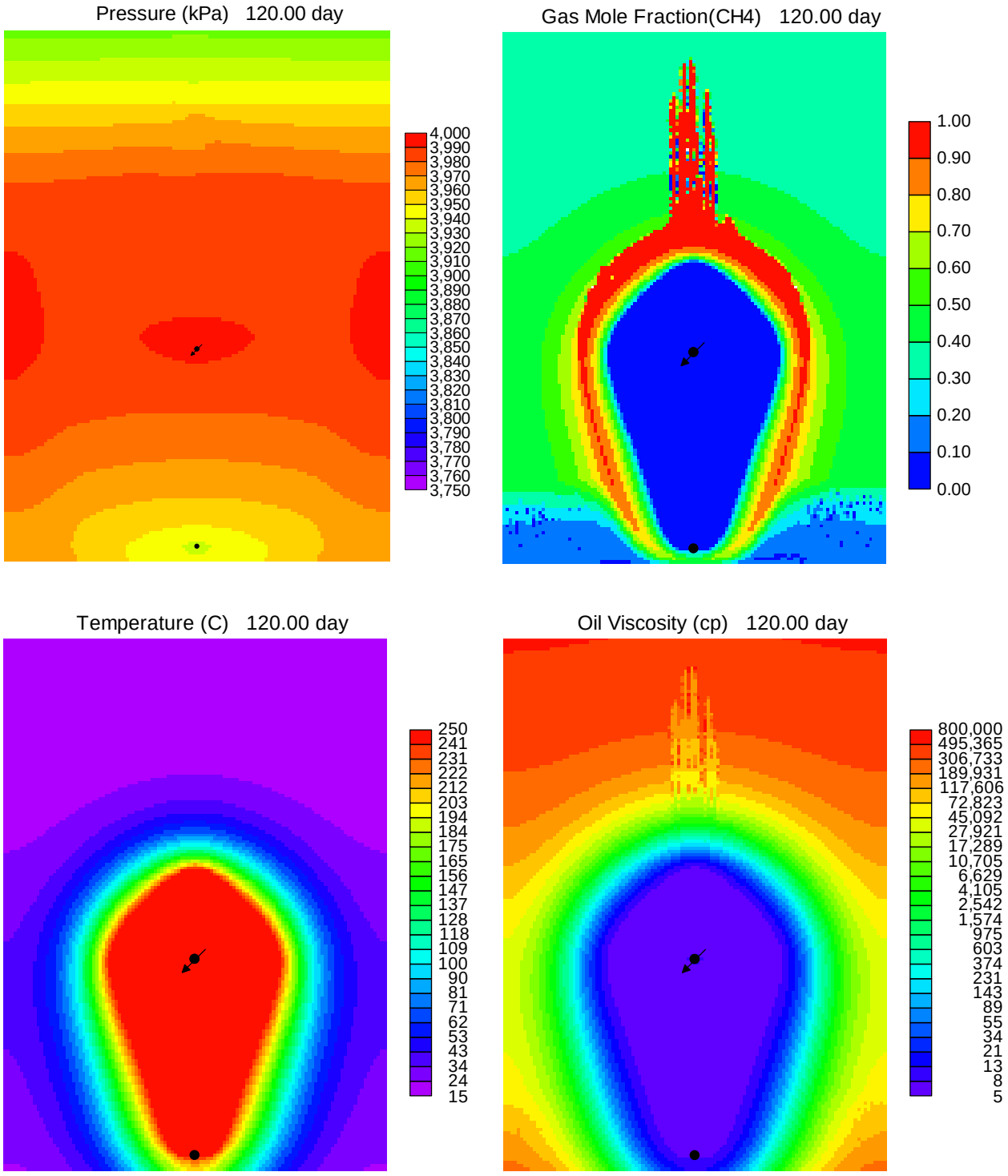

Figure 4-11 Case 1: Pressure, gas mole fraction solution gas, temperature, and oil viscosity distribution at Day 120.

Figure 4.11 displays the initial temperature in the reservoir after the steam circulation period for Case 2 (where the oil phase viscosity varies vertically in the reservoir). As with the homogeneous case, the region between the wells is heated to about 70°C providing sufficient oil mobility to move the bitumen enabling the creation of the depletion chamber. After Day 97, with the start of steam injection into the upper well, the pressure rises to 4,000 kPa near that well and the temperature and oil viscosity respond accordingly. By Day 100, as shown in Figure 4.13, as steam is being injected into the reservoir, even though the hot chamber (as indicated by the temperature distribution) has reached about 0.5 m below the injection well, the gas that exsolved from the oil due to heating fingers down to the production well. With a heterogeneous viscosity profile, the results are distinctly different from that of the homogeneous viscosity case. The distribution of the mole fraction of solution gas at above the hot chamber reveals the onset of instability with fingers of gas moving into the formation. A similar result is seen at Day 100 as displayed in Figure 4.13. The distribution of the oil viscosity also shows the start of oil viscosity variations which are not aligned with the temperature distribution thus showing that the temperature distribution is not sufficient to view the onset of instability. By Day 103, presented in Figure 4.14, the fingers at the top of the depletion chamber have grown but the extension of the chamber towards the production well is slower than that in the homogeneous viscosity case. Figure 4.15 shows the results at Day 107. At this point of time, the hot chamber has not yet still reached the production well yet there are gas phase fingers above the hot chamber. The fingers are smaller than that of the fingers that resulted in the homogeneous viscosity case. This suggests that the heterogeneous viscosity profile is blunting the instability – the system is still unstable but the growth rate of the instability is reduced. This is further seen at Day 110, shown in Figure 4.16, where the gas phase fingers are still evident but they are muted compared to the

homogeneous case. The results reveal that the chamber has reached the production well. After 120 Days, as shown in Figure 4.17, the gas phase fingers have grown further from the hot chamber but they are smaller than that achieved in the homogeneous viscosity case. The fingers are also evident from the distribution of oil viscosity. Despite the variability of the oil viscosity distribution, gas phase fingers resulted and grew as the process evolved which indicates instability of the system especially since the fingers are non-symmetric. These results indicate the potential for steam conformance issues even in reservoir with variable oil viscosity with homogeneous geological properties.

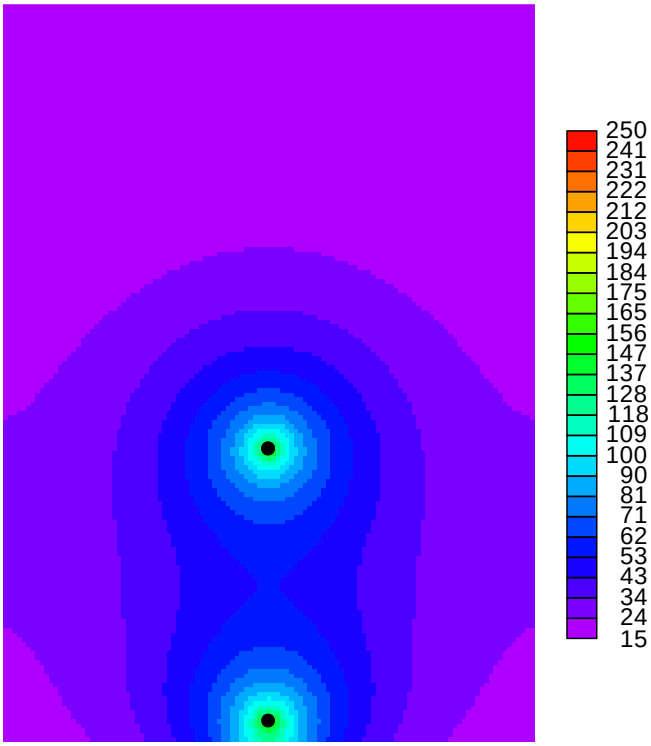

Figure 4-12 Case 2: initial temperature distribution after the steam circulation period.

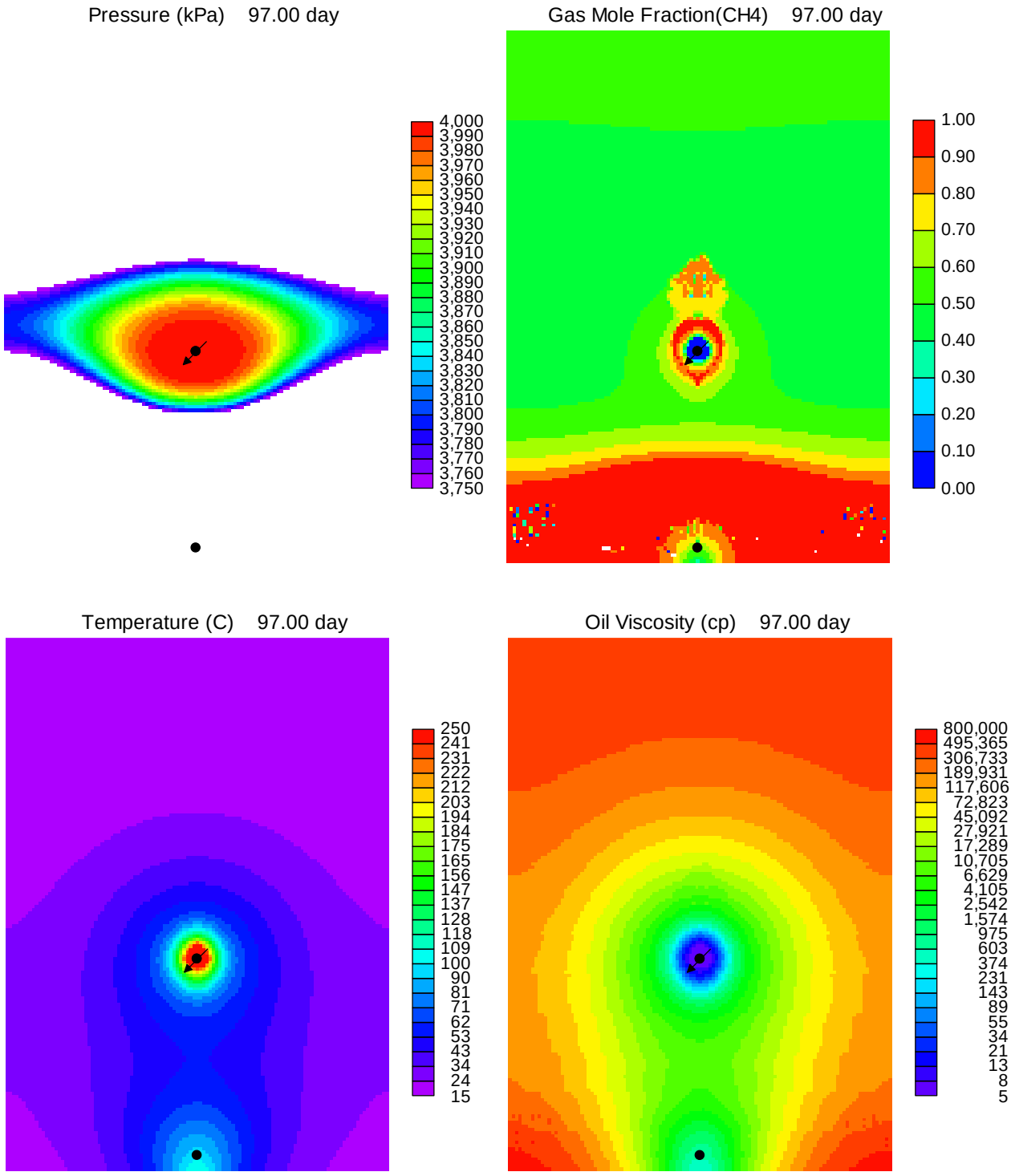

Figure 4-13 Case 2: Pressure, gas mole fraction solution gas, temperature, and oil viscosity distributions at Day 97.

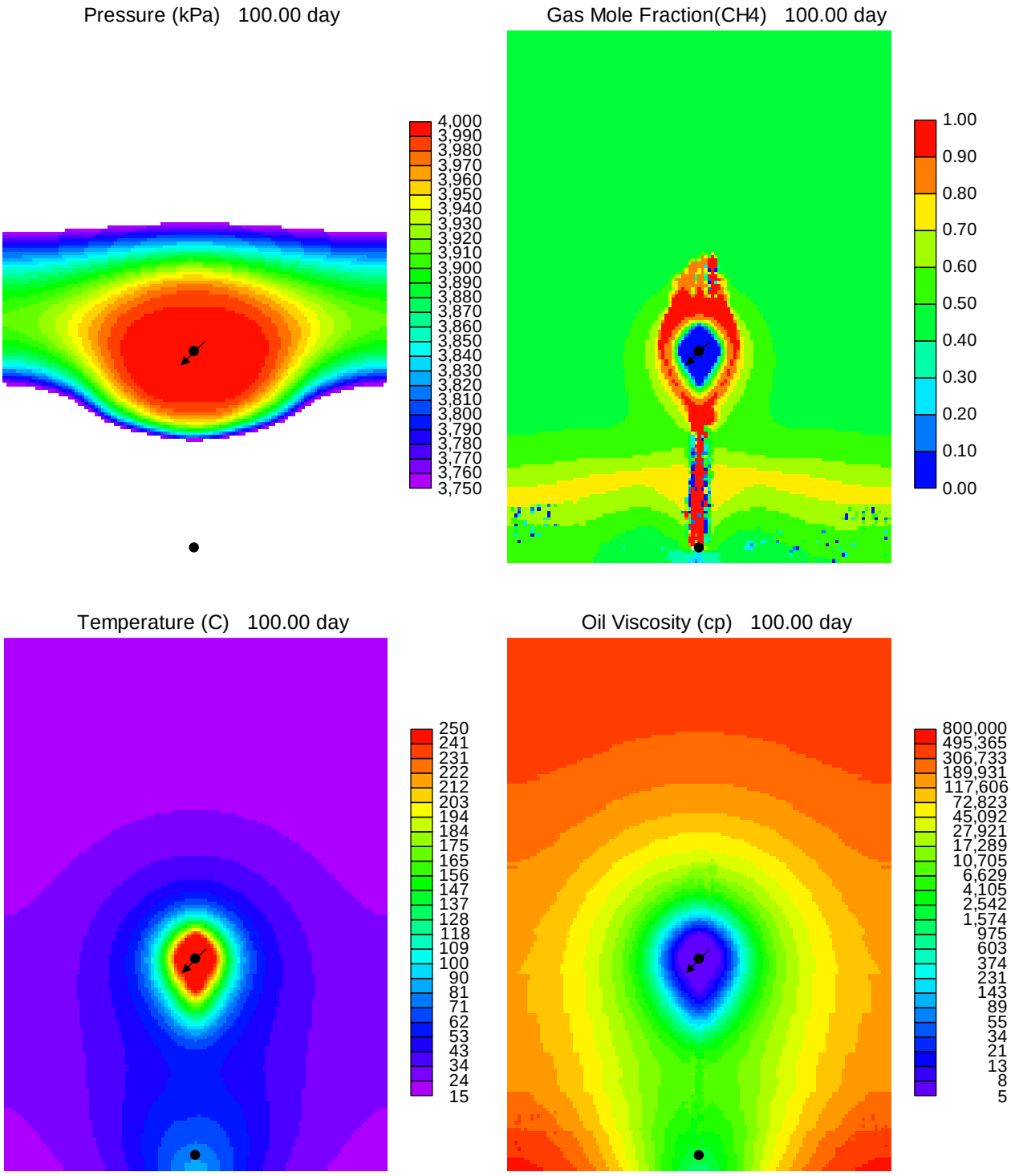

Figure 4-14 Case 2: Pressure, gas mole fraction solution gas, temperature, and oil viscosity distributions at Day 100.

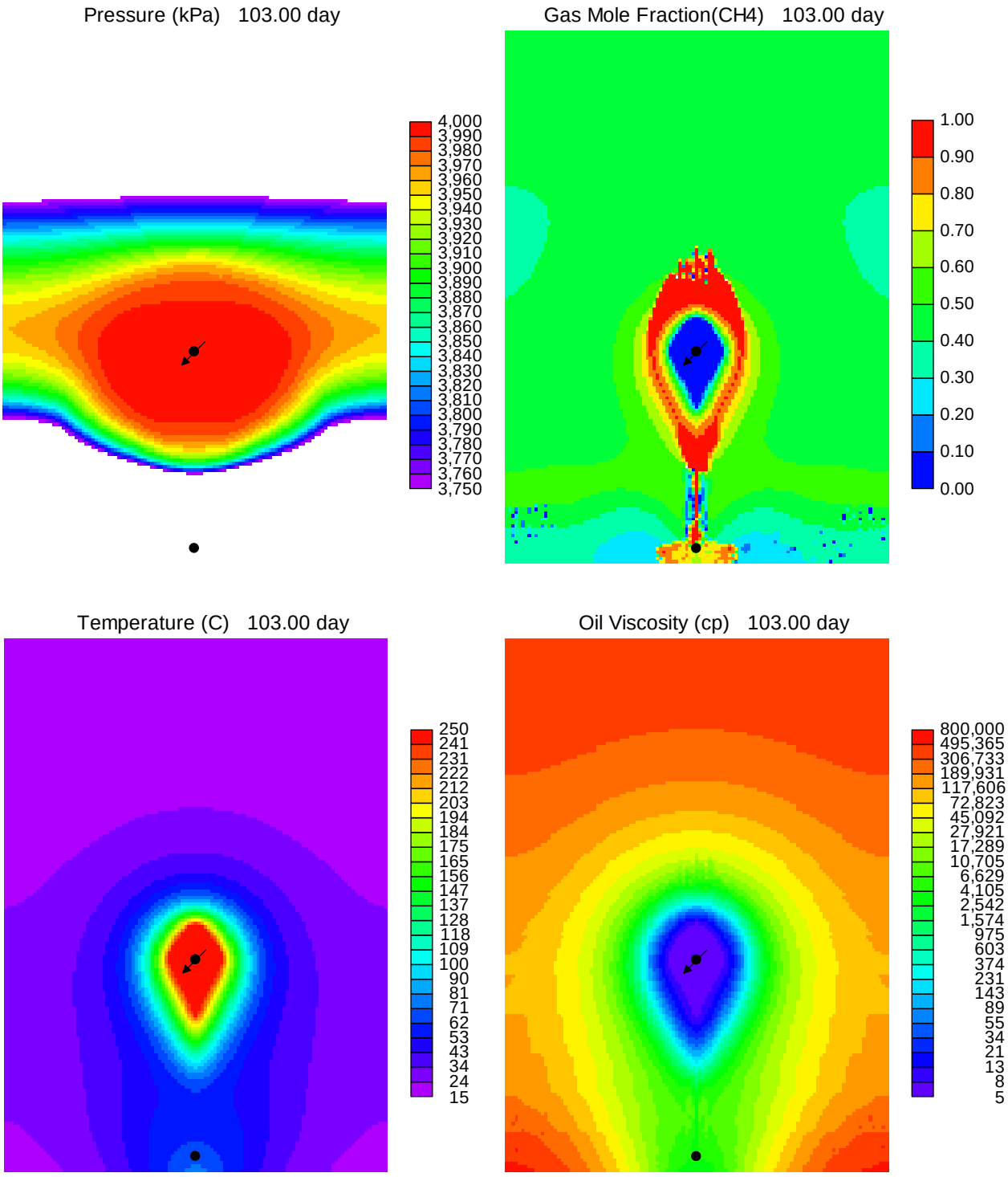

Figure 4-15 Case 2: Pressure, gas mole fraction solution gas, temperature, and oil viscosity distributions at Day 103.

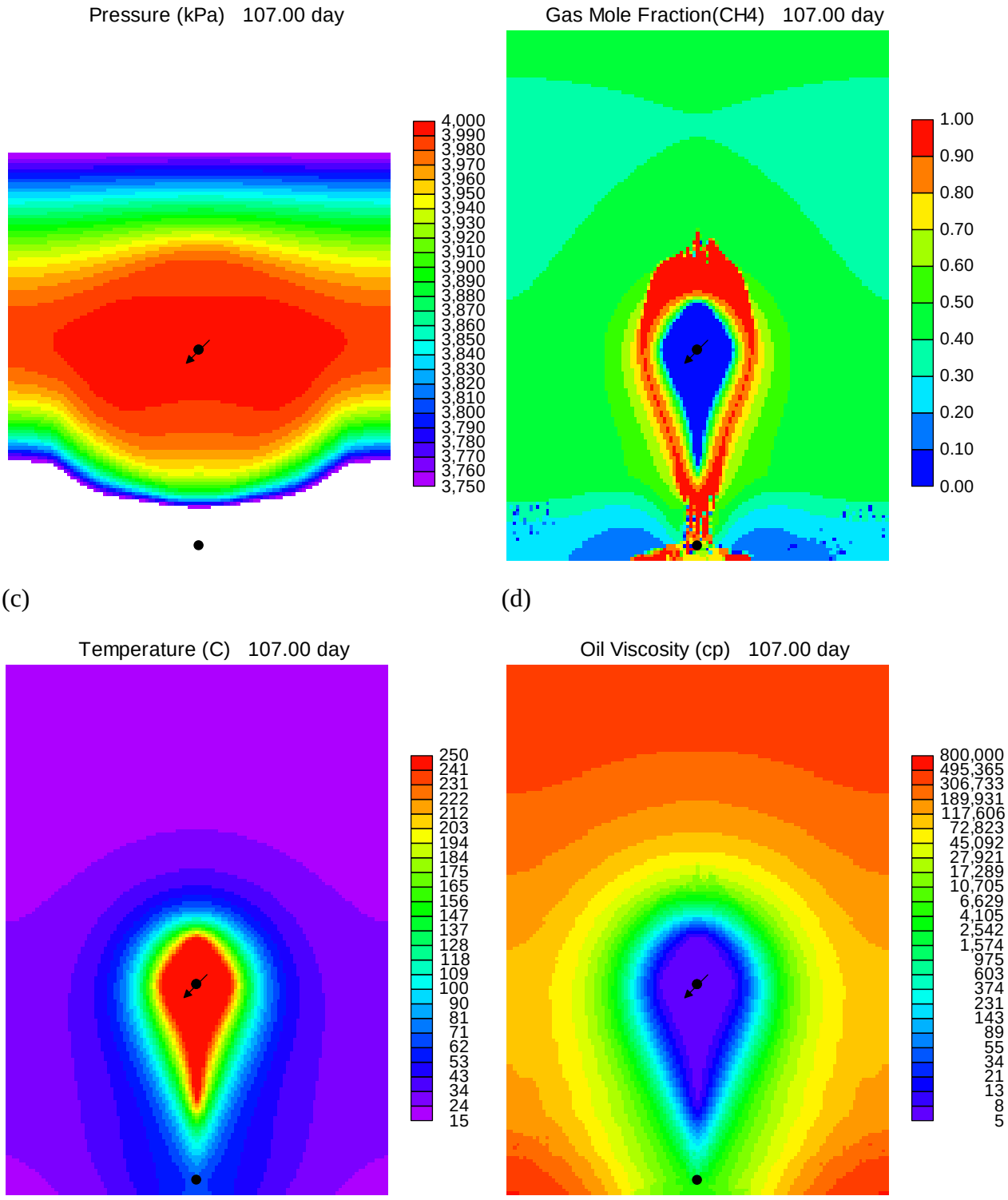

Figure 4-16 Case 2: Pressure, gas mole fraction solution gas, temperature, and oil viscosity distributions at Day 107.

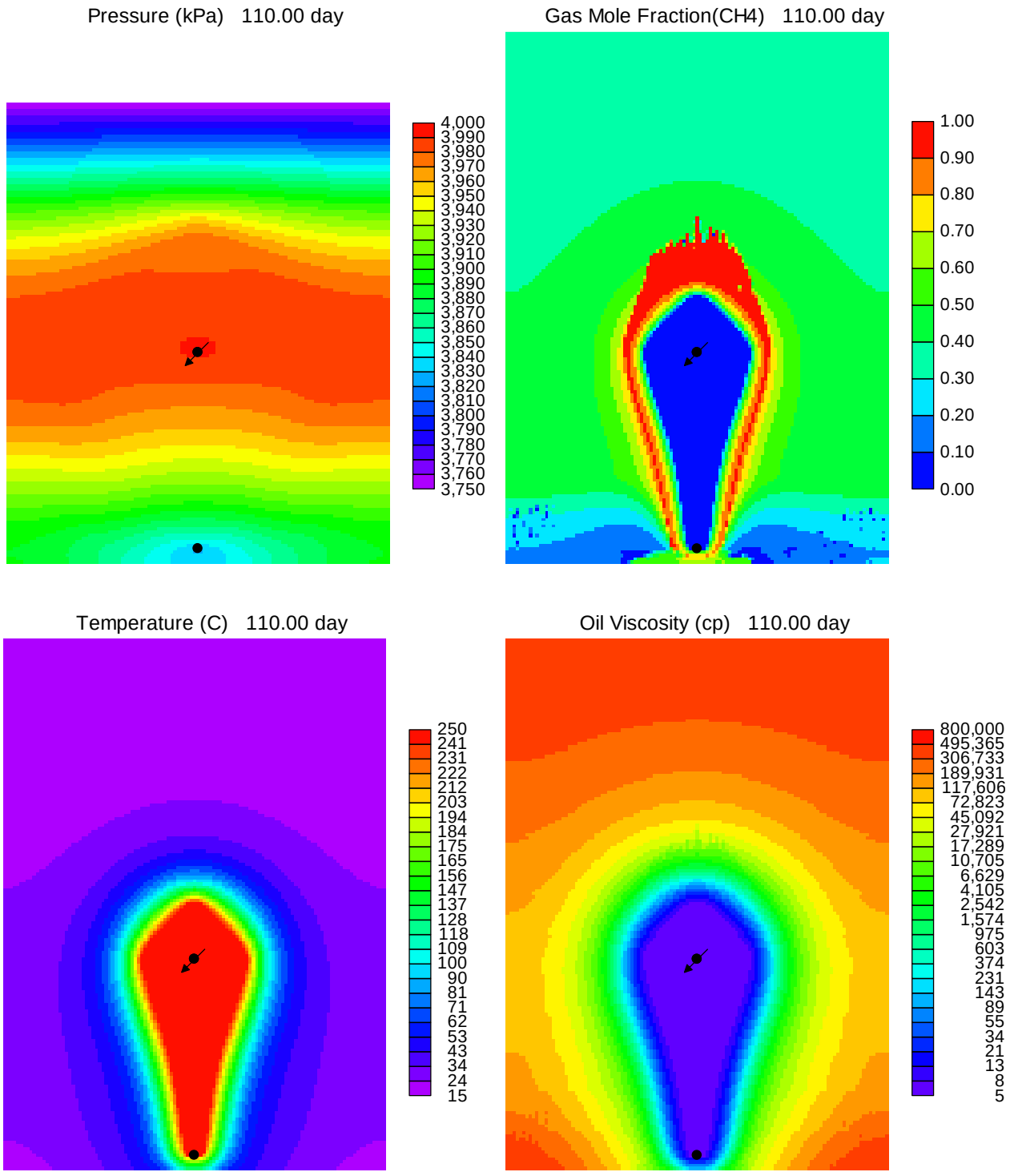

Figure 4-17 Case 2: Pressure, gas mole fraction solution gas, temperature, and oil viscosity distributions at Day 110.

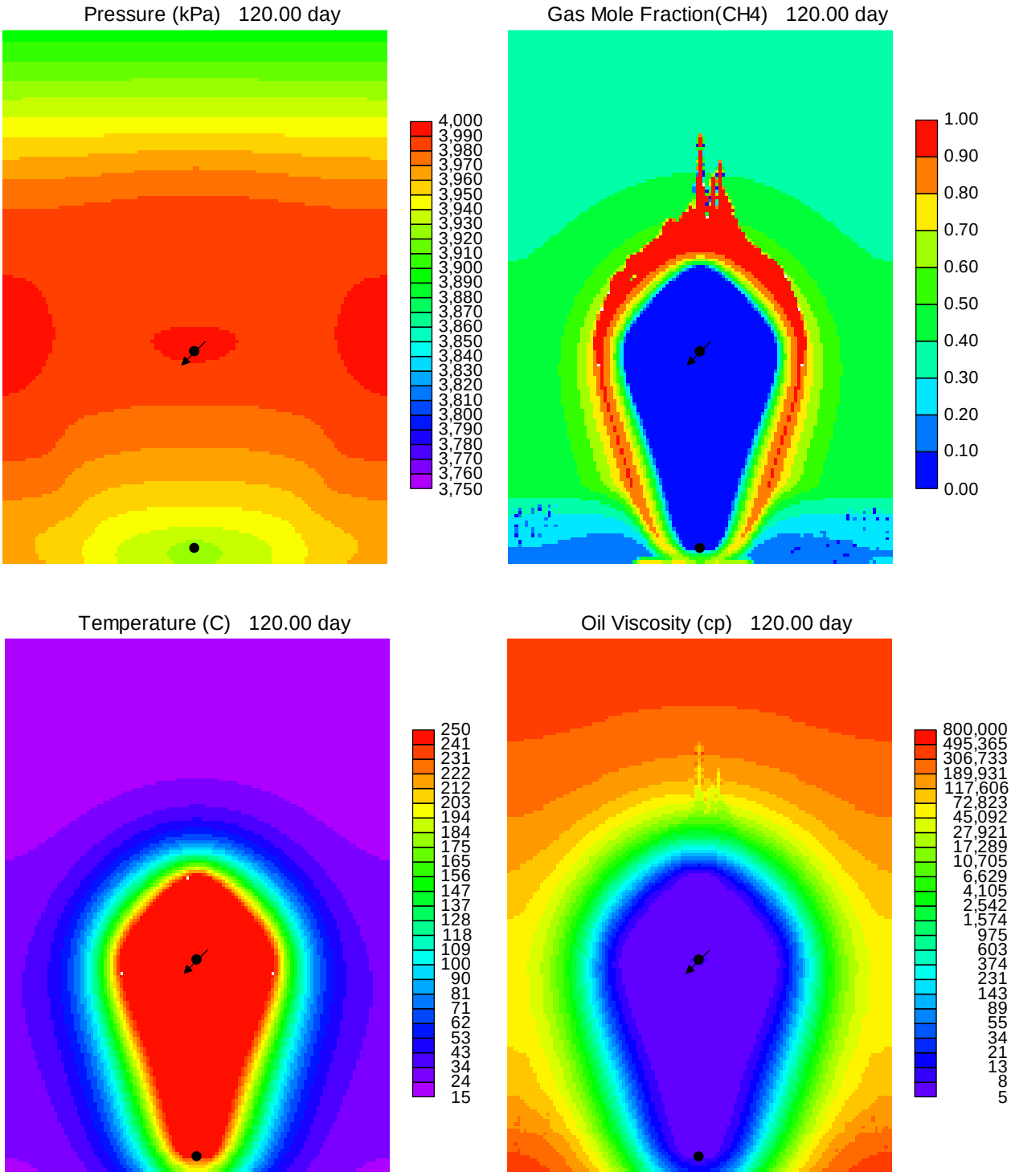

Figure 4-18 Case 2: Pressure, gas mole fraction solution gas, temperature, and oil viscosity distributions at Day 120.

Figure 4.18 displays the oil rates of Cases 1 and 2. The results show that the average oil rate per unit length of well is equal to about 0.2 m^3/day/m of well (this value is taken before Day 180 where the steam chamber has not yet largely emptied the model of oil). This value is very typical of that of oil productivity from SAGD wellpairs in Alberta. The difference between the homogeneous and heterogeneous viscosity cases is relatively small.

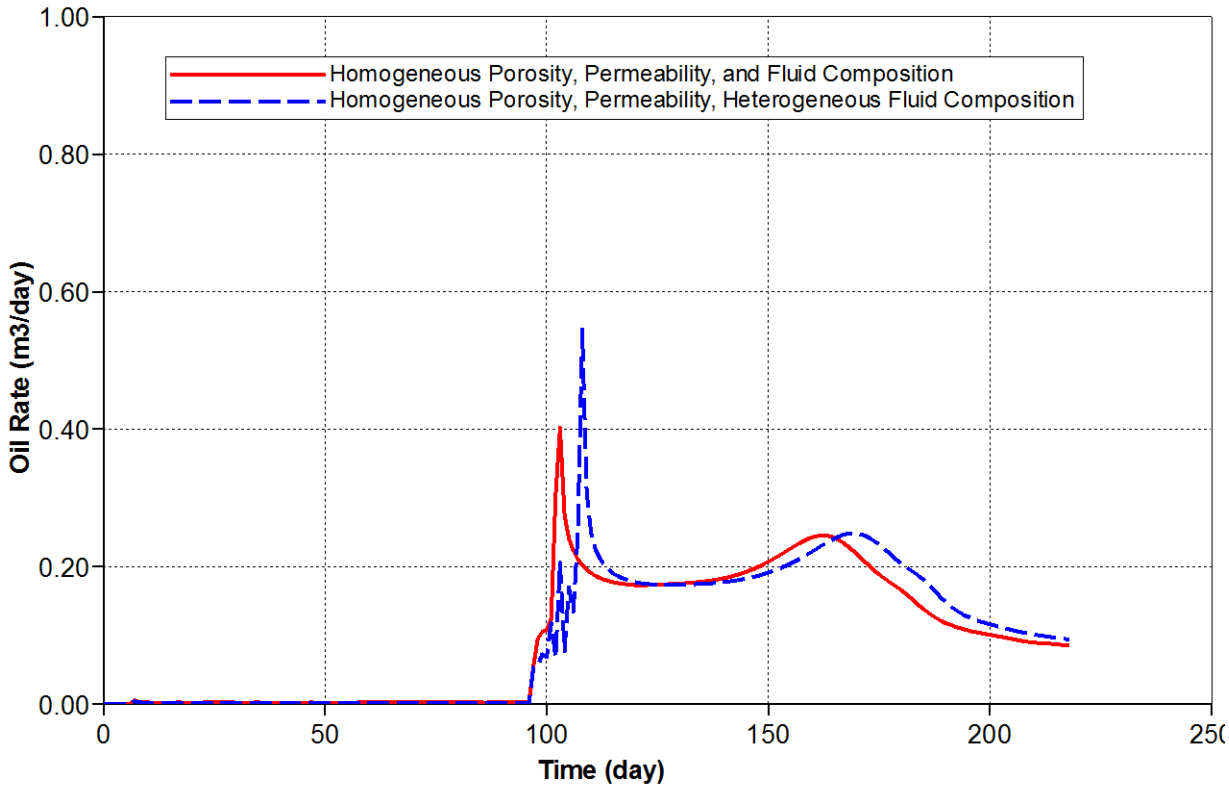

Figure 4-19: Case 1 and Case 2 oil rates. Since the model has a downwell dimension of 1 m, the rates are per m of wellpair length.

4.5 Discussion

The results from the analytical theory shows that when the steam quality is greater than 75%, that is, the volume is largely vapor phase, the system is unstable and as a consequence the edge of the chamber becomes wavy with subsequent growth of fingers. Past reservoir simulation studies have not seen the onset of fingers at the edges or top of the steam chamber. The results of the SAGD reservoir simulations, due to the scale of the grid blocks, have enabled the observation of fingering just beyond the edge of the chamber. Figure 4.19 displays the distribution of the mole fraction of solution gas in the gas phase for models with grid blocks with dimensions equal to 0.25 and 1 m.

The results make it clear that the fingering phenomena does not result when the grid block dimensions are too large. The surprising new result is that the fingering does not occur from the steam chamber but rather by the solution gas that exsolves from the oil just beyond the edge of the chamber due to the elevated temperature arising from conduction from the edge of the chamber. This gas, due to its low viscosity viscously fingers into the oil sand displacing mobile water. This added gas leads to a slight drop of the viscosity of the oil corresponding to the gas fingers within the reservoir. Thus, the analytical theory produces the correct result which at 100% quality (100% vapour steam) yields an unstable edge of the chamber but the region over which it happens is not at the edge of the chamber where the steam is condensing.

(a)

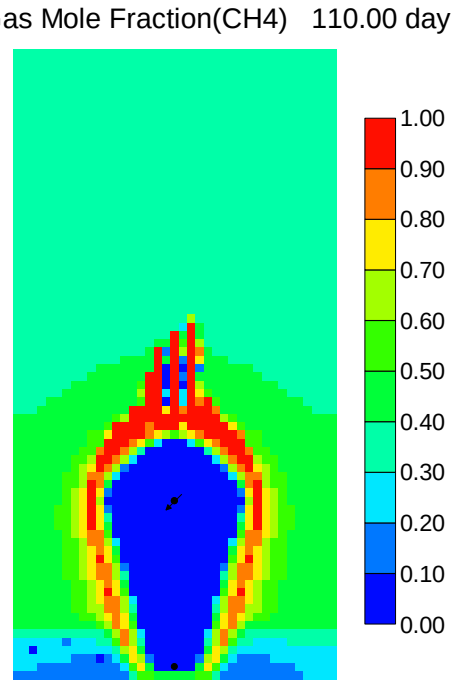

(b)

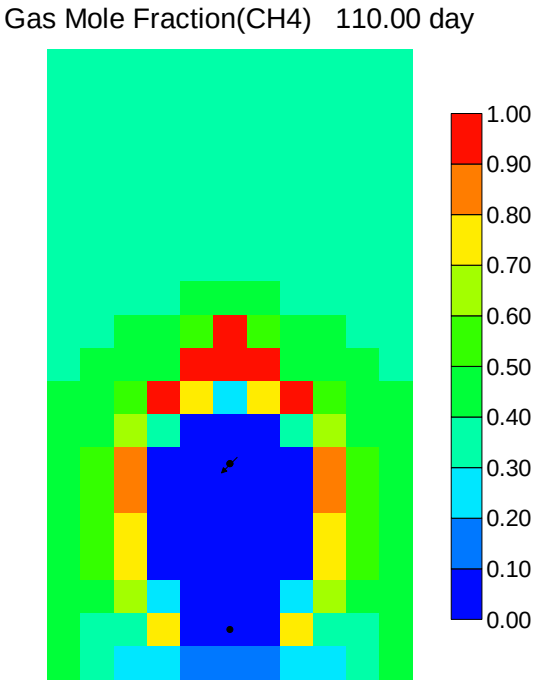

Figure 4-20: Distribution of mole fraction of solution gas in the gas phase for models with grid.block dimensions equal to (a) 0.25 m and (b) 1 m at Day 110. The viscosity is homogeneous in both cases.

As discussed earlier, there exist two potential causes for fingering a) Saffman-Taylor type, which occurs when a lower viscosity phase displaces a higher viscosity phase and b) Rayleigh-Taylor type, which occurs when a higher density phase is placed on top of a lower density one. We want to emphasize here that the fingering phenomena shown here involves both mechanisms. The results above demonstrate the fingering of lower viscosity oil into higher viscosity oil. Figure 4.20 displays the spatial distribution of the oil mass density at Day 120 for the homogeneous viscosity case. The results show that there exists higher density oil above lower density oil (and steam condensate and vapour). Thus both modes are playing a role in the onset and evolution of the instability.

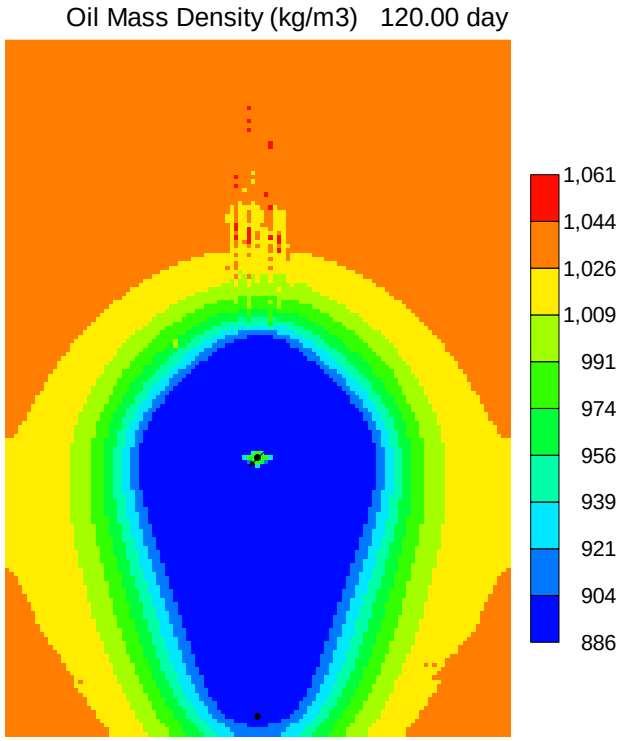

Figure 4-21: Distribution of oil mass density at Day 110 (Case 1).

The results show that non-uniform steam chambers can result in perfectly homogeneous reservoir which for many sounds counter intuitive. The reason for this is that the system is inherently unstable and as a consequence the steam conformance within the reservoir cannot be uniform – the perturbations grow within the chamber and as shown by the results of the research documented here, they result in non-symmetric growth of fingers from the chamber. The results also show that the primary site of growth of the instability is above the top of the chamber. At the sides of the chamber, no instability is evident. This is mainly associated with the pressure gradient that is greater in the vertical direction than that in the horizontal direction. This is due to the combination of the injected steam pressure versus the original reservoir pressure as well as the hydrostatic pressure (the pressure is lower at shallower depths). If the lateral pressure gradient was greater, there is potential that side-directed instabilities could occur. This could be the case in Cyclic Steam Stimulation (CSS) operations where injection pressures reach as high as 13 MPa and production pressures drop as low as 0.5 MPa and injection and production wells could be separated by of order of a few hundreds of meters. With this pressure gradient, there is potential that instability sideways from the chamber could occur. This coupled with steam fracturing might explain why early cycle CSS performs better than SAGD with respect to thermal efficiency. This will be examined in future work.

4.6 Conclusions

In this chapter, we mainly discussed another type of instability—Rayleigh-Taylor instability and its extension to the SAGD process. The conclusions of the research are as follows:

1. Both linear and nonlinear instability analysis demonstrates that instability occurs at the edge of steam chambers which leads to non-uniform chambers even in homogeneous reservoirs.
2. The instability is more focused above the top of the reservoir where the pressure gradient is highest.
3. The instability takes place in the gas phase beyond the edge of the hot steam chamber in the gas zone that is created due to gas exsolution.
4. The growth rate of the instability appears to be reduced when the viscosity of the oil is heterogeneous.
5. The results suggest that non-ideal steam conformance may occur in perfectly homogeneous reservoirs.
6. The nonlinear instability that is exhibited by the fine grid reservoir simulation results can be triggered by the difference in either viscosity (Saffman-Taylor) or density (Rayleigh-Taylor).
7. To observe fingering at the edges of depletion chambers in steam-based recovery processes, fin grid simulations are required. Given that the fingers are of order of 30 cm in width, this implies grid blocks of this order of length scale.

Chapter Five: **Conclusions and Recommendations**

The main theme of this thesis is to investigate the occurrence of fluid mechanical instability at the edge of steam chamber.

The conclusions from the research documented in this thesis are as follows:

1. Even at low Reynolds' number (equal to about 1 as expected in a pore containing steam and mobilized bitumen), the flow is unstable at pore scales.
2. The larger is the convective heat transfer relative to conductive heat transfer, the less stable is the system.
3. The smaller is the ratio of interfacial forces relative to inertial forces, the greater is the growth rate of the instability in the pore.
4. The larger is the inclination, the greater is the growth rate of the instability.
5. Both linear and nonlinear instability analysis demonstrates that instability occurs at the edge of steam chambers which leads to non-uniform chambers even in homogeneous reservoirs.
6. The instability is more focused above the top of the reservoir where the pressure gradient is highest.
7. The instability takes place in the gas phase beyond the edge of the hot steam chamber in the gas zone that is created due to gas exsolution.
8. The growth rate of the instability appears to be reduced when the viscosity of the oil is heterogeneous.
9. The results suggest that non-ideal steam conformance may occur in perfectly homogeneous reservoirs.

10. The nonlinear instability that is exhibited by the fine grid reservoir simulation results can be triggered by the difference in either viscosity (Saffman-Taylor) or density (Rayleigh-\Taylor).
11. To observe fingering at the edges of depletion chambers in steam-based recovery processes, fin grid simulations are required. Given that the fingers are of order of 30 cm in width, this implies grid blocks of this order of length scale.

The recommendations of the research documented in this thesis are:

1. Thermal reservoir simulation models should be of sufficiently fine grid block dimensions to capture instability. It is recommended that fine grid models are used (with spacing at least as small as 10 cm) to observe the fingering phenomena. Also, it is recommended that further research is done on upscaling fingering and instability phenomena for steam recovery processes.
2. Linear stability analysis should be extended to the role of solution gas at the edge of the steam chamber.
3. Further studies should be done to determine if well orientation and placement can be used to take advantage of instabilities to yield improved steam conformance along wells.
4. Further study is required to connect results at pore scale to those at continuum scales.

References

Alberta Energy Regulator 2014. Alberta's Energy Reserves 2013 and Supply/Demand Outlook 2014–2023

Anand, J., Somerton, W.H., and Gomaa, E., "Predicting Thermal Conductivities of formations from Other Known Properties," SPEJ, Vol. 13, No. 5, October 1973, pp. 267-273.

Beattie, C.I., Boberg, T.C., and McNab, G.S. 1991. Reservoir Simulation of Cyclic Steam Stimulation in the Cold Lake Oil Sands. *SPE Res Eng 6 (2): 200–206. SPE-18752-PA*

Bois A., Tec C. Mainguy M., 2013. Importance of Thermal Consolidation of Shale During SAGD Process. *Paper SPE 150420 presented at the SPE Heavy Oil Conference and Exhibition. Kuwait City, Kuwait. 12-14 December 2011.*

Butler, R.M. 1987. Rise of interfering steam chambers *SPE JCPT, paper 87-03-07.*

Butler, R.M. 1994. Horizontal wells for the recovery of oil, gas, and bitumen. *Petroleum Society of the Canadian Institute of Mining, Metallurgy and Petroleum, Calgary Section Monograph 2, 169-199.*

Chung, K.H., and Butler, R.M. 1987, Geometrical effect of steam injection on the formation of emulsions in the steam-assisted gravity drainage process: *Paper 87-38-22., 38th Ann. Tech. Meet. Of the Pet. Soc. of CIM, Calgary June.*

Cenovus, AER In-situ performance presentation, 2013

Cokar, M., Kallos, M.S., and Gates, I.D. Reservoir Simulation of Steam Fracturing in Early Cycle Cyclic Steam Stimulation. SPE Reservoir Evaluation & Engineering-Reservoir Engineering, 15(6):676-687, 2012.

ConocoPhillips, AER In-situ performance presentation, 2013

Devon Canada, AER In-situ performance presentation, 2013

Dongarra, J. Straughan B., Walker, D.W. 1996 Chebyshev tau-QZ algorithm methods for calculating spectra of hydrodynamic stability problems, *Applied Numerical Mathematics 22 (4) 399-435 1999, ISSN 0168-9274*

Edmunds, N.R. 1998, Investigation of SAGD steam trap control in two and three dimensions, *Paper SAPE 50413 presented at the SPE international conference on horizontal well technology, Calgary 1-4 November*

Edmunds, N.R. 1999, On the difficult birth of SAGD, *JCPT 38(1), January.*

Edmunds, N.R. 2006, Analysis of the solution gas effect on SAGD slope drainage rate, *Paper 2006-406, World Heavy Oil Conference, Beijing Nov 2006*

Etminan, S., Haghighat, P., Maini, B. , Chen Z. Molecular Diffusion and Dispersion Coefficient in a Propane-Bitumen System: Case of Vapour Extraction (VAPEX) Process, *SPE EUROPEC/EAGE Annual Conference and Exhibition, 23-26 May, Vienna, Austria*

Farouq-Ali, S.M., 1997. Is there life after SAGD, *JCPT 36 (6) (97-06-DAS., June)*

Gates, I. D., 2011. Basic Reservoir Engineering, *Kendall Hunt Publishing Company*

Gates, I.D., Kenny, J., Hernandez-Hdez, I.L., Bunio, G.L. 2005, Steam-injection strategy and energetics of steam-assisted gravity drainage: *SPE/PS-CIM/CHOA 97742, SPE/PS-CIM/CHOA Int. Thml. Opr. And Heavy Oil Sym. Calgary Canada. Nov.*

Gates, I.D., Leskiw. C. 2010, Impact of steam trap control on performance of steam-assisted gravity drainage: *J. Pet. Sci. Eng. 75 (1-2): 215-222*

Gates, I.D. 2013 Basic Reservoir Engineering. ISBN: 978-1-4652-3684-5.

Gotawala, D. and Gates, I.D., 2008, Steam Fingering in Steam-Assisted Gravity Drainage. *Canadian Journal of Chemical Engineering, 86:1011-1022*

Gupta, S.C. and Gittins, S.D., Christina Lake SolventAided Process Pilot, *JCPT, Vol. 38, No. 13, pp. 44-53,September 1999.*

Hein, F.J. 2006. Heavy oil and oil (tar) sands in North America: An overview and summary of contributions: Natural Resources Research, v. 15, no. 2, p.67-84, doi: 10.1007/s11053-006-9016-3

Hejazi, S.H. and J. Azaiez (2012). Stability of reactive interfaces in saturated porous media under gravity in the presence of transverse flows*: J. of Fluid Mech., Vol. 695, 439-466.*

Hill, S. 1952, Channeling in packed columns. Chemical Engineering Science 1 (6*), 247-253*

Hubbard S.M., Smith D.G., Nielsen H., Leckie D.A., Fustic M., Spencer R.J., Bloom L. 2011. Seismic geomorphology and sedimentology of a tidally influenced river deposit, Lower Cretaceous Athabasca oil sands, Alberta, Canada. *The American Association of Petroleum Geologists. V. 95, No. 7, PP. 1123-1145.*

Imperial Oil, AER In-situ performance presentation, 2013

Islam, M.N. and Azaiez, J., 2006 Nonlinear simulation of thermo-viscous fingering in nonisothermal miscible displacements in porous media. *In: SPE Annual Technical Conference and Exhibition, San Antonio, TX, USA, SPE-97729*

Ito, Y., Ipek, G. 2005, Steam-fingering phenomenon during SAGD process, *SPE/PS-CIM/CHOA 97729, SPE/PS-CIM/CHOA Int. Thml. Opr. And Heavy Oil Sym. Calgary Canada. Nov*

Ito, Y., Suzuki, S. 1999, Numerical simulation of the SAGD process in the Hangingstone oil sands reservoir, *J Can Pet Technol 38 (9): 27-35. Petsoc-99-09-02.*

Ito, Y., Suzuki, S. 1996, Numerical simulation of the SAGD process in the Hangingstone oil sands reservoir, *Paper 96-57, 47th Ann, Tech. Meet. Of the Pet. Soc., in Calgary, Alberta, Canada, June*

Irani, M. and Gates, I.D. Understanding the Convection Heat Transfer Mechanism in Steam-Assisted Gravity Drainage (SAGD) Process. *SPE Journal, 18(6):1202-1215, 2013.*

Irani, M. and Gates, I.D. On the Stability of the Edge of a SAGD Steam Chamber. *Accepted. SPE Journal, August 2013.*

Leaute, R.P. and Carey, B.S. 2005. Liquid addition to steam for enhancing recovery (LASER) of bitumen with CSS: Results from the first pilot cycle. *Paper 2005-161 presented at the 56th Canadian International Petroleum Conference (CIPC), Calgary, 7–9 June.*

Mehrotra, A.K. and W.Y. Svrcek, 1986, Viscosity of compressed Athabasca bitumen, *Canadian Journal of Chemical Engineering, 64(5), 844-847.*

Nakamura,N., Zhu, D., 2010, Finite-Amplitude Wave Activity and Diffusive Flux of Potential Vorticity in Eddy–Mean Flow Interaction, *Journal of Atmospheric Sciences, 67, 2701-2716*

Nakamura,N., Zhu, D., 2010, Formation of Jets through Mixing and Forcing of Potential Vorticity: Analysis and Parameterization of Beta-Plane Turbulence, *Journal of Atmospheric Sciences, 67, 2717-2733*

Nasr, T. and Isaacs, E. 2001 Process For Enhancing Hydrocarbon Mobility Using a Steam Additive. *U.S. Patent* 6230814

O´Connor, P. A., 2001. Constant-Pressure Measurement of Steam-Water Relative Permeability. Stanford Geothermal Program, Stanford University, USA. Report: SGP-TR-169.

Orr, W.M.F. 1907 The stability or instability of the steady motions of a perfect liquid and of a viscous liquid. Part I: A perfect fluid. Part II: A viscous fluid. *Proc. R. Irish. Acad. A 27 9-138*

Pritchard, D. 2004, The instability of thermal and fluid fronts during radial injection in a porous medium, *Journal of Fluid Mechanics 508, 133-163*

Saffman, P.G. Taylor, G.I. 1958 The penetration of a fluid into a porous medium or Hele-Shaw cell containing a more viscous liquid, *Proceedings of the Royal Society 245 (1242), 312-329*

Sasaki, K., Akibayashi, S., Yazawa, N. Doan, Q.T., Farouq Ali, S.M., 2001, Experimental modeling of the SAGD process—enhancing SAGD performance with periodic stimulation of the horizontal producer, *SPE 69742 SPEJ March*

Sharma, J. and Gates, I.D. Convection at the Edge of a SAGD Steam Chamber. *SPE Journal, 16(3):503-512, 2011.*

Somerton, W.H., Keese, J.A., and Chu, S.L., "Thermal Behavior of Unconsolidated Oil Sands," SPEJ, Vol. 14, No. 5, October 1974, pp. 513-521.

Sommerfeld, A. 1908 Ein Beitrag zur hydrodynamischen Erklarung derturbulenten Flussigkeitbewegungen. *In Att. Del 4. Congr. Internat. Dei Mat. III, pp. 116-124 Roma*

Su Y., Wang J. Y., Gates I.D., 2012. SAGD Well Placement in Ultra-Defined Point Bar Deposit. Paper SPE 157857 presented at the SPE Heavy Oil Conference. Calgary, Alberta, Canada 12-14 June 2012

Wang, Z. 2011 Stability analysis of two-layer immiscible viscous fluids in an inclined closed tube, *WHOI GFD summer school*

Weideman, J.A., Reddy, S.C. 2000, A MATLAB differentiation matrix suite, *ACM Transactions on Mathematical Software (TOMS), Vol 26, Issue 4, 465-519.*

Appendix A: Matlab Code

Growthrate.m

```
clear
nbre=100;
nbal=100;

renolds=1;

alpha=linspace(0.000,30,nbal);

p=0;

%pe=[1.35,1.4,0.1,1.5,1.55];
gr=zeros(1,nbal);
   p=0
for i=1:nbal

       gr(i)=alpha(i)*(min(eigencomp(renolds,alpha(i),10)),2000)
   p=p+1

end

plot(alpha,gr,'b','linewidth',3)
xlabel('Wavenumber','fontsize',20)
ylabel('Growth Rate','fontsize',20)
xlim([0,30])
ylim([0,15*10^6])
set(findobj('type','axes'),'fontsize',15)
```

eigencomp.m

```
function st=eigencomp(Re,kx,Pe)

[AR,AI,BR,BI]=matgentest15(Re,kx,Pe);


%QZ-factorization
[AA,BB,Q,Z]=qz((AR+1i*AI),(BR+1i*BI));

k=size(AA,1);
S=[];
dia=diag(AA);
```

```
dib=diag(BB);
for i=1:k
   if(dib(i)~=0)
      S=[S,dia(i)/dib(i)];
   end
end

stt=sort(imag(S),'descend');
st=stt(1);
```

matgentest15.m

```
function [AR,AI,BR,BI]=matgentest15(Re,kx,Pe)


%clear all
N=100;%number of collocation points in wall normal direction (new)

theta=pi/4;

%Matrix parameters
n=1; %h2/h1
m=440; %nu2/nu1
gamma=1000; %rho2/rho1

a=kx;
F=0.1;
S=10;
wb=0.1;
%Re=100;

qo=0.9;
sor=3.5;
qs=sor*qo;

a1=-(6*m*(qo-qs))/(m+1)-3*(m*qo+qs)/2;
a2=(6*m*(qo-qs))/(m+1);
a3=3*(m*qo+qs)/2;


u1=cos(theta)*a1*((yvec+1)/2).^2+a2*((yvec+1)/(-2))+a3;

b1=-(6*(qo-qs))/(m+1)-3*(m*qo+qs)/2;
b2=(6*(qo-qs))/(m+1);
b3=3*(m*qo+qs)/2;

u2=cos(theta)*b1*((n*yvec+n)/2).^2+b2*((n*yvec+n)/2)+b3;


U0=1*cos(theta);
U1P=a2*cos(theta);
U2P=b2*cos(thata);
```

```
U1PP=2*a1*cos(theta)*ones(1,N+1);
U2PP=2*b1*cos(theta)*ones(1,N+1);


TP=-0.5;

AR=zeros(5*(N+3),5*(N+3));
AI=zeros(5*(N+3),5*(N+3));
BR=zeros(5*(N+3),5*(N+3));
BI=zeros(5*(N+3),5*(N+3));



AR11=[4*D2(1:N+1,1:N+3)-a^2*eye(N+1,N+3) -eye(N+1,N+3) zeros(N+1,N+3) zeros(N+1,N+3)
zeros(N+1,N+3)];
AR12=[ones(1,N+3) zeros(1,N+3) zeros(1,N+3) zeros(1,N+3) zeros(1,N+3)];
AR13=[((0:N+2)).^2 zeros(1,N+3) zeros(1,N+3) zeros(1,N+3) zeros(1,N+3)];


AR21=[zeros(N+1,N+3) 4*D2(1:N+1,1:N+3)-a^2*eye(N+1,N+3) zeros(N+1,N+3) zeros(N+1,N+3)
zeros(N+1,N+3)];
AR22=[(-1).^[(0:N+2)] zeros(1,N+3) (-1).^[(1:N+3)] zeros(1,N+3) zeros(1,N+3)];
AR23=[2*a^2*(-1).^[(0:N+2)] (-1).^[(0:N+2)] -2*a^2*m*(-1).^[(0:N+2)] -m*(-1).^[(0:N+2)] zeros(1,N+3)];

AR31=[zeros(N+1,N+3) zeros(N+1,N+3) 4/n^2*D2(1:N+1,1:N+3)-a^2*eye(N+1,N+3) zeros(N+1,N+3)
zeros(N+1,N+3)];
AR32=[zeros(1,N+3) zeros(1,N+3) ones(1,N+3) zeros(1,N+3) zeros(1,N+3)];
AR33=[zeros(1,N+3) zeros(1,N+3) ((0:N+2)).^2 zeros(1,N+3) zeros(1,N+3)];

AR41=[zeros(N+1,N+3) zeros(N+1,N+3) zeros(N+1,N+3) 4/n^2*D2(1:N+1,1:N+3)-a^2*eye(N+1,N+3)
zeros(N+1,N+3)];
AR42=[-2*a^2*(-1).^[(0:N+2)-1].*[(0:N+2)].^2 (-1).^[(0:N+2)-1].*[(0:N+2)].^2 -2*m/n*a^2*(-1).^[(0:N+2)-
1].*[(0:N+2)].^2 m/n*(-1).^[(0:N+2)-1].*[(0:N+2)].^2 zeros(1,N+3)];
AR43=wb*[(U0-1/(U2P-U1P)*((1-gamma)*sin(theta)/F^2+a^2))*(-1).^[(0:N+2)-1].*[(0:N+2)].^2+1/2*(U1P-
gamma*U2P)*(-1).^[(0:N+2)] zeros(1,N+3) (U0*gamma/n-1/(U2P-U1P)*(1/n)*((1-
gamma)*sin(theta)/F^2+a^2))*(-1).^[(0:N+2)-1].*[(0:N+2)].^2 zeros(1,N+3) zeros(1,N+3)];
AR51=[zeros(N+1,N+3) zeros(N+1,N+3) zeros(N+1,N+3) zeros(N+1,N+3) (-(4*D2(1:N+1,1:N+3)/n^2-
a^2*eye(N+1,N+3)))];
AR52=[zeros(1,4*(N+3)) ones(1,N+3)];
AR53=[zeros(1,4*(N+3)) (-1).^[(0:N+2)-1].*[(0:N+2)].^2];
AR=[AR11;AR12;AR13;AR21;AR22;AR23;AR31;AR32;AR33;AR41;AR42;AR43;AR51;AR52;AR53];


 AI1=[zeros(N+3,4*(N+3)+N+3)];
%
 AI21=[a*diag(U1PP)*Re*eye(N+1,N+3) -a*Re*diag(u1)*eye(N+1,N+3) zeros(N+1,N+3) zeros(N+1,N+3)
zeros(N+1,N+3)];
 AI22=zeros(2,4*(N+3)+N+3);
%
 AI3=zeros(N+3,4*(N+3)+N+3);
%
 AI41=[zeros(N+1,N+3) zeros(N+1,N+3) diag(U2PP)*a*Re*gamma/m*eye(N+1,N+3) -
a*Re*gamma/m*diag(u2)*eye(N+1,N+3) zeros(N+1,N+3)];
 AI42=[zeros(2,4*(N+3)+N+3)];
```

```
 AI51=[zeros(N+1,N+3) zeros(N+1,N+3) -a*Pe*diag(TP)*eye(N+1,N+3) zeros(N+1,N+3)
a*Pe*diag(u2)*eye(N+1,N+3)];
 AI52=[zeros(2,5*(N+3))];
 AI=[AI1;AI21;AI22;AI3;AI41;AI42;AI51;AI52];

BR1=zeros(4*(N+3)-1,4*(N+3)+N+3);
BR2=wb*[(-1).^[(0:N+2)-1].*[(0:N+2)].^2 zeros(1,N+3) gamma/n*(-1).^[(0:N+2)-1].*[(0:N+2)].^2 zeros(1,N+3)
zeros(1,N+3)];
BR3=[zeros(N+1,4*(N+3)+N+3)];
BR4=[zeros(2,5*(N+3))];
BR=[BR1;BR2;BR3;BR4];

BI1=zeros(N+3,4*(N+3)+N+3);

BI21=[zeros(N+1,N+3) -a*Re*eye(N+1,N+3) zeros(N+1,N+3) zeros(N+1,N+3) zeros(N+1,N+3)];
BI22=zeros(2,4*(N+3)+N+3);

BI3=zeros(N+3,4*(N+3)+N+3);

BI41=[zeros(N+1,N+3) zeros(N+1,N+3) zeros(N+1,N+3) -a*Re*gamma/m*eye(N+1,N+3) zeros(N+1,N+3)];
BI42=zeros(2,4*(N+3)+N+3);

BI51=[zeros(N+1,4*(N+3)) a*Pe*eye(N+1,N+3)];
BI52=[zeros(2,5*(N+3))];

BI=[BI1;BI21;BI22;BI3;BI41;BI42;BI51;BI52];
```

Appendix B: CMG Input Files

Heterogeneous Viscosity Model

```
RESULTS SIMULATOR STARS 201210

** ====================  INPUT/OUTPUT  ======================
FILENAMES OUTPUT INDEX-OUT MAIN-RESULTS-OUT MAIN-RESULTS-IN

*TITLE1  'Model'
*TITLE2  'SAGD'
*CASEID  'GEOSTAT'
*INUNIT  *SI
*OUTUNIT *SI

**OUTPRN *grid *NONE
**OUTPRN *ITER *NEWTON

*WRST *TIME
*WSRF *GRID *TIME
*WSRF *SECTOR  *TIME
**OUTPRN *WELL *WELLCOMP
**OUTPRN *GRID *PRES *TEMP
OUTSRF GRID HEATCAP KRG KRO KRW MASDENG MASDENO MASDENW PRES SG SO STEAMQUAL
         SW TEMP THCONDUCT VELOCRC VISG VISO VISW X Y
OUTSRF SPECIAL SOR  'INJ1_INJ' 'INJ1_PRD'
           SOR  'INJ1_INJ' 'INJ1_PRD' CUM
**             SOR  'INJ2_INJ' 'PRD2_PRD'
**             SOR  'INJ2_INJ' 'PRD2_PRD' CUM
OUTSRF WELL LAYER ALL

*MAXERROR  1
RESULTS SUBMODEL_REFSS 5353
RESULTS SUBMODEL_REFSS 5353
RESULTS SUBMODEL_REFSS 5353
RESULTS SUBMODEL_REFSS 160
RESULTS SUBMODEL_REFSS 5353
RESULTS SUBMODEL_REFSS 0.0
RESULTS SUBMODEL_REFSS 0
**$  Distance units: m
RESULTS XOFFSET       1050.0000
RESULTS YOFFSET         0.0000
RESULTS ROTATION        0.0000  **$  (DEGREES)
RESULTS AXES-DIRECTIONS 1.0 -1.0 1.0
RESULTS SUBMODEL_REFSS 5353
**$ ************************************************************************
**$ Definition of fundamental cartesian grid
**$ ************************************************************************
GRID VARI 117 1 228
KDIR DOWN
DI IVAR
 117*0.08333333
```

```
DJ JVAR
 1
DK ALL
 26676*0.08333333
DTOP
 117*300
**$  0 = null block, 1 = active block
NULL CON           1
POR CON         0.3
PERMI CON      6500.44
PERMJ EQUALSI
PERMK EQUALSI * 0.25
**$  0 = pinched block, 1 = active block
PINCHOUTARRAY CON           1

*END-GRID

**Thermal Properties

*ROCKTYPE 1         ** Matrix Heat Properties

*PRPOR 3300.0
*CPOR   2.90E-06
*ROCKCP 2.35E+06
*THCONR 6.60E+05
*THCONW 5.35E+04
*THCONO 1.25E+04
*THCONG 3.20E+03
*THCONMIX *COMPLEX
*HLOSST 15.0
*HLOSSTDIFF 0.1
*HLOSSPROP *OVERBUR  2.350E+06 1.496E+05
          *UNDERBUR 2.350E+06 1.496E+05

*DILATION
*PBASE 2650.
*PDILA 9000.
*PPACT 5000.
*CRD 1.016E-04
*FR 0.45
*PORRATMAX 1.25
PERMULI CON          5
PERMULJ CON          5
PERMULK CON           5
THTYPE CON          1

** ================ FUILD DEFINITIONS ================

model 4 4 4 1

compname 'WATER' 'TOIL' 'BOIL' 'CH4'

cmm                 0          0.4067   1.0928   0.01604
pcrit               0          1478     792      4600
```

tcrit	0	618.85	903.85	-82.55	
kv1	0	1.9E+07	0	5.45E+05	
kv2	0	0	0	0	
kv3	0	0	0	0	
kv4	0	-6562.3	0	-879.84	
kv5	0	-80.13	0	-265.99	
massden	0	983.2	1158	320.4	
cp	0	7.00E-07		7.00E-07	1.00E-06
ct1	0	7.00E-04		7.00E-04	8.00E-04
avg	0	0.00010573		0.00010573	0.00010573
bvg	0	0.82	0.82	0.8126	
cpg1	0	0	0	19.251	
cpg2	0	0	0	5.21E-02	
cpg3	0	0	0	1.20E-05	
cpg4	0	0	0	-1.13E-08	
cpl1	0	994.1184		2514.584	-0.018
cpl2	0	0	0	1.20E+00	
cpl3	0	0	0	-9.87E-03	
cpl4	0	0	0	3.17E-05	
**hvr	0	1500	1500	2565.14	
**ev	0	0.38	0.38	0.265	

**TEMP		'WATER'	'TOIL'	'BOIL'	'GAS'
VISCTABLE				
5	0	4523613.536	14627862.150	1.15E+02
12	0	1246217.106	4420687.1044	9.81E+01
20	0	336922.8540	1291721.5943	6.84E+01
30	0	81167.37620	331656.03280	5.41E+01
40	0	23833.29160	100864.59230	4.34E+01
50	0	8256.561200	35419.211700	3.52E+01
60	0	3286.742100	14062.172500	2.89E+01
70	0	1471.422700	6203.0386000	2.40E+01
80	0	727.8683000	2996.2711000	2.01E+01
90	0	392.1015000	1565.6454000	1.70E+01
100	0	227.2724000	875.97330000	1.46E+01
110	0	140.3285000	520.25010000	1.26E+01
120	0	91.52780000	325.58540000	1.09E+01
130	0	62.61830000	213.36760000	9.56E+00
140	0	44.66740000	145.63780000	8.43E+00
150	0	33.05240000	103.06220000	7.49E+00
160	0	25.25990000	75.314100000	6.70E+00
170	0	19.86230000	56.637500000	6.03E+00
180	0	16.01640000	43.699400000	5.46E+00
190	0	13.20650000	34.502100000	4.97E+00
200	0	11.10700000	27.810400000	4.55E+00
210	0	9.506700000	22.838600000	4.18E+00
220	0	8.264900000	19.074100000	3.86E+00
230	0	7.285500000	16.174500000	3.58E+00
240	0	6.501900000	13.905800000	3.34E+00

250	0	5.866600000	12.105600000	3.12E+00
260	0	5.345400000	10.658300000	2.93E+00
270	0	4.913200000	9.4811000000	2.76E+00
280	0	4.551200000	8.5129000000	2.61E+00
300	0	3.984600000	7.0349000000	2.36E+00

** Reference conditions
prsr 2000
temr 10
psurf 101.325
tsurf 15.5

** ============== RELATIVE PERMEABILTIES ======================

rockfluid

rpt 1 stone2 ** ---------- good zone ----------

SWT	** KRW	KROW
0.1500	0.0000	0.9920
0.2000	0.0002	0.9790
0.2500	0.0016	0.9500
0.3000	0.0055	0.7200
0.3500	0.0130	0.6000
0.4000	0.0254	0.4700
0.4500	0.0440	0.3500
0.5000	0.0698	0.2400
0.5500	0.1040	0.1650
0.6000	0.1480	0.1100
0.6500	0.2040	0.0700
0.7000	0.2710	0.0400
0.7500	0.3520	0.0150
0.8000	0.4470	0.0000
0.8500	0.5590	0.0000
0.9000	0.6870	0.0000
0.9500	0.8340	0.0000
1.0000	1.0000	0.0000

SLT	** KRG	KROG	PCG
0.1500	1.0000	0.0000	
0.2000	0.9500	0.0002	
0.2500	0.8400	0.0016	
0.3000	0.7200	0.0055	
0.3500	0.6000	0.0130	
0.4000	0.4700	0.0254	
0.4500	0.3500	0.0440	
0.5000	0.2400	0.0698	
0.5500	0.1650	0.1040	
0.6000	0.0930	0.1480	
0.6500	0.0750	0.2040	
0.7000	0.0450	0.2710	
0.7500	0.0270	0.3520	
0.8000	0.0200	0.4470	
0.8500	0.0100	0.5590	

```
0.9000   0.0050   0.6870
0.9500   0.0000   0.8340
1.0000   0.0000   0.9920

swr         0.15       ** irreducible water saturation
sgr         0.005      ** critical gas saturation
sorg        0.005
krwro       0.1        ** end point
KRTYPE CON          1

** ================  INITIAL CONDITIONS  ====================
INITIAL
VERTICAL DEPTH_AVE

REFPRES 2670.0
REFDEPTH 300.0
TEMP CON          15
SW CON         0.2
SG CON          0
MFRAC_OIL 'TOIL' KVAR
 72*0.9246 9*0.921 9*0.9145 9*0.9047 9*0.8912 9*0.8736 9*0.8514 9*0.8241
 9*0.7912 12*0.752 12*0.7056 12*0.6512 12*0.5875 12*0.5126 12*0.4242
 12*0.3183
MFRAC_OIL 'CH4' CON        0.06
MFRAC_OIL 'BOIL' KVAR
 72*0.0154 9*0.019 9*0.0255 9*0.0353 9*0.0488 9*0.0664 9*0.0886 9*0.1159
 9*0.1488 12*0.188 12*0.2344 12*0.2888 12*0.3525 12*0.4274 12*0.5158
 12*0.6217
MFRAC_WAT 'WATER' CON          1
MFRAC_GAS 'CH4' CON          1

** ================  NUMERICAL CONTROL  ==================

*NUMERICAL
MAXSTEPS 8000000
DTMAX 90.
**SDEGREE 1
**ITERMAX 300
**AIM *STAB
**UPSTREAM *NLEVEL
**MINPRES 100.
**NCUTS 7
**NORTH 100
**NEWTONCYC 30
**CONVERGE   *PRESS 1.          *TEMP 0.5         *Y 0.01             *X 0.01             *SATUR 0.01
**NORM                        *PRESS 1500.     *TEMP 80.         *Y 0.1              *X 0.1              *SATUR 0.1
**CONVERGE TOTRES 1e-005

*RUN

** ================  RECURRENT DATA  ====================

*DATE 2006 12 26
DTWELL 0.1
```

```
** SAGD WP1
**$
WELL  'PRD1_PRD' FRAC  0.5
PRODUCER 'PRD1_PRD'
OPERATE MIN BHP  2650. CONT REPEAT
**OPERATE MAX STEAM   2. CONT REPEAT
OPERATE MAX STL   800. CONT REPEAT
** I J K
**$ UBA      ff  Status  Connection
**$ UBA      ff  Status  Connection
**$ UBA     ff  Status  Connection
**$         rad  geofac  wfrac  skin
GEOMETRY  K  0.1111  0.249  1.  0.
PERF  GEO  'PRD1_PRD'
**$ UBA       ff  Status  Connection
   59 1 224  1.
**$
WELL  'INJ1_INJ' FRAC  0.5
INJECTOR MOBWEIGHT 'INJ1_INJ'
TINJW 250.00
QUAL 0.95
INCOMP  WATER  1.  0.  0.  0.
OPERATE MAX STF   250. CONT REPEAT
OPERATE MAX BHP  4000. CONT REPEAT
** I J K
**$ UBA      ff  Status  Connection
**$ UBA     ff  Status  Connection
**$         rad  geofac  wfrac  skin
GEOMETRY  K  0.1111  0.249  1.  0.
PERF  GEO  'INJ1_INJ'
**$ UBA       ff  Status  Connection
   59 1 164  1.
**$
WELL  'INJ1_PRD' FRAC  0.5
PRODUCER 'INJ1_PRD'
OPERATE MIN BHP  2650. CONT REPEAT
**OPERATE MAX STEAM   2. CONT REPEAT
OPERATE MAX STL   800. CONT REPEAT
** I J K
**$ UBA      ff  Status  Connection
**$ UBA     ff  Status  Connection
**$         rad  geofac  wfrac  skin
GEOMETRY  K  0.1111  0.249  1.  0.
PERF  GEO  'INJ1_PRD'
**$ UBA       ff  Status  Connection
   59 1 164  1.



*SHUTIN 'PRD1_PRD'
*SHUTIN 'INJ1_INJ'
*SHUTIN 'INJ1_PRD'
```

```
** START CIRCULATION

*DATE 2007 01 01.
DTWELL 0.1
DTMAX 1.0

*OPEN 'INJ1_PRD'
*OPEN 'PRD1_PRD'
**$ Property: Temp. Setpoint for Controller (C)   Max: 200  Min: 200
TMPSET   *IJK 59 1 164   200
          59 1 224   200
**$ Property: Prop. Heat Transfer Coeff. (J/(day*C))   Max: 5e+009  Min: 5e+009
UHTR   *IJK 59 1 164   5e+009
          59 1 224   5e+009

*DATE 2007 02 01.
*DATE 2007 03 01.
*DATE 2007 04 01.                    ** START SAGD
DTWELL 0.05
DTMAX 1.0

*SHUTIN 'INJ1_PRD'


INJECTOR MOBWEIGHT 'INJ1_INJ'
TINJW 250.00

QUAL 0.95
INCOMP  WATER  1.  0.  0.  0.
OPERATE MAX BHP  4000. CONT REPEAT
**OPERATE MAX STF   300. CONT REPEAT

PRODUCER 'PRD1_PRD'
**OPERATE MIN STEAMTRAP 5.0 CONT REPEAT
**OPERATE MIN BHP  500. CONT REPEAT
OPERATE MAX STEAM  1. CONT REPEAT
**$ Property: Temp. Setpoint for Controller (C)   Max: 10  Min: 10
TMPSET   *IJK 59 1 164   10
          59 1 224   10
**$ Property: Prop. Heat Transfer Coeff. (J/(day*C))   Max: 0  Min: 0
UHTR   *IJK 59 1 164   0
          59 1 224   0

DATE   2007     4          2
DATE   2007     4          3
DATE   2007     4          4
DATE   2007     4          5
DATE   2007     4          6
DATE   2007     4          7
DATE   2007     4          8
DATE   2007     4          9
DATE   2007     4          10
DATE   2007     4          11
```

DATE 2007 4 12
DATE 2007 4 13
DATE 2007 4 14
DATE 2007 4 15
DATE 2007 4 16
DATE 2007 4 17
DATE 2007 4 18
DATE 2007 4 19
DATE 2007 4 20
DATE 2007 4 21
DATE 2007 4 22
DATE 2007 4 23
DATE 2007 4 24
DATE 2007 4 25
DATE 2007 4 26
DATE 2007 4 27
DATE 2007 4 28
DATE 2007 4 29
DATE 2007 4 30
DATE 2007 5 1
DATE 2007 5 2
DATE 2007 5 3
DATE 2007 5 4
DATE 2007 5 5
DATE 2007 5 6
DATE 2007 5 7
DATE 2007 5 8
DATE 2007 5 9
DATE 2007 5 10
DATE 2007 5 11
DATE 2007 5 12
DATE 2007 5 13
DATE 2007 5 14
DATE 2007 5 15
DATE 2007 5 16
DATE 2007 5 17
DATE 2007 5 18
DATE 2007 5 19
DATE 2007 5 20
DATE 2007 5 21
DATE 2007 5 22
DATE 2007 5 23
DATE 2007 5 24
DATE 2007 5 25
DATE 2007 5 26
DATE 2007 5 27
DATE 2007 5 28
DATE 2007 5 29
DATE 2007 5 30
DATE 2007 5 31
DATE 2007 6 1
DATE 2007 6 2
DATE 2007 6 3
DATE 2007 6 4

DATE 2007 6 5
DATE 2007 6 6
DATE 2007 6 7
DATE 2007 6 8
DATE 2007 6 9
DATE 2007 6 10
DATE 2007 6 11
DATE 2007 6 12
DATE 2007 6 13
DATE 2007 6 14
DATE 2007 6 15
DATE 2007 6 16
DATE 2007 6 17
DATE 2007 6 18
DATE 2007 6 19
DATE 2007 6 20
DATE 2007 6 21
DATE 2007 6 22
DATE 2007 6 23
DATE 2007 6 24
DATE 2007 6 25
DATE 2007 6 26
DATE 2007 6 27
DATE 2007 6 28
DATE 2007 6 29
DATE 2007 6 30
DATE 2007 7 1
DATE 2007 7 2
DATE 2007 7 3
DATE 2007 7 4
DATE 2007 7 5
DATE 2007 7 6
DATE 2007 7 7
DATE 2007 7 8
DATE 2007 7 9
DATE 2007 7 10
DATE 2007 7 11
DATE 2007 7 12
DATE 2007 7 13
DATE 2007 7 14
DATE 2007 7 15
DATE 2007 7 16
DATE 2007 7 17
DATE 2007 7 18
DATE 2007 7 19
DATE 2007 7 20
DATE 2007 7 21
DATE 2007 7 22
DATE 2007 7 23
DATE 2007 7 24
DATE 2007 7 25
DATE 2007 7 26
DATE 2007 7 27
DATE 2007 7 28

```
DATE   2007    7       29
DATE   2007    7       30
DATE   2007    7       31
DATE   2007    8       1

STOP
```

Homogeneous Viscosity Model

```
RESULTS SIMULATOR STARS 201210

** ==================  INPUT/OUTPUT  ======================
FILENAMES OUTPUT INDEX-OUT MAIN-RESULTS-OUT MAIN-RESULTS-IN

*TITLE1  'Model'
*TITLE2  'SAGD'
*CASEID  'GEOSTAT'
*INUNIT  *SI
*OUTUNIT *SI

**OUTPRN *grid *NONE
**OUTPRN *ITER *NEWTON

*WRST *TIME
*WSRF *GRID *TIME
*WSRF *SECTOR  *TIME
**OUTPRN *WELL *WELLCOMP
**OUTPRN *GRID *PRES *TEMP
OUTSRF GRID HEATCAP KRG KRO KRW MASDENG MASDENO MASDENW PRES SG SO STEAMQUAL
          SW TEMP THCONDUCT VELOCRC VISG VISO VISW X Y
OUTSRF SPECIAL SOR  'INJ1_INJ' 'INJ1_PRD'
             SOR  'INJ1_INJ' 'INJ1_PRD' CUM
**              SOR  'INJ2_INJ' 'PRD2_PRD'
**              SOR  'INJ2_INJ' 'PRD2_PRD' CUM
OUTSRF WELL LAYER ALL

*MAXERROR  1
RESULTS SUBMODEL_REFSS 5353
RESULTS SUBMODEL_REFSS 5353
RESULTS SUBMODEL_REFSS 5353
RESULTS SUBMODEL_REFSS 160
RESULTS SUBMODEL_REFSS 5353
RESULTS SUBMODEL_REFSS 0.0
RESULTS SUBMODEL_REFSS 0
**$  Distance units: m
RESULTS XOFFSET        1050.0000
RESULTS YOFFSET           0.0000
RESULTS ROTATION          0.0000  **$  (DEGREES)
RESULTS AXES-DIRECTIONS 1.0 -1.0 1.0
RESULTS SUBMODEL_REFSS 5353
**$ ************************************************************************
**$ Definition of fundamental cartesian grid
**$ ************************************************************************
GRID VARI 117 1 228
KDIR DOWN
DI IVAR
 117*0.08333333
DJ JVAR
 1
DK ALL
```

```
 26676*0.08333333
DTOP
 117*300
**$  0 = null block, 1 = active block
NULL CON           1
POR CON         0.3
PERMI CON      6500.44
PERMJ EQUALSI
PERMK EQUALSI * 0.25
**$  0 = pinched block, 1 = active block
PINCHOUTARRAY CON           1

*END-GRID

**Thermal Properties

*ROCKTYPE 1         ** Matrix Heat Properties

*PRPOR 3300.0
*CPOR   2.90E-06
*ROCKCP 2.35E+06
*THCONR 6.60E+05
*THCONW 5.35E+04
*THCONO 1.25E+04
*THCONG 3.20E+03
*THCONMIX *COMPLEX
*HLOSST 15.0
*HLOSSTDIFF 0.1
*HLOSSPROP *OVERBUR  2.350E+06 1.496E+05
          *UNDERBUR 2.350E+06 1.496E+05

*DILATION
*PBASE 2650.
*PDILA 9000.
*PPACT 5000.
*CRD 1.016E-04
*FR 0.45
*PORRATMAX 1.25
PERMULI CON          5
PERMULJ CON          5
PERMULK CON           5
THTYPE CON          1

** ================ FUILD DEFINITIONS ================

model 4 4 4 1

compname 'WATER' 'TOIL' 'BOIL' 'CH4'

cmm              0          0.4067   1.0928   0.01604
pcrit            0          1478     792      4600
tcrit            0          618.85   903.85   -82.55
kv1              0          1.9E+07  0        5.45E+05
kv2              0          0        0        0
```

kv3	0	0	0	0	
kv4	0	-6562.3	0	-879.84	
kv5	0	-80.13	0	-265.99	
massden	0	983.2	1158	320.4	
cp	0	7.00E-07		7.00E-07	1.00E-06
ct1	0	7.00E-04		7.00E-04	8.00E-04
avg	0	0.00010573		0.00010573	0.00010573
bvg	0	0.82	0.82	0.8126	
cpg1	0	0	0	19.251	
cpg2	0	0	0	5.21E-02	
cpg3	0	0	0	1.20E-05	
cpg4	0	0	0	-1.13E-08	
cpl1	0	994.1184		2514.584	-0.018
cpl2	0	0	0	1.20E+00	
cpl3	0	0	0	-9.87E-03	
cpl4	0	0	0	3.17E-05	
**hvr	0	1500	1500	2565.14	
**ev	0	0.38	0.38	0.265	

**TEMP		'WATER'	'TOIL'	'BOIL'	'GAS'
VISCTABLE					
5	0	4523613.536	14627862.150		1.15E+02
12	0	1246217.106	4420687.1044		9.81E+01
20	0	336922.8540	1291721.5943		6.84E+01
30	0	81167.37620	331656.03280		5.41E+01
40	0	23833.29160	100864.59230		4.34E+01
50	0	8256.561200	35419.211700		3.52E+01
60	0	3286.742100	14062.172500		2.89E+01
70	0	1471.422700	6203.0386000		2.40E+01
80	0	727.8683000	2996.2711000		2.01E+01
90	0	392.1015000	1565.6454000		1.70E+01
100	0	227.2724000	875.97330000		1.46E+01
110	0	140.3285000	520.25010000		1.26E+01
120	0	91.52780000	325.58540000		1.09E+01
130	0	62.61830000	213.36760000		9.56E+00
140	0	44.66740000	145.63780000		8.43E+00
150	0	33.05240000	103.06220000		7.49E+00
160	0	25.25990000	75.314100000		6.70E+00
170	0	19.86230000	56.637500000		6.03E+00
180	0	16.01640000	43.699400000		5.46E+00
190	0	13.20650000	34.502100000		4.97E+00
200	0	11.10700000	27.810400000		4.55E+00
210	0	9.506700000	22.838600000		4.18E+00
220	0	8.264900000	19.074100000		3.86E+00
230	0	7.285500000	16.174500000		3.58E+00
240	0	6.501900000	13.905800000		3.34E+00
250	0	5.866600000	12.105600000		3.12E+00
260	0	5.345400000	10.658300000		2.93E+00
270	0	4.913200000	9.4811000000		2.76E+00

280	0	4.551200000	8.5129000000	2.61E+00
300	0	3.984600000	7.0349000000	2.36E+00

** Reference conditions
prsr 2000
temr 10
psurf 101.325
tsurf 15.5

** ========== RELATIVE PERMEABILTIES ==========

rockfluid

rpt 1 stone2 ** ---------- good zone ----------

SWT	** KRW	KROW
0.1500	0.0000	0.9920
0.2000	0.0002	0.9790
0.2500	0.0016	0.9500
0.3000	0.0055	0.7200
0.3500	0.0130	0.6000
0.4000	0.0254	0.4700
0.4500	0.0440	0.3500
0.5000	0.0698	0.2400
0.5500	0.1040	0.1650
0.6000	0.1480	0.1100
0.6500	0.2040	0.0700
0.7000	0.2710	0.0400
0.7500	0.3520	0.0150
0.8000	0.4470	0.0000
0.8500	0.5590	0.0000
0.9000	0.6870	0.0000
0.9500	0.8340	0.0000
1.0000	1.0000	0.0000

SLT	** KRG	KROG	PCG
0.1500	1.0000	0.0000	
0.2000	0.9500	0.0002	
0.2500	0.8400	0.0016	
0.3000	0.7200	0.0055	
0.3500	0.6000	0.0130	
0.4000	0.4700	0.0254	
0.4500	0.3500	0.0440	
0.5000	0.2400	0.0698	
0.5500	0.1650	0.1040	
0.6000	0.0930	0.1480	
0.6500	0.0750	0.2040	
0.7000	0.0450	0.2710	
0.7500	0.0270	0.3520	
0.8000	0.0200	0.4470	
0.8500	0.0100	0.5590	
0.9000	0.0050	0.6870	
0.9500	0.0000	0.8340	
1.0000	0.0000	0.9920	

```
swr         0.15       ** irreducible water saturation
sgr         0.005      ** critical gas saturation
sorg        0.005
krwro       0.1        ** end point
KRTYPE CON          1

** ================  INITIAL CONDITIONS  ====================
INITIAL
VERTICAL DEPTH_AVE

REFPRES 2670.0
REFDEPTH 300.0
TEMP CON          15
SW CON         0.2
SG CON          0
MFRAC_OIL 'TOIL' con 0.752
MFRAC_OIL 'CH4' CON        0.06
MFRAC_OIL 'BOIL' con 0.1880
MFRAC_WAT 'WATER' CON          1
MFRAC_GAS 'CH4' CON          1

** ================  NUMERICAL CONTROL  ==================

*NUMERICAL
MAXSTEPS 8000000
DTMAX 90.
**SDEGREE 1
**ITERMAX 300
**AIM *STAB
**UPSTREAM *NLEVEL
**MINPRES 100.
**NCUTS 7
**NORTH 100
**NEWTONCYC 30
**CONVERGE   *PRESS 1.         *TEMP 0.5         *Y 0.01             *X 0.01             *SATUR 0.01
**NORM                       *PRESS 1500.    *TEMP 80.         *Y 0.1              *X 0.1              *SATUR 0.1
**CONVERGE TOTRES 1e-005

*RUN

** ================  RECURRENT DATA  ====================

*DATE 2006 12 26
DTWELL 0.1

** SAGD WP1
**$
WELL  'PRD1_PRD' FRAC  0.5
PRODUCER 'PRD1_PRD'
OPERATE MIN BHP  2650. CONT REPEAT
**OPERATE MAX STEAM   2. CONT REPEAT
OPERATE MAX STL   800. CONT REPEAT
** I J K
```

```
**$ UBA      ff  Status  Connection
**$ UBA      ff  Status  Connection
**$ UBA     ff  Status  Connection
**$         rad  geofac  wfrac  skin
GEOMETRY  K  0.1111  0.249  1.  0.
PERF  GEO  'PRD1_PRD'
**$ UBA      ff  Status  Connection
   59 1 224  1.
**$
WELL  'INJ1_INJ' FRAC  0.5
INJECTOR MOBWEIGHT 'INJ1_INJ'
TINJW 250.00
QUAL 0.95
INCOMP  WATER  1.  0.  0.  0.
OPERATE MAX STF   250. CONT REPEAT
OPERATE MAX BHP  4000. CONT REPEAT
** I J K
**$ UBA      ff  Status  Connection
**$ UBA     ff  Status  Connection
**$         rad  geofac  wfrac  skin
GEOMETRY  K  0.1111  0.249  1.  0.
PERF  GEO  'INJ1_INJ'
**$ UBA      ff  Status  Connection
   59 1 164  1.
**$
WELL  'INJ1_PRD' FRAC  0.5
PRODUCER 'INJ1_PRD'
OPERATE MIN BHP  2650. CONT REPEAT
**OPERATE MAX STEAM   2. CONT REPEAT
OPERATE MAX STL   800. CONT REPEAT
** I J K
**$ UBA      ff  Status  Connection
**$ UBA     ff  Status  Connection
**$         rad  geofac  wfrac  skin
GEOMETRY  K  0.1111  0.249  1.  0.
PERF  GEO  'INJ1_PRD'
**$ UBA      ff  Status  Connection
   59 1 164  1.



*SHUTIN 'PRD1_PRD'
*SHUTIN 'INJ1_INJ'
*SHUTIN 'INJ1_PRD'


** START CIRCULATION

*DATE 2007 01 01.
DTWELL 0.1
DTMAX 1.0

*OPEN 'INJ1_PRD'
*OPEN 'PRD1_PRD'
```

```
**$ Property: Temp. Setpoint for Controller (C)   Max: 200  Min: 200
TMPSET   *IJK 59 1 164   200
          59 1 224   200
**$ Property: Prop. Heat Transfer Coeff. (J/(day*C))   Max: 5e+009  Min: 5e+009
UHTR   *IJK 59 1 164   5e+009
          59 1 224   5e+009

*DATE 2007 02 01.
*DATE 2007 03 01.
*DATE 2007 04 01.                    ** START SAGD
DTWELL 0.05
DTMAX 1.0

*SHUTIN 'INJ1_PRD'


INJECTOR MOBWEIGHT 'INJ1_INJ'
TINJW 250.00

QUAL 0.95
INCOMP  WATER  1.  0.  0.  0.
OPERATE MAX BHP  4000. CONT REPEAT
**OPERATE MAX STF   300. CONT REPEAT

PRODUCER 'PRD1_PRD'
**OPERATE MIN STEAMTRAP 5.0 CONT REPEAT
**OPERATE MIN BHP  500. CONT REPEAT
OPERATE MAX STEAM  1. CONT REPEAT
**$ Property: Temp. Setpoint for Controller (C)   Max: 10  Min: 10
TMPSET   *IJK 59 1 164   10
          59 1 224   10
**$ Property: Prop. Heat Transfer Coeff. (J/(day*C))   Max: 0  Min: 0
UHTR   *IJK 59 1 164   0
          59 1 224   0

DATE   2007     4          2
DATE   2007     4          3
DATE   2007     4          4
DATE   2007     4          5
DATE   2007     4          6
DATE   2007     4          7
DATE   2007     4          8
DATE   2007     4          9
DATE   2007     4          10
DATE   2007     4          11
DATE   2007     4          12
DATE   2007     4          13
DATE   2007     4          14
DATE   2007     4          15
DATE   2007     4          16
DATE   2007     4          17
DATE   2007     4          18
DATE   2007     4          19
DATE   2007     4          20
```

DATE 2007 4 21
DATE 2007 4 22
DATE 2007 4 23
DATE 2007 4 24
DATE 2007 4 25
DATE 2007 4 26
DATE 2007 4 27
DATE 2007 4 28
DATE 2007 4 29
DATE 2007 4 30
DATE 2007 5 1
DATE 2007 5 2
DATE 2007 5 3
DATE 2007 5 4
DATE 2007 5 5
DATE 2007 5 6
DATE 2007 5 7
DATE 2007 5 8
DATE 2007 5 9
DATE 2007 5 10
DATE 2007 5 11
DATE 2007 5 12
DATE 2007 5 13
DATE 2007 5 14
DATE 2007 5 15
DATE 2007 5 16
DATE 2007 5 17
DATE 2007 5 18
DATE 2007 5 19
DATE 2007 5 20
DATE 2007 5 21
DATE 2007 5 22
DATE 2007 5 23
DATE 2007 5 24
DATE 2007 5 25
DATE 2007 5 26
DATE 2007 5 27
DATE 2007 5 28
DATE 2007 5 29
DATE 2007 5 30
DATE 2007 5 31
DATE 2007 6 1
DATE 2007 6 2
DATE 2007 6 3
DATE 2007 6 4
DATE 2007 6 5
DATE 2007 6 6
DATE 2007 6 7
DATE 2007 6 8
DATE 2007 6 9
DATE 2007 6 10
DATE 2007 6 11
DATE 2007 6 12
DATE 2007 6 13

```
DATE   2007    6       14
DATE   2007    6       15
DATE   2007    6       16
DATE   2007    6       17
DATE   2007    6       18
DATE   2007    6       19
DATE   2007    6       20
DATE   2007    6       21
DATE   2007    6       22
DATE   2007    6       23
DATE   2007    6       24
DATE   2007    6       25
DATE   2007    6       26
DATE   2007    6       27
DATE   2007    6       28
DATE   2007    6       29
DATE   2007    6       30
DATE   2007    7       1
DATE   2007    7       2
DATE   2007    7       3
DATE   2007    7       4
DATE   2007    7       5
DATE   2007    7       6
DATE   2007    7       7
DATE   2007    7       8
DATE   2007    7       9
DATE   2007    7       10
DATE   2007    7       11
DATE   2007    7       12
DATE   2007    7       13
DATE   2007    7       14
DATE   2007    7       15
DATE   2007    7       16
DATE   2007    7       17
DATE   2007    7       18
DATE   2007    7       19
DATE   2007    7       20
DATE   2007    7       21
DATE   2007    7       22
DATE   2007    7       23
DATE   2007    7       24
DATE   2007    7       25
DATE   2007    7       26
DATE   2007    7       27
DATE   2007    7       28
DATE   2007    7       29
DATE   2007    7       30
DATE   2007    7       31
DATE   2007    8       1

STOP
```